# Influence of basement heterogeneity on the architecture of low subsidence rate Paleozoic intracratonic basins (Reggane, Ahnet, Mouydir and Illizi basins, Hoggar massif)

Paul Perron[1], Michel Guiraud[1], Emmanuelle Vennin[1], Isabelle Moretti[2], Éric Portier[3], Laetitia Le Pourhiet[4], Moussa Konaté[5]

[1]Université de Bourgogne Franche-Comté, Centre des Sciences de la Terre, UMR CNRS 6282 Biogéosciences, 6 Bd Gabriel, 21000 Dijon, France.

[2]ENGIE, Département Exploration & Production, 1, place Samuel de Champlain, Faubourg de l'Arche, 92930 Paris La Défense, France.

[3]NEPTUNE Energy International S.A., 9-11 Allée de l'Arche – Tour EGEE – 92400 Courbevoie, France.

[4]Sorbonne Université, CNRS-INSU, Institut des Sciences de la Terre Paris, ISTeP UMR 7193, F-75005 Paris, France.

[5]Département de Géologie, Université Abdou Moumouni de Niamey, BP :10662, Niamey, Niger.

Corresponding author: paul.perron@u-bourgogne.fr, paul.perron@hotmail.fr

## Abstract

The Paleozoic intracratonic North African Platform is characterized by an association of arches (ridges, domes, swells or paleo-highs) and low subsidence rate syncline basins of different wavelengths (75–620 km). In the Reggane, Ahnet, Mouydir and Illizi basins are successively delimited from east to west by the Amguid El Biod, Arak-Foum Belrem, and Azzel Matti arches. Through the analysis of new unpublished geological data (i.e. satellite images, well-logs, seismic lines), the deposits associated with these arches and syncline basins exhibit thickness variations and facies changes ranging from continental to marine environments. The arches are characterized by thin amalgamated deposits with condensed and erosional surfaces, whereas the syncline basins exhibit thicker and well-preserved successions. In addition, the vertical facies succession evolves from thin Silurian to Givetian deposits into thick Upper Devonian sediments. Synsedimentary structures and major unconformities are related to several tectonic events such as the Cambrian–Ordovician extension, Ordovician–Silurian glacial rebound, Silurian–Devonian "Caledonian" extension/compression, late Devonian extension/compression, and "Hercynian" compression. Locally, deformation is characterized by near-vertical planar normal faults responsible for horst and graben structuring associated with folding during the Cambrian–Ordovician–Silurian period. These structures may have been inverted or reactivated during the Devonian (i.e. Caledonian, Mid-Late Devonian) compression and the Carboniferous (i.e. pre-Hercynian to Hercynian). Additionally, basement characterization from geological and geophysics data (aeromagnetic and gravity maps), shows an interesting age-dependent zonation of the terranes which are bounded by mega shear zones with the arches-basins framework. The "old" terranes are situated under arches while the "young" terranes are located under the basins depocenter. This structural framework results from the accretion of Archean and Proterozoic terranes inherited from former orogeny (e.g. Pan-African orogeny 900-520 Ma). So, the sedimentary infilling pattern and the nature of deformation result from the slow Paleozoic repeatedly reactivation of Precambrian terranes bounded by sub-vertical lithospheric fault systems. Alternating periods of tectonic quiescence and low-rate subsidence acceleration associated with extension and local inversion tectonics correspond to a succession of Paleozoic geodynamic events (i.e. far-field orogenic belt, glaciation).

Keywords: intracratonic basin, Paleozoic, arches, low-rate subsidence, tectonic heritage, terranes, Central Sahara

# 1 Introduction

Paleozoic deposits fill numerous intracratonic basins, which may also be referred to as “cratonic basins”, “interior cratonic basins”, or “intracontinental sags”. Intracratonic basins are widespread around the world (Heine et al., 2008) and exploration for non-conventional petroleum has revived interest in them. They are located in “stable” lithospheric areas and share several common features (Allen and Armitage, 2011). Their geometries are large circular, elliptical, saucer-shaped to oval. Their stratigraphy is filled with continental to shallow-water sediments. Their subsidence rate is low (5 to 50 m/Ma) and long (sometimes more than 540 Myr). Their structural framework shows reactivation of structures and emergence of arches also referred to in the literature as “ridges”, “paleo-highs”, “domes”, and “swells”. Multiple hypotheses and models have been proposed to explain how these slowly subsiding, long-lived intracratonic basins formed and evolved (see Allen and Armitage, 2011 and references therein or Hartley and Allen, 1994). However, their tectonic and sedimentary architectures are often poorly constrained.

The main specificities of intracratonic basins are found on the Paleozoic North Saharan Platform. The sedimentary infilling during c. 250 Myr is relatively thin (i.e. around a few hundred to a few thousand meters), of great lateral extent (i.e. 9 million km$^2$), and is separated by major regional unconformities (Beuf et al., 1968a, 1971; Carr, 2002; Eschard et al., 2005, 2010; Fabre, 1988, 2005; Fekirine and Abdallah, 1998; Guiraud et al., 2005; Kracha, 2011; Legrand, 2003a). Depositional environments were mainly continental to shallow-marine and homogeneous. Very slow and subtle lateral variations occurred over time (Beuf et al., 1971; Carr, 2002; Fabre, 1988; Guiraud et al., 2005; Legrand, 2003a). The Paleozoic North Saharan Platform is arranged (Fig. 1) into an association of long-lived broad synclines (i.e. basins or sub-basins) and anticlines (i.e. arches) of different wavelengths (λ: 75–620 km). Burov and Cloetingh (2009) report deformation wavelengths of the order of 200–600 km when the whole lithosphere is involved and of 50–100 km when the crust is decoupled from the lithospheric mantle. This insight suggests that the inherited basement fabric influences intracratonic basin architecture at a large scale. Besides, pre-existing structures, such as shear zones and terrane suture zones, are present throughout the lithosphere, affecting the geometry and evolution of upper-crustal structural framework forming during later tectonic events (Peace et al., 2018; Phillips et al., 2018).

In this study of the Reggane, Ahnet, Mouydir and Illizi basins, a multidisciplinary workflow involving various tools (e.g. seismic profiles, satellite images) and techniques (e.g. photo-geology, seismic interpretation, well correlation, geophysics, geochronology) has enabled us to (1) make a tectono-sedimentary analysis, (2) determine the spatial arrangement of depositional environments calibrated by biostratigraphic zonation, (3) characterize basin geometry, and (4) ascertain the inherited architecture of the basement and its tectonic evolution. We propose a conceptual coupled model explaining the architecture of the intracratonic basins of the North Saharan Platform. This model highlights the role of basement heritage heterogeneities in an accreted mobile belt and their influence on the structure and evolution of intracratonic basins. It is a first step towards a better understanding of the factors and mechanisms that drive intracratonic basins.

## 2 Geological setting: The Paleozoic North Saharan Platform and the Reggane, Ahnet, Mouydir and Illizi basins

The Reggane, Ahnet, Mouydir and Illizi basins (Figs. 1 and 2) are located in south-western Algeria, north of the Hoggar massif (Ahaggar). They are depressions filled by Paleozoic deposits. The basins are bounded to the south by the Hoggar massif (Tuareg Shield) and they are separated from together by the Azzel Matti, the Arak-Foum Belrem the Amguid El Biod arches.

Figure 3 synthetizes the lithostratigraphy, the large-scale sequence stratigraphic framework delimited by six main regional unconformities (A to F), and the tectonic events proposed in the literature (cf. references under Fig. 3) affecting the Paleozoic North Saharan Platform.

During the Paleozoic, the Reggane, Ahnet, Mouydir and Illizi basins were part of a set of the super-continent Gondwana (Fig. 1). This super-continent resulted from the collision of the West African Craton (WAC) and the East Saharan Craton (ESC), sandwiching the Tuareg Shield (TS) mobile belt during the Pan-African orogeny (Craig et al., 2008; Guiraud et al., 2005; Trompette, 2000). This orogenic cycle followed by the chain's collapse (c. 1000–525 Ma) was also marked by phases of oceanization and continentalization (c. 900–600 Ma) giving rise to the heterogeneous terranes in the accreted mobile belt (Trompette, 2000). The Hoggar massif is composed of several accreted, sutured, and amalgamated terranes of various ages and compositions resulting from multiple phases of geodynamic events (Bertrand and Caby, 1978; Black et al., 1994; Caby, 2003; Liégeois et al., 2003). Twenty-three well preserved terranes in the Hoggar were identified and grouped into Archean, Paleoproterozoic, and Mesoproterozoic–Neoproterozoic juvenile Pan-African terranes (see legend in Fig. 1). In the West African Craton, the Reguibat shield is composed of Archean terrains in the west and of Paleoproterozoic terranes in the east (Peucat et al., 2003, 2005).

Then, there is evidence of a complex and polyphased history throughout the Paleozoic (Fig. 3), with alternating periods of quiescence and tectonic activity, individualizing and rejuvenating ancient NS, NE–SW, or NW–SE structures in arch and basin configurations (Badalini et al., 2002; Boote et al., 1998; Boudjema, 1987; Coward and Ries, 2003; Craig et al., 2008; Guiraud et al., 2005; Logan and Duddy, 1998; Lüning, 2005). The Paleozoic successions of the North Saharan Platform are predominantly composed of siliciclastic detrital sediments (Beuf et al., 1971; Eschard et al., 2005). They form the largest area of detrital sediments ever found on continental crust (Burke et al., 2003), dipping gently NNW

(Beuf et al., 1971, 1969; Fabre, 1988, 2005; Fröhlich et al., 2010; Gariel et al., 1968; Le Heron et al., 2009). Carbonate deposits are observed from the Mid–Late Devonian to the Carboniferous (Wendt, 1985, 1988, 1995; Wendt et al., 1993, 1997, 2006, 2009a; Wendt and Kaufmann, 1998). From south to north, the facies progressively evolve from continental fluviatile to shallow marine (i.e. upper to lower shoreface) and then to offshore facies (Beuf et al., 1971; Carr, 2002; Eschard et al., 2005; Fabre, 1988; Fekirine and Abdallah, 1998; Legrand, 1967a).

## 3 Data and methods

A multidisciplinary approach has been used in this study integrating new data (i.e. satellite images, seismic lines and well-logs data) in particular from the Reggane, Ahnet, Mouydir, Illizi basins and Hoggar massif (Fig. 4):

The Paleozoic series of the Ahnet and Mouydir basins are well-exposed over an area of approximately 170,000 km$^2$ and are well observed in satellite images (Google Earth and Landsat from USGS). Furthermore, a significant geological database (i.e. wells, seismic records, geological reports) has been compiled in the course of petroleum exploration since the 1950s. The sedimentological dataset is based on the integration and analysis of cores, outcrops, well-logs, and of lithological and biostratigraphic data. They were synthetized from internal SONATRACH (Dokka, 1999), IFP-SONATRACH consortium reports (Eschard et al., 1999), and published articles (Beuf et al., 1971; Biju-Duval et al., 1968; Wendt et al., 2006). Facies described from cores and outcrops of these studies were grouped into facies associations corresponding to the main depositional environments observed on the Saharan Platform (Table 1). Characteristic gamma-ray patterns (electrofacies) are proposed to illustrate the different facies associations. The gamma-ray (GR) peaks are commonly interpreted as the maximum flooding surfaces (MFS) (e.g. Catuneanu et al., 2009; Galloway, 1989; Milton et al., 1990; Serra and Serra, 2003). Time calibration of well-logs is based on palynomorphs (essentially Chitinozoans and spores) and outcrops on conodonts, goniatites, and brachiopods (Wendt et al., 2006). Palynological data of wells (W1, W7, W12, W19 and W20) from internal unpublished data (Abdesselam-Rouighi, 1991; Azzoune, 1999; Hassan, 1984; Khiar, 1974) are based on biozonations from Magloire, (1967) and Boumendjel et al., (1988). Well W18 is supported by palynological data and biozonations from Hassan Kermandji et al., (2008).

Synsedimentary extensional and compressional markers are characterized in this structural framework based on the analyses of satellite images (Figs. 5 and 6), seismic profiles (Fig. 7), 21 wells (W1 to W21), and 12 outcrop cross-sections (O1 to O12). Wells and outcrop sections are arranged into three E–W sections (Figs. 10, 11 and 12) and one N–S section (Fig. 13). Satellite images (Figs. 5 and 6) and seismic profiles (Fig. 7) are located at key areas (i.e. near arches) illustrating the relevant structures (Fig. 2). The calibration of the key stratigraphic horizon on seismic profiles (Fig. 7) was settled by sonic well-log data using PETREL and OPENDTECT software. Nine key horizons easily extendable at the regional scale are identified and essentially correspond to major depositional unconformities: near top Infra-Cambrian, near top Ordovician, near top Silurian, near top Pragian, near top Givetian, near top mid-Frasnian, near top Famennian, near base Quaternary and near Hercynian unconformities (Figs 7). The stratigraphic layers are identified by the integration of satellite images (Google Earth and Landsat USGS: https://earthexplorer.usgs.gov/), digital elevation model (DEM) and the 1:200,000 geological maps of Algeria (Bennacef et al., 1974; Bensalah et al., 1971).

Subsidence analysis characterizes the vertical displacements of a given sedimentary depositional surface by tracking its subsidence and uplift history (Van Hinte, 1978). The resulting curve details the total subsidence history for a given stratigraphic column (Allen and

Allen, 2005; Van Hinte, 1978). Backstripping is also used to restore the initial thicknesses of a sedimentary column (Allen and Allen, 2005; Angevine et al., 1990). Lithologies and paleobathymetries have been defined using facies analysis or literature data. Porosity and the compaction proxy are based on experimental data from (Sclater and Christie, 1980). In this study, subsidence analyses were performed on sections using OSXBackstrip software performing 1D Airy backstripping (after Allen and Allen, 2005; Watts, 2001); available at: http://www.ux.uis.no/nestor/work/programs.html).

The 800 km$^2$ outcrop of basement rocks of the Hoggar massif provides an exceptional case study of an exhumed mobile belt composed of accreted terranes of different ages. To reconstruct the nature of the basement, a terrane map (Figs. 15 and 16) was put together by integrating geophysical data (aeromagnetic anomaly map: https://www.geomag.us/, Bouguer gravity anomaly map: http://bgi.omp.obs-mip.fr/), satellite images (7ETM+ from Landsat USGS: https://earthexplorer.usgs.gov/) data, geological maps (Berger et al., 2014; Bertrand and Caby, 1978; Black et al., 1994; Caby, 2003; Fezaa et al., 2010; Liégeois et al., 1994, 2003, 2005, 2013), and geochronological data (e.g. U-Pb radiochronology, see supplementary data 1). Geochronological data from published studies were compiled and georeferenced (Fig. 1). Thermo-tectonic ages were grouped into eight main thermo-orogenic events (Fig. 1): The Liberian-Ouzzalian event (Arcehan, >2500 Ma), (the Archean, Eburnean (i.e. Paleproterozoic, 2500-1600 Ma), the Kibarian (i.e. Mesosproterozoic, 1600-1100 Ma), the Neoproterozoic oceanization-rifting (1100-750 Ma), the syn-Pan-African orogeny (i.e. Neoproterozoic, 750-541 Ma), the post-Pan-African (i.e. Neoproterozoic, 541-443 Ma), the Caledonian orogeny (i.e. Siluro-Devonian, 443-358 Ma), and the Hercynian orogeny (i.e. Carbo-Permian, 358-252 Ma).

# 4 Structural framework and tectono-sedimentary structure analyses

The structural architecture of the North Saharan Platform is characterized by mostly circular to oval shaped basins structured by major faults frequently associated with broad asymmetrical folds displayed by three main trends (Fig. 1): (1) near-N–S, varying from N0° to N10° or N160°, (2) from N40° to 60°, and (3) N100° to N140° directions (Figs 1, 3A, and 4). These fault zones are about 100 km (e.g. faults F1 and F2, Fig. 5) to tens of kilometers long (e.g. faults F3 to F8, Fig. 5). They correspond to the mainly N–S Azzel-Matti, Arak-Foum Belrem, Amguid El Biod, and Tihemboka arches, the NE–SW Bou Bernous, Ahara, and Gargaf arches, and the NW–SE Saoura and Azzene arches (Fig. 1).

### 4.1 Synsedimentary extensional markers

Extensional markers are characterized by the settlement of steeply west- or eastward-dipping basement normal faults associated with colinear syndepositional folds of several kilometers in length (e.g. Fig. 6A to E and 7A), represented by footwall anticline and hanging wall syncline-shaped forced folds. They are located in the vicinity of different arches (Fig. 2) such as the Tihemboka arch (Figs. 5B and 6A, 6B), Arak-Foum Belrem arch (Figs. 5A, 6C to 6F and 7A, 7C), Azzel Matti arch (Fig. 7B), and Bahar El Hamar area intra-basin arch (Fig. 7D). These tectonic structures can be featured by basement blind faults (e.g. fault F1 in Fig. 7A). The deformation pattern is mainly characterized by brittle faulting in Cambrian–Ordovician series down to the basement and fault-damping in Silurian series (e.g. faults F1 to F6 in Fig. 7B). The other terms of the series (i.e. Silurian to Carboniferous) are usually affected by folding except (see F1 faults in Figs. 6F, 7B, 7D and 7C) where the brittle deformation can be propagated to the Upper Devonian (due to reactivation and/or inversion as suggested in the next paragraph).

In association with the extensional markers, thickness variations and tilted divergent onlaps of the sedimentary series (i.e. wedge-shaped units, progressive unconformities) in the hanging wall syncline of the fault escarpments are observed (Figs. 6 and 7). These are attested using photogeological analysis of satellite images (Fig. 6) and are marked by a gentler dip angle of the stratification planes away from the fault plane (i.e. fault core zone). The markers of syndepositional deformation structures are visible in the hanging-wall synclines of Precambrian to Upper Devonian series (Figs. 6 and 7).

The footwall anticline and hanging-wall syncline-shaped forced folds recognized in this study are very similar to those described in the literature by Grasemann et al., (2005); Khalil and McClay, (2002); Schlische, (1995); Stearns, (1978); Withjack et al., (1990), (2002); Withjack and Callaway, (2000). The wedge-shaped units (DO0 to DO3; Figs. 5, 6 and 7) associated with the hanging-wall synclines are interpreted as synsedimentary normal fault-related folding. The whole tectonic framework forms broad extensional horsts and graben related to synsedimentary forced folds controlling basin shape and sedimentation.

Following Khalil and McClay, (2002); Lewis et al., (2015); Shaw et al., (2005); Withjack et al., (1990), we use the ages of the growth strata (i.e. wedge-shaped units) to determine the timing of the deformation. The main four wedge-shaped units identified (DO0 to DO3) are indicative of the activation and/or reactivation of the normal faults (extensional settings) during Neoproterozoic (DO0), Cambrian–Ordovician (DO1), Early to Mid-Silurian (DO2) and Mid to Late Devonian (DO3) times.

In planar view, straight (F1 in Fig. 5A) and sinuous faults (F2, F3, F3', F4, F4', and F5 in Fig. 5A) can be identified. The sinuous faults are arranged "en echelon" into several segments with relay ramps. These faults are 10 to several tens of kilometers long with vertical throws of hundreds of meters that fade rapidly toward the fault tips. The sinuous geometry of normal undulated faults as well as the rapid lateral variation in fault throw are controlled by the propagation and the linkage of growing parent and tip synsedimentary normal faults (Marchal et al., 2003, 1998). We use the stratigraphic age of impacted layers (here Tamadjert Fm.) to date (re)activation of the faults.

According to Holbrook and Schumm, (1999), river patterns are extremely sensitive to tectonic structure activity. Here we find that the synsedimentary activity of the extensional structures is also evidenced by the influence of the fault scarp on the distribution and orientation of sinuous channelized sandstone body systems (dotted red lines in Fig. 5B). It highlights the (re)activation of the faults during the deposition of these channels, i.e. late Hirnantian dated by (Girard et al., 2012).

### 4.2 Synsedimentary compressional markers (inversion tectonics)

After the development of the extensional tectonism described previously, evidence of synsedimentary compressional markers can be identified. These markers are located and preferentially observable near the Arak-Foum Belrem arch (Fig. 6F; F2 in Fig. 7C), the Azzel Matti arch (2 in Figs 7B), and the Bahar El Hamar area intra-basin arch (2 in Fig. 7D). The tectonic structures take the form of inverse faulting reactivating former basement faults (F1' in Fig. 6F, F1 in Fig. 7C, F1' in Fig. 7D, F1 in Fig. 7B). The synsedimentary inverse faulting is demonstrated by the characterization of asymmetric anticlines especially observable in satellite images and restricted to the fault footwalls (Figs 5A along F1-F2).

Landsat image analysis combined with the line drawing of certain seismic lines reveals several thickness variations reflecting divergent onlaps (i.e. wedge-shaped units) which are restricted to the hanging-wall asymmetric anticlines (2 in Figs 6F, 7B, 7C and 7D). The compressional synsedimentary markers clearly post-date extensional divergent onlaps at hanging-wall syncline-shaped forced folds (1 in Figs 7B, 7C and 7D). This architecture is very similar to classical positive inversion structures of former inherited normal faults (Bellahsen and Daniel, 2005; Bonini et al., 2012; Buchanan and McClay, 1991; Ustaszewski et al., 2005). Tectonic transport from the paleo-graben hanging-wall toward the paleo-horst footwall (F1, F2-F2', F4-F4' in Fig. 7B; F1-F1' in Fig. 7D) is evidenced. Further positive tectonic inversion architecture is identified by tectonic transport from the paleo-horst footwall to the paleo-graben hanging wall (F1-F1' in Fig. 6F; F1, F5, and F6 in Fig. 7C). This second type of tectonic inversion is very similar to the transported fault models defined by (Butler, 1989; Madritsch et al., 2008). The local positive inversions of inherited normal faults occurred during Silurian–Devonian (F4' Fig. 7B) and Mid to Late Devonian times (Figs. 7B, 7C and 7D). A late significant compression event between the end of the Carboniferous and the Early Mesozoic was responsible for the exhumation and erosion of the tilted Paleozoic series. This series is related to the Hercynian angular unconformity surface (Fig. 7B).

## 5 Stratigraphy and sedimentology

The whole sedimentary series described in the literature is composed of fluviatile to Braid-deltaic plain Cambrian, not only fluviatile (e.g. Brahmaputra River analogue), with a transitional facies from continental to shallow marine (Beuf et al., 1968b, 1968a, 1971; Eschard et al., 2005, 2010; Sabaou et al., 2009), Upper Ordovician glaciogenic deposits (Beuf et al., 1968a, 1968b, 1971; Eschard et al., 2005, 2010), argillaceous deep marine Silurian deposits (Djouder et al., 2018; Eschard et al., 2005, 2010; Legrand, 1986, 2003b; Lüning et al., 2000) and offshore to embayment Carboniferous deposits (Wendt et al., 2009). In this complete sedimentary succession, we have focused on the Devonian deposits as they are very sensitive to and representative of basin dynamics. The architecture of the Devonian deposits allows us to approximate the main forcing factors controlling the sedimentary infilling of the basin and its synsedimentary deformation. Eleven facies associations organized into four depositional environments (Table 1) are defined to reconstruct the architecture and the lateral and vertical sedimentary evolution of the basins (Figs. 10, 11, 12 and 13).

### 5.1 Facies association, depositional environments, and erosional unconformities

Based on the compilation and synthesis of internal studies (Eschard et al., 1999), published papers on the Saharan platform (Beuf et al., 1971; Eschard et al., 2005, 2010; Henniche, 2002) and on the Ahnet and Mouydir basins (Biju-Duval et al., 1968; Wendt et al., 2006), eleven main facies associations (AF1 to AF5) and four depositional environments are proposed for the Devonian succession (Table 1). They are associated with their gamma-ray responses (Figs 8 and 9). They are organized into two continental/fluvial (AF1 to AF2), four transitional/coastal plain (AF3a to AF3d), three shoreface (AF4a to AF4c), and two offshore (AF5a to AF5b) sedimentary environments.

#### 5.1.1 Continental fluvial environments

This depositional environment features the AF1 (fluvial) and the AF2 (flood plain) facies association (Table 1). Facies association AF1 is mainly characterized by a thinning-up sequence with a basal erosional surface and trough cross-bedded intraformational conglomerates with mud clast lag deposits, quartz pebbles, and imbricated grains (Table 1). It passes into medium to coarse trough cross-bedded sandstones, planar cross-bedded siltstones, and laminated shales. These deposits are associated with rare bioturbations (expect at the surface of the sets), ironstones, phosphorites, corroded quartz grains, and phosphatized pebbles. Laterally, facies association AF2 is characterized by horizontally laminated and very poorly sorted silt to argillaceous fine sandstones. They contain frequent root traces, plant debris, well-developed paleosols, bioturbations, nodules, and ferruginous horizons. Current ripples and climbing ripples are associated in prograding thin sandy layers.

In AF1, the basal erosional reworking and high energy processes are characteristic of channel-filling of fluvial systems (Allen, 1983; Owen, 1995). Eschard et al., (1999) identify three fluvial systems (see A, B, and C in Fig. 9) in the Tassili-N-Ajjers outcrops: braided dominant

(AF1a), meandering dominant (AF1b), and straight dominant (AF1c). They differentiate them by their different sinuosity, directions of accretion (lateral or frontal), the presence of mud drapes, bioturbations, and giant epsilon cross-bedding. Gamma-ray signatures of these facies associations (A, B, and C in Fig. 9) are cylindrical with an average value of 20 gAPI. The gamma ray shapes are largely representative of fluvial environments (Rider, 1996; Serra and Serra, 2003; Wagoner et al., 1990). The bottom is sharp with high value peaks and the tops are frequently fining-up, which may be associated with high values caused by argillaceous flood plain deposits and roots (Eschard et al., 1999). AF2 is interpreted as humid floodplain deposits (Allen, 1983; Owen, 1995) with crevasse splays or preserved levees of fluvial channels (Eschard et al., 1999). Gamma-ray curves of AF2 (D, Fig. 9) show a rapid succession of low to very high peak values, ranging from 50 to 120 gAPI. AF1 and AF2 are typical of the Pragian "Oued Samene" Formation (Wendt et al., 2006). In the Illizi basin, these facies are mainly recorded in the Ajjers Formation (dated Upper Cambrian? to Ordovician see Fabre, 2005; Vecoli, 2000; Vecoli et al., 1995, 1999, 2008; Vecoli and Playford, 1997) and the Lochkovian to Pragian "Barre Moyenne" and "Barre Supérieure" Formations (Beuf et al., 1971; Eschard et al., 2005).

#### 5.1.2 Transitional coastal plain environments

This depositional environment comprises facies associations AF3a (delta/estuarine), AF3b (fluvial/tidal distributary channels), AF3c (tidal sand flat), AF3d (lagoon/mudflat) (table 1). AF3a is mainly dominated by sigmoidal cross-bedded heterolithic rocks with mud drapes. It is also characterized by fine to coarse, poorly sorted sandstones and siltstones often structured by combined flow ripples, flaser bedding, wavy bedding, and some rare planar bedding. Mud clasts, root traces, desiccation cracks, water escape features, and shale pebbles are common. The presence of epsilon bedding is attested, which is formed by lateral accretion of a river point bar (Allen, 1983). The bed surface sets are intensively bioturbated (*Skolithos* and

*Planolites*) indicating a shallow marine subtidal setting (Pemberton and Frey, 1982). Faunas such as brachiopods, trilobites, tentaculites, and graptolites are present. AF3b exhibits a fining-up sequence featured by a sharp erosional surface, trough cross-bedded, very coarse-grained, poorly sorted sandstone at the base and sigmoidal cross-bedding at the top (Figs 8 and 9). AF3c is formed by fine-grained to very coarse-grained sigmoidal cross-bedded heterolithic sandstones with multidirectional tidal bundles. They are also structured by lenticular, flaser bedding and occasional current and oscillation ripples with mud cracks. They reveal intense bioturbation composed of *Skolithos* (Sk), *Thalassinoides* (Th), and *Planolites* (Pl) ichnofacies indicating a shallow marine subtidal setting (Frey et al., 1990; Pemberton and Frey, 1982). AF4d is characterized by horizontally laminated mudstones associated with varicolored shales and fine-grained sandstones. They exhibit mud cracks, occasional wave ripples, and rare multidirectional current ripples. These sedimentary structures are poorly preserved because of intense bioturbation composed of *Skolithos* (Sk), *Thalassinoides* (Th), and *Planolites* (Pl). Fauna includes ammonoids (rare), goniatites, calymenids, pelecypod molds, and brachiopod coquinas.

In AF3a, both tidal and fluvial systems in the same facies association can be interpreted as an estuarine system (Dalrymple et al., 1992; Dalrymple and Choi, 2007). The gamma-ray signature is characterized by a convex bell shape with rapidly alternating low to mid values (30 to 60 gAPI) due to the mud draping of the sets (see E Fig. 9). These forms of gamma ray are typical of fluvial-tidal influenced environments with upward-fining parasequences (Rider, 1996; Serra and Serra, 2003; Wagoner et al., 1990). AF3a is identified at the top of the Pragian "Oued Samene" Formation and in Famennian "Khenig" Formation (Wendt et al., 2006) in the Ahnet and Mouydir basins. In the Illizi basin, AF3a is mostly recorded at the top Cambrian of the Ajjers Formation, in the Lochkovian "Barre Moyenne", and at the top Pragian of the "Barre Supérieure" Formation (Beuf et al., 1971; Eschard et al., 2005). The

AF3b association can be characterized by a mixed fluvial and tidal dynamic based on criteria such as erosional basal contacts, fining-upward trends or heterolythic facies (Dalrymple et al., 1992; Dalrymple and Choi, 2007). They are associated with abundant mud clasts, mud drapes, and bioturbation indicating tidal influences (Dalrymple et al., 1992, 2012; Dalrymple and Choi, 2007). The major difference with the estuarine facies association (AF3a) is the slight lateral extent of the channels which are only visible in outcrops (Eschard et al., 1999). The gamma-ray pattern is very similar to the estuarine electrofacies (see F Fig. 9). AF3c is interpreted as a tidal sandflat laterally present near a delta (Lessa and Masselink, 1995) and associated with an estuarine environment (Leuven et al., 2016). The gamma-ray signature (see G Fig. 9) is distinguishable by its concave funnel shape with alternating low and mid peaks (25 to 60 gAPI) due to the heterogeneity of the deposits and rapid variations in the sand/shale ratio. These facies are observed in the "Talus à Tigillites" Formation of the Illizi basin (Eschard et al., 2005). In AF4d, both ichnofacies and facies are indicative of tidal mudflat/lagoonal depositional environments (Dalrymple et al., 1992; Dalrymple and Choi, 2007; Frey et al., 1990). The gamma-ray signature has a distinctively high value (80 to 130 gAPI) and an erratic shape (see H Fig. 9). AF4d is observed in the "Atafaitafa" Formation and in the Emsian prograding shoreface sequence of the Illizi basin (Eschard et al., 2005). It is also recorded in the Lochkovian "Oued Samene" Formation and the Famennian "Khenig" Sandstones (Wendt et al., 2006).

#### 5.1.3 Shoreface environments

This depositional environment is composed of AF4a (subtidal), AF4b (upper shoreface), and AF4c (lower shoreface) facies associations (Table 1). AF4a is characterized by the presence of brachiopods, crinoids, and diversified bioturbations, by the absence of emersion, and by the greater amplitude of the sets in a dominant mud lithology (Eschard et al., 1999). AF4b is heterolithic and composed of fine to medium-grained sandstones (brownish) interbedded with argillaceous siltstones and bioclastic carbonated sandstones. Sedimentary structures include oscillation ripples, swaley cross-bedding, flaser bedding, cross-bedding, convolute bedding, wavy bedding, and low-angle planar cross-stratification. Sediments were affected by moderate to highly diversified bioturbation by *Skolithos* (Sk), *Cruziana*, *Planolites*, (Pl) *Chondrites* (Ch), *Teichichnus* (Te), *Spirophytons* (Sp) and are composed of ooids, crinoids, bryozoans, stromatoporoids, tabulate and rugose corals, pelagic styliolinids, neritic tentaculitids, and brachiopods. AF4c can be distinguished by a low sand/shale ratio, thick interbeds, abundant HCS, deep groove marks, slumping, and intense bioturbation (Table 1).

AF4a is interpreted as a lagoonal shoreface. The gamma-ray pattern (see I Fig. 9) is characterized by a concave bell shape influenced by a low sand/shale ratio with values fluctuating between 100 and 200 gAPI. AF4a is identified in the "Talus à Tigillites" Formation and the Emsian sequence of the Illizi basin (Eschard et al., 2005) and in the Lochkovian "Oued Samene" Formation (Wendt et al., 2006). AF4b is interpreted as a shoreface environment. The presence of swaley cross-bedding produced by the amalgamation of storm beds (Dumas and Arnott, 2006) and other cross-stratified beds is indicative of upper shoreface environments (Loi et al., 2010). The gamma-ray pattern (see J and K Fig. 9) displays concave erratic egg shapes with a very regularly decreasing-upward trend and ranging from offshore shale with mid values (80 to 60 gAPI) to clean sandstone with lower values at the top (40 to 60 gAPI). AF4b is observed in the "Atafaitafa" Formation corresponding to the "Zone de passage" Formation of the Illizi basin (Eschard et al., 2005). AF4c is interpreted as a lower shoreface environment (Dumas and Arnott, 2006; Suter, 2006). The gamma-ray pattern displays the same features as the upper shoreface deposits with higher values (i.e. muddier facies) ranging from 100 to 80 gAPI (see J and K Fig. 9).

### 5.1.4 Offshore marine environments

This depositional environment is composed of AF5a and AF5b facies associations (Table 1). AF5a is mainly defined by wavy to planar-bedded heterolithic silty-shales interlayered with fine-grained sandstones. It also contains bundles of skeletal wackestones and calcareous mudstones. The main sedimentary structures are lenticular sandstones, rare hummocky cross-bedding (HCS), mud mounds, low-angle cross-bedding, tempestite bedding, slumping, and deep groove marks. Sediments can present rare horizontal bioturbation such as *Zoophycos* (Z), *Teichichnus* (Te), and *Planolites* (Pl). AF5b is characterized by an association of black silty shales with occasional bituminous wackestones and packstones. It is composed of graptolites, gonitaties, orthoconic nautiloids, pelagic pelecypods, limestone nodules, tentaculitids, ostracods, and rare fish remains. Rare bioturbation such as *Zoophycos* (Z) is visible.

In AF5a, the occurrence of HCS, the decrease in sand thickness and grain size together with the bioturbation and the floro-faunal associations indicate a deeper marine environment under the influence of storms (Aigner, 1985; Dott and Bourgeois, 1982; Reading and Collinson, 2009). AF5a is interpreted as upper offshore deposits (i.e. offshore transitional). The gamma-ray pattern is serrated and erratic with values well grouped around high values from 120 to 140 gAPI (see L Fig. 9). Positive peaks may indicate siltstone to sandstone ripple beds. AF5b is interpreted as lower offshore deposits (Aigner, 1985; Stow et al., 2001; Stow and Piper, 1984). Here again the gamma-ray signature is serrated and erratic with values well grouped around 140 gAPI (see L Fig. 9). Hot shales with anoxic conditions are characterized by gamma-ray peaks (>140 gAPI). These gamma-ray patterns are typical of offshore environments dominated by shales (Rider, 1996; Serra and Serra, 2003; Wagoner et al., 1990). AF5a and AF5b are observed in the Silurian “Argiles à Graptolites” Formation and the Emsian “Orsine” Formation of the Illizi basin (Beuf et al., 1971; Eschard et al., 2005;

Legrand, 1986, 2003b). The “Argiles de Mehden Yahia” and “Argiles de Temertasset“ shales have the same facies (Wendt et al., 2006).

## 5.2 Sequential framework and unconformities

The high-resolution facies analysis, depositional environments, stacking patterns, and surface geometries observed in the Devonian succession reveal at least two different orders of depositional sequences (large and medium scale, Fig. 8) considered as transgressive/regressive T/R (Catuneanu et al., 2009). The sequential framework proposed in Fig. 8B result from the integration of the vertical evolution the main surfaces (Fig. 8A) and the gamma-ray pattern (Fig. 9). The Devonian series under focus exhibits nine medium-scale sequences (D1 to D9, Fig. 8; Figs. 10, 11, 12 and 13) bounded by 10 major sequence boundaries (HD0 to HD9), and nine major flooding surfaces (MFS1 to MFS9). The correlation of the different sequences at the scale of the different basins and arches is used to build two E–W (Figs. 10, 11 and 12) and one N–S (Fig. 13) cross-sections.

The result of the analysis of the general pattern displayed by the successive sequences reveal two major patterns (Figs. 10, 12 and 13) limited by a major flooding surface MFS5. The first pattern extends from the Oued Samene to Adrar Morrat Formations and is dated from the Lochkovian to Givetian. D1 to D5 medium-scale sequences indicate a general proximal clastic depositional environment (dominated by fluvial to transitional and shoreface facies) with intensive lateral facies evolution. This first pattern is thin (from 500 m in the basin depocenter to 200 m around the basin rim) and with successive amalgamated surfaces on the edge of the arches between the “Zone de passage” and “Oued Samene” Formations (e.g. Figs. 10 and 13). It is delimited at the bottom by the HD0 surface corresponding to the Silurian/Devonian boundary. D1 to D3 are composed of T-R sequences with a first deepening transgressive trend indicative of a transition from continental to marine deposits bounded by a major MFS and evolving into a second shallowing trend from deep marine to shallow marine depositional environments. D1 to D3 thin progressively toward the edge and the continental deposits, in the central part of the basin, pass laterally into a major unconformity. The amalgamation of the surfaces and lateral variations of facies between the Ahnet basin and Azzel Matti and Arak-Foum Belrem arches demonstrate a tectonic control related to the presence of subsiding basins and paleo-highs (i.e. arches).

D4 and D5 display the same T-R pattern with a reduced continental influence and upward decrease in lateral facies variations and thicknesses where the MFS4 marks the beginning of a marine-dominated regime in the entire area. It is identified as the early Eifelian transgression defined by Wendt et al., (2006). The D5 sequence is mainly composed of shoreface carbonates. Evidence of mud mounds preferentially located along faults are well-documented in the area for that time (Wendt et al., 1993, 1997, 2006; Wendt and Kaufmann, 1998). This change in the general pattern indicates reduced tectonic influence.

MFS5, at the transition between the two main patterns, represents a major flooding surface on the platform and is featured worldwide by deposition of "hot shales" during the early Frasnian (Lüning et al., 2003, 2004; Wendt et al., 2006).

The second pattern extends from the "Mehden Yahia", "Temertasset" to "Khenig" Formations dated Frasnian to Lower Tournaisian. This pattern is composed of part of D5 to D9 medium-scale sequences. It corresponds to homogenous offshore depositional environments with no lateral facies variations. However, local deltaic (fluvio-marine) conditions are observed during the Frasnian at the Arak Foum Belrem arch ("Grès de Mehden Yahia" in Fig. 12). A successive alternation of shoreface and offshore deposits is organized into five medium-scale sequences (part of D5, and D6 to D9; Figs. 10, 11 and 12). They in particular show some regressive phases with the deposition of both "Grès de Mehden Yahia" and "Grès du Khnig" sandstones (bounded by HD6 and HD9). This pattern (i.e. part of D5 to D9) corresponds to the general maximum flooding (Lüning et al., 2003, 2004; Wendt et al., 2006) under eustatic control with no tectonic influences.

## 6 Subsidence and tectonic history: An association of low rate extensional subsidence and positive inversion pulses

The backstripping approach (Fig. 14) was applied to five wells (W1, W5, W7, W17, and W21). The morphology of the backstripped curve and subsidence rates can provide clues as to the nature of the sedimentary basin (Xie and Heller, 2006). In intracratonic basins, reconstructed tectonic subsidence curves are almost linear to gently exponential in shape, similar to those of passive margins and rifts (Xie and Heller, 2006). The compilation of tectonic backstripped curves from several wells in peri-Hoggar basins (Fig. 14A, see Fig. 1 for location) and from wells in the study area (Fig. 14B) display low rates of subsidence (from 5 to 50 m/Myr) organized in subsidence patterns of: Inversion of the Low Rate Subsidence (ILRS type c, red line, Fig. 14C), Deceleration of the Low Rate Subsidence (DLRS type b, black line), and Acceleration of the Low Rate Subsidence (ALRS type a, blue line).

Each period of ILRS, DLRS, and ALRS may be synchronous among the different wells studied (see B1 to J, Fig. 14B) and some wells of published data (see D to J Fig. 14A).

The Saharan Platform is marked by a rejuvenation of basement structures, around arches (Figs. 1, 2, and 3), linked to regional geodynamic pulses during Neoproterozoic to Paleozoic times (Fig. 14). A compilation of the literature shows that the main geodynamic events are associated with discriminant association of subsidence patterns:

(A) Late Pan-African compression and collapse (patterns a, b, and c, A Fig. 14A). The Infra-Cambrian (i.e. top Neoproterozoic) is characterized by horst and graben architecture associated with wedge-shaped unit DO0 in the basement (Fig. 7). This structuring probably related to Pan-African post-orogenic collapse is illustrated by intracratonic basins infilled with volcano-sedimentary molasses series (Ahmed and Moussine-Pouchkine, 1987; Coward and Ries, 2003; Fabre et al., 1988; Oudra et al., 2005).

(B) Cambrian-Ordovician geodynamic pulse (Fig. 14). Highlighted by the wedge-shaped units DO1 (Figs. 6A and 7), the horst-graben system is correlated with deceleration (DLRS pattern a, B1) and with local acceleration of the subsidence (ALRS pattern b, B2). The Cambrian–Ordovician extension is documented on arches (Arak-Foum Belrem, Azzel Matti, Amguid El Biod, Tihemboka, Gargaf, Murizidié, Dor El Gussa, etc.) of the Saharan Platform by synsedimentary normal faults, reduced sedimentary successions (Bennacef et al., 1971; Beuf et al., 1968b, 1968a, 1971; Beuf and Montadert, 1962; Borocco and Nyssen, 1959; Claracq et al., 1958; Echikh, 1998; Eschard et al., 2010; Fabre, 1988; Ghienne et al., 2003, 2013; Zazoun and Mahdjoub, 2011) and by stratigraphic hiatuses (Mélou et al., 1999; Oulebsir and Paris, 1995; Paris et al., 2000; Vecoli et al., 1995, 1999).

(C) Late Ordovician geodynamic pulse (i.e. Hirnantian glacial and isostatic rebound; Fig. 14). Late Ordovician incisions mainly situated at the hanging walls of normal faults (Fig. 7C and 7D) are interpreted as Hirnantian glacial-Palaeovalleys (Le Heron, 2010; Smart, 2000) and followed by local inversion of low rate subsidence (ILRS of type c, C in Fig. 14).

(D) Silurian extensional geodynamic pulse (D, Figs 14). The Silurian post-glaciation period is featured by the reactivation and sealing of the inherited horst and graben fault system (i.e. wedge-shaped unit DO2; Figs. 6B, 6C, 7A and 7B). It is linked to an acceleration of the subsidence (ALRS of pattern b in Fig. 14). This tectonic extension is documented in seismic (Najem et al., 2015) and is associated to the Silurian major transgression on the Saharan platform (e.g. Eschard et al., 2005; Lüning et al., 2000).

(E) Late Silurian to -Early Devonian geodynamic pulse (Caledonian compression; E Fig. 14). Late Silurian times are marked by reactivation and local positive inversion of the former structures (Figs. 6C and 7B); by truncations located at fold hinges (Figs 6C and 7); and by a major shift from marine to fluvial/transitional environments (e.g. Figs 10). Backstripped curves register an inversion of the subsidence (ILRS of pattern c, in Fig. 14). The Caledonian event is mentioned as related to large-scale folding or uplifted arches (e.g. the Gargaff, Tihemboka, Ahara, Murizidé-Dor el Gussa and Amguid El Biod arches) and it is associated with breaks in the series and with angular unconformities (Beuf et al., 1971; Biju-Duval et al., 1968; Boote et al., 1998; Boudjema, 1987; Boumendjel et al., 1988; Carruba et al., 2014; Chavand and Claracq, 1960; Coward and Ries, 2003; Dubois and Mazelet, 1964; Echikh, 1998; Eschard et al., 2010; Fekirine and Abdallah, 1998; Follot, 1950; Frizon de Lamotte et al., 2013; Ghienne et al., 2013; Gindre et al., 2012; Legrand, 1967b, 1967a; Magloire, 1967).

(F) Early Devonian tectonic quiescence (F Fig. 14). This is characterized by a deceleration of the low rate subsidence (DLRS of pattern a, F in Fig. 14). During this period, we have detected Emsian truncation from satellite images (Figs. 6D and 6E) and erosion and pinch out of upper Emsian to Eifelian series from well cross sections (Figs. 10, 12 and 13). In previous works, these hiatuses/gaps (i.e. Upper Lochkovian, Lower Pragian, Upper Pragian, Upper Emsian, Lower Eifelian) are observed in the Ahnet basin (Kermandji, 2007; Kermandji et al., 2003, 2008, 2009; Wendt et al., 2006), in the Illizi (Boudjema, 1987) and in the Reggane (Jäger et al., 2009).

(G and H) Middle to late Devonian geodynamic pulse (extension and local inversions, G and H Fig. 14). The Mid to Late Devonian period is characterized by large wedge hiatuses and truncations associated with the reactivation of horst and graben structures and local positive inversion (OD3 in Figs. 6D, 6E, 6F, 7 and 10 to 13). This period is characterized by inversion and acceleration of low rate subsidence (patterns c and b: ILRS - ALRS, Fig. 14). Some of the

Middle to Late Devonian syn-tectonic structures and hiatuses (e.g. Givetian/Frasnian) are noticed in the Ahnet basin (Wendt et al., 2006), on the Amguid Ridge (Wendt et al., 2009b), in the Illizi basin (Boudjema, 1987; Chaumeau et al., 1961; Eschard et al., 2010; Fabre, 2005; Legrand, 1967a), on the Gargaf (Carruba et al., 2014; Collomb, 1962; Fabre, 2005; Massa, 1988) and elsewhere on the platform (Frizon de Lamotte et al., 2013).

(I and J) Pre-Hercynian to Hercynian geodynamic pulses (I and J Fig. 14). This period is organized in Early Carboniferous pre-Hercynian (I, Fig. 14) to Late Carboniferous–Early Permian Hercynian compressions limited by Mid Carboniferous tectonic quiescence/extension (J, Fig. 14). The Carboniferous period is characterized by a normal reactivation and local positive inversion of the previous structural patterns involving reverse faults, overturned folds, transpressional flower structures along strike-slip fault zones (Figs. 6F, 7B, 7C and 7D). The major Carboniferous tectonic event on the Saharan Platform impacted all arches and it is mainly controlled by near-vertical basement faults with a strike-slip component (Boote et al., 1998; Caby, 2003; Carruba et al., 2014; Haddoum et al., 2001, 2013; Liégeois et al., 2003; Wendt et al., 2009a; Zazoun, 2001, 2008). According these authors basement fabric features exerted a very strong control on the structural evolution during the Hercynian deformation. Two major hiatuses (i.e. Mid Tournaisian to Mid Visean–Serpukhovian) are recognized (Wendt et al., 2009a).

The geodynamic pulses attest to the reactivation of the terranes and associated lithospheric fault zones. This observation questions the nature of the Precambrian basement and associated structural heritage.

## 7 Basement characterization: Precambrian structural heritage

Geochronological data show that the different terranes were reworked during several main thermo-orogenic events. The two main events deduced from geochronological data are the

Neoproterozoic (i.e. Pan-African) and Paleoproterozoic (i.e. Eburnean) episodes (Bertrand and Caby, 1978). Aeromagnetic anomaly surveys are commonly used to analyze geological features such as rock types and fault zones (e.g. Turner et al., 2007). A similar study was led in the meantime showing similar interpretations (Bournas et al., 2003; Brahimi et al., 2018). In this study, these data highlight the geometries and the extension of the different terranes under the sedimentary cover. Four main domains can be identified from the aeromagnetic anomaly map, delimited by contrasted magnetic signatures and interpreted as suture zones (thick black lines, Fig. 15A). The study area is bounded to the south by the Tuareg Shield (TS), to the north, by the south Atlasic Range, to the west by the West African Craton (WAC) and at the east by the East Saharan Craton (ESC) or Saharan Metacraton (Abdelsalam et al., 2002).

The magnetic disturbance features (Fig. 15A) show three main magnetic trends. A major NS sinuous fabric and two minor sinuous 130–140°E and N45°E trends. The major NS lineaments coincide with terrane boundaries and mega-shear zones (e.g. 4°50', 4°10', WOSZ, EOSZ, 8°30', RSZ shear zones; Fig. 1). Sigmoidal-shaped terranes 200 to 500 km long and 100 km wide are characterized (red lines in Fig. 15A). The whole assemblage forms a typical SC-shaped shear fabric (Choukroune et al., 1987) associated with vertical mega-shear zones and suture zones (e.g. WOSZ, EOSZ, 4°10', 4°50' or 8°30' Hoggar shear zones in Fig. 1). The SC fabrics combined with subvertical lithospheric shear zones (Fig. 16B and C) are typical features of the Paleoproterozoic accretionary orogens (Cagnard et al., 2011; Chardon et al., 2009). This architecture is concordant with the Neoproterozoic collage of the Tuareg Shield (i.e. mobile belt) between the West African Craton and the East Saharan Craton (i.e. cratonic blocks) described by (Coward and Ries, 2003; Craig et al., 2008).

The gravimetric anomaly map (Fig. 15B) shows a correlation between gravimetric anomalies and tectonic architecture (intracratonic syncline-shaped basin and neighboring arches).

Positive anomalies (> 66 mGal) are mainly associated with arches whereas negative anomalies are related to intracratonic basins (< 66 mGal). Nevertheless, negative anomaly disturbance is found in the Hoggar massif probably due to Cenozoic volcanism and the Hoggar swell (Liégeois et al., 2005) or to Eocene Alpine intraplate lithospheric buckling (Rougier et al., 2013).

The Precambrian structural heritage is characterized by accreted lithospheric terranes limited by vertical strike-slip mega shear zones (Fig. 16B and C). A zonation is observed between the Paleozoic basins and arches configurations and the different terranes (thermo-tectonic age). Arches are linked to Archean to Paleoproterozoic continental terranes in contrast to syncline-shaped basins which are associated with Meso-Neoproterozoic terranes (Figs. 1, 2 and 16A).

# 8 Low subsidence rate intracratonic Paleozoic basins of the Central Sahara provide a basis for an integrated modeling study

Paleozoic intracratonic basins with similar characteristics (architecture, subsidence rate, stratigraphic partitioning, alternating episodes of intraplate extension and short duration compressions with periods of tectonic quiescence, etc.) have been documented in North America (e.g. Allen and Armitage, 2011; Beaumont et al., 1988; Burgess, 2008; Burgess et al., 1997; Eaton and Darbyshire, 2010; Pinet et al., 2013; Potter, 2006; Sloss, 1963; Xie and Heller, 2006), South America (Allen and Armitage, 2011; de Brito Neves et al., 1984; Milani and Zalan, 1999; de Oliveira and Mohriak, 2003; Soares et al., 1978; Zalan et al., 1990), Russia (Allen and Armitage, 2011; Nikishin et al., 1996) and Australia (Harris, 1994; Lindsay and Leven, 1996; Mory et al., 2017). However, the nature of the potential driving processes (lithospheric folding, far-field stresses, local increase in the geotherm, mechanical anisotropy from lithospheric rheological heterogeneity, etc.) associated with the formation of intracratonic Paleozoic basins remains highly speculative (Allen and Armitage, 2011;

Armitage and Allen, 2010; Braun et al., 2014; Burgess and Gurnis, 1995; Burov and Cloetingh, 2009; Cacace and Scheck-Wenderoth, 2016; Célérier et al., 2005; Gac et al., 2013; Heine et al., 2008; Leeder, 1991; Vauchez et al., 1998).

The multiscale and multidisciplinary analysis performed in this study enable us to document a model of Paleozoic intracratonic Central Saharan basins coupling basin architecture and basement structures (Fig. 17). While we do not provide any quantitative explanations for the dynamics of these basins, our synthesis highlights that their subsidence is not the result of a single process and we attempt here to make a check-list of the properties that a generic model of formation of such basins must capture:

(A) The association of syncline-shaped wide basins and neighboring arches (i.e. paleo-highs). The structural framework shows a close association of syncline-shaped basins, inter-basin principal to secondary arches, and intra-basin secondary arches (see Fig. 2).

(B) By local horst and graben architecture linked to steep-dipping planar normal faults and associated with normal fault-related fold structures (i.e. forced folds; a, Fig. 17A). Locally, the extensional structures are disrupted by positive inversion structures (b, Fig. 17A) or transported normal faults (c, Fig. 17A).

(C) A low rate of subsidence ranging between 5 to 50 m/Myr (Fig. 14).

(D) Long periods of extension and tectonic quiescence are interrupted by brief periods of compression or glaciation/deglaciation events (Beuf et al., 1971; Denis et al., 2007; Le Heron et al., 2006). These periods of compression are possibly related to intraplate compression linked to distal orogenies (i.e. Late Silurian Caledonian event, Late Carboniferous Hercynian, (Frizon de Lamotte et al., 2013) or to intraplate arch uplift related to magmatism (Derder et al., 2016; Fabre, 2005; Frizon de Lamotte et al., 2013; Moreau et al., 1994).

(E) Synsedimentary divergent onlaps and local unconformities are identified from integrated seismic data, satellite images, and borehole data (Figs. 5, 6, 7 and 10 to 13). The periods of tectonic activity are characterized by normal to reverse reactivation of border faults, emplacement of wedge-shaped units, and erosional unconformities neighboring the arches.

(F) The stratigraphic architecture displays a lateral facies variation and partitioning between distal marine facies infilling the intracratonic basins (i.e. offshore deposits) and proximal amalgamated facies (i.e. fluvio-marine, shoreface) associated with prominent stratigraphic hiatus and erosional unconformities in the vicinity of the arches.

(G) A close connection is evidenced between the period of tectonic deformation and the presence of erosional unconformities (i.e. 2, 3, 6, 8, 10 geodynamic events in Fig. 17B). By contrast, the periods of tectonic quiescence and extension are characterized by low lateral facies variations, thin deposits, and the absence of erosional surfaces.

(H) The Precambrian heritage corresponds to Archean to Paleoproterozoic terranes identified in the Hoggar massif and reactivated during the Meso-Neoproterozoic Pan-African cycle (Fig. 1). The Precambrian lithospheric heterogeneity illustrated by the different characteristics of Precambrian terranes (wavelength, age, nature, fault zones) spatially control the emplacement of the syncline-shaped intracratonic basins underlain by Meso–Neoproterozoic oceanic terranes and the arches underlain by Archean to Paleoproterozoic continental terranes (Figs. 1, 2 and 16). Many authors suggest control of the basement fabrics is inherited from the Pan-African orogeny in the Saharan basins (Beuf et al., 1968b, 1971; Boote et al., 1998; Carruba et al., 2014; Coward and Ries, 2003; Eschard et al., 2010; Guiraud et al., 2005; Sharata et al., 2015).

# 9 Conclusion

Our integrated approach using both geophysical (seismic, gravity, aeromagnetic, etc.) and geological (well, seismic, satellite images, etc.) data has enabled us to decrypt the characteristics of the intracratonic Paleozoic Saharan basins and the control of the heterogeneous lithospheric heritage of the horst and graben architecture, low rate subsidence, association of long-lived broad synclines and anticlines (i.e. arches swells, domes, highs or ridges) with very different wavelengths (λ) (tens to hundreds of kilometers). A coupled basin architecture and basement structures model is proposed (Fig. 17).

This study highlights a tight control of the heterogeneous lithosphere zonation over the structuring of the intracratonic Central Saharan basin. This particular type of basin is characterized by a low rate of subsidence and fault activation controlling the homogeneity of sedimentary facies and the distribution of the main unconformities. The low rate activation of vertical mega-shear zones bounding the intracratonic basin during Paleozoic times contrasts markedly with classic rift kinematics and architecture. Three different periods of tectonic compressional pulses (i.e. Caledonian, Middle to Late Devonian, Pre-Hercynian), extension and quiescence are identified and controlled the sedimentary distribution (Fig. 17). An understanding of tectono-sedimentary interaction is key to understanding the distribution of the Paleozoic petroleum reservoirs of this first-order oil province.

**Acknowledgements**

We are most grateful to ENGIE/NEPTUNE who provided the database used in this paper and who funded the work. Special thanks to the data management service of ENGIE/NEPTUNE (especially Aurelie Galvani) for their help with the database. Specific appreciations for detailed reviews/comments from Jobst Wendt, Réda Samy Zazoun and Fabio Lottaroli, along with a short comment from Alexander Peace, which have considerably enriched and improved this paper.

## References


Abdelsalam, M. G., Liégeois, J.-P. and Stern, R. J.: The saharan metacraton, J. Afr. Earth Sci., 34(3), 119–136, 2002.

Abdesselam-Rouighi, F.: Etude palynologique du sondage Sebkhet El Melah (unpublished), Entreprise nationale Sonatrach division hydrocarbures direction Laboratiore central des hydrocarbures, Boumerdès., 1977.

Abdesselam-Rouighi, F.: Résultats de l'étude palynologiques des sondage Garet El Guefoul Bassin de l'Ahnet-Mouydir (unpublished), Entreprise nationale Sonatrach division hydrocarbures direction Laboratiore central des hydrocarbures, Boumerdès., 1991.

Ahmed, A. A.-K. and Moussine-Pouchkine, A.: Lithostratigraphie, sédimentologie et évolution de deux bassins molassiques intramontagneux de la chaine Pan-Africaine: la Série pourprée de l'Ahnet, Nord-Ouest du Hoggar, Algérie, J. Afr. Earth Sci. 1983, 6(4), 525–535, 1987.

Aigner, T.: Storm depositional systems: dynamic stratigraphy in modern and ancient shallow-marine sequences, Lect. Notes Earth Sci. Berl. Springer Verl., 3, 1–158, 1985.

Allen, J. R. L.: Studies in fluviatile sedimentation: bars, bar-complexes and sandstone sheets (low-sinuosity braided streams) in the Brownstones (L. Devonian), Welsh Borders, Sediment. Geol., 33(4), 237–293, 1983.

Allen, P. A. and Allen, J. R.: Subsidence and thermal history, in Basin analysis: Principles and applications, pp. 349–401, Wiley-Blackwell, Oxford., 2005.

Allen, P. A. and Armitage, J. J.: Cratonic Basins, in Tectonics of Sedimentary Basins, edited by C. Busby and A. Azor, pp. 602–620, John Wiley & Sons, Ltd., 2011.

Angevine, C. L., Heller, P. L. and Paola, C.: Quantitative sedimentary basin modeling, American Association of Petroleum Geologists., 1990.

Armitage, J. J. and Allen, P. A.: Cratonic basins and the long-term subsidence history of continental interiors, J. Geol. Soc., 167(1), 61–70, doi:10.1144/0016-76492009-108, 2010.

Askri, H., Belmecheri, A., Benrabah, B., Boudjema, A., Boumendjel, K., Daoudi, M., Drid, M., Ghalem, T., Docca, A. M., Ghandriche, H. and others: Geology of Algeria, in Well Evaluation Conference Algeria, pp. 1–93, Schlumberger-Sonatrach., 1995.

Azzoune, N.: Analyse palynologique de trois (03) échantillons de carottes du sondages W7, Sonatrach (unpublished), Entreprise nationale Sonatrach division hydrocarbures direction Laboratiore central des hydrocarbures, Boumerdès., 1999.

Badalini, G., Redfern, J. and Carr, I. D.: A synthesis of current understanding of the structural evolution of North Africa, J. Pet. Geol., 25(3), 249–258, 2002.

Beaumont, C., Quinlan, G. and Hamilton, J.: Orogeny and stratigraphy: Numerical models of the Paleozoic in the eastern interior of North America, Tectonics, 7(3), 389–416, 1988.

Bellahsen, N. and Daniel, J. M.: Fault reactivation control on normal fault growth: an experimental study, J. Struct. Geol., 27(4), 769–780, doi:10.1016/j.jsg.2004.12.003, 2005.

Bennacef, A., Beuf, S., Biju-Duval, B., Charpal, O. de, Gariel, O. and Rognon, P.: Example of Cratonic Sedimentation: Lower Paleozoic of Algerian Sahara, AAPG Bull., 55(12), 2225–2245, 1971.

Bennacef, A., Attar, A., Froukhi, R., Beuf, S., Philippe, G., Schmerber, G. and Vermeire, J. C.: Cartes Géologiques d'Iherir-Dider (NG-32-IX), Iherir (NG-32-X), Illizi (NG-32-XV), Aharhar (NG-32-VIII), Oued Samène (NG-32-XIV), Erg Tihodaine (NG-32-VII), Tin

Alkoum (NG-32-V), Djanet (NG-32-IV), Ta-N-Mellet (NG-32-XIII) , Ta-N-Elak (NG-32-XIX), Fort Tarat (NG-32-XVI), Tilmas El Mra (NG-31-XXIV), Ers Oum El Lil (NG-31-XXII), Amguid (NG-31-XVIII), 1/200000 Sonatrach-Ministère de l'Industrie et des Mines, Algérie, 1974.

Bensalah, A., Beuf, S., Gabriel, O., Philippe, G., Lacot, R., Paris, A., Basseto, D., Conrad, J. and Moussine-Pouchkine, A.: Cartes Géologiques de Khanguet El Hadid (NG-31-XVII), Aïn Tidjoubar (NG-31-XVI), Oued Djaret (NG-31-XV), Aoulef El Arab (NG-31-XIV), Reggane (NG-31-XIII), Ifetessene (NG-31-IX), Arak (NG-31-X et NG-31-IV), Meredoua (NG-31-XIII), Tanezrouft (NG-31-VII et NG-31-I), In Heguis (NG-31-IX), Tin Senasset (NG-31-III), Ouallene (NG-31-II)1/200000 Sonatrach-Ministère de l'Industrie et des Mines, Algérie, 1971.

Berger, J., Ouzegane, K., Bendaoud, A., Liégeois, J.-P., Kiénast, J.-R., Bruguier, O. and Caby, R.: Continental subduction recorded by Neoproterozoic eclogite and garnet amphibolites from Western Hoggar (Tassendjanet terrane, Tuareg Shield, Algeria), Precambrian Res., 247, 139–158, doi:10.1016/j.precamres.2014.04.002, 2014.

Bertrand, J. M. L. and Caby, R.: Geodynamic evolution of the Pan-African orogenic belt: A new interpretation of the Hoggar shield (Algerian Sahara), Geol. Rundsch., 67(2), 357–388, doi:10.1007/BF01802795, 1978.

Beuf, S. and Montadert, L.: Géologie-sur une discordance angulaire entre les unites II et III du Cambro-Ordovicien au sud-est de la plaine de Dider (Tassili des Ajjers), Compte Rendus Hebd. Séances L'Académie Sci., 254(6), 1108, 1962.

Beuf, S., Biju-Duval, B., Mauvier, A. and Legrand, P.: Nouvelles observations sur le 'Cambro-Ordovicien'du Bled El Mass (Sahara central), Publ. Serv. Géologique Algér. Bull., 38, 39–51, 1968a.

Beuf, S., Biju-Duval, B., De Charpal, O., Gariel, O., Bennacef, A., Black, R., Arene, J., Boissonnas, J., Chachau, F., Guérangé, B. and others: Une conséquence directe de la structure du bouclier Africain: L'ébauche des bassins de l'Ahnet et du Mouydir au Paléozoique inférieur, Publ. Serv. Géologique L'Algérie Nouv. Sér. Bull., 38, 105–34, 1968b.

Beuf, S., Biju-Duval, B., De Charpal, O. and Gariel, O.: Homogénéité des directions des paléocourants du Dévonien inférieur au Sahara central, Comptes Rendus L'Académie Sci. Sér. D, 268, 2026–9, 1969.

Beuf, S., Biju-Duval, B., de Charpal, O., Rognon, P., Gabriel, O. and Bennacef, A.: Les grès du Paléozoïque inférieur au Sahara: Sédimentation et discontinuités évolution structurale d'un craton, Technip., Paris., 1971.

Biju-Duval, B., de Charpal, O., Beuf, S. and Bennacef, A.: Lithostratigraphie du Dévonien inférieur dans l'Ahnet et le Mouydir (Sahara Central), Bull Serv Géologique Algèrie, (38), 83–104, 1968.

Black, R., Latouche, L., Liégeois, J. P., Caby, R. and Bertrand, J. M.: Pan-African displaced terranes in the Tuareg shield (central Sahara), Geology, 22(7), 641–644, 1994.

Bonini, M., Sani, F. and Antonielli, B.: Basin inversion and contractional reactivation of inherited normal faults: A review based on previous and new experimental models, Tectonophysics, 522–523, 55–88, doi:10.1016/j.tecto.2011.11.014, 2012.

Boote, D. R. D., Clark-Lowes, D. D. and Traut, M. W.: Palaeozoic petroleum systems of North Africa, Geol. Soc. Lond. Spec. Publ., 132(1), 7–68, doi:10.1144/GSL.SP.1998.132.01.02, 1998.

Borocco, J. and Nyssen, R.: Nouvelles observations sur les “gres inferieurs” cambro-ordoviciens du Tassili interne (Nord-Hoggar), Bull. Société Géologique Fr., S7-I(2), 197–206, doi:10.2113/gssgfbull.S7-I.2.197, 1959.

Boudjema, A.: Evolution structurale du bassin pétrolier" triasique" du Sahara nord oriental (Algérie), Doctoral dissertation, Paris 11, France., 1987.

Boumendjel, K.: Les chitinozoaires du silurien superieur et du devonien du sahara algerien (cadre geologique, systematique, biostratigraphie), Doctoral dissertation, Rennes 1, France., 1987.

Boumendjel, K., Loboziak, S., Paris, F., Steemans, P. and Streel, M.: Biostratigraphie des Miospores et des Chitinozoaires du Silurien supérieur et du Dévonien dans le bassin d’Illizi (S.E. du Sahara algérien), Geobios, 21(3), 329–357, doi:10.1016/S0016-6995(88)80057-3, 1988.

Bournas, N., Galdeano, A., Hamoudi, M. and Baker, H.: Interpretation of the aeromagnetic map of Eastern Hoggar (Algeria) using the Euler deconvolution, analytic signal and local wavenumber methods, J. Afr. Earth Sci., 37(3–4), 191–205, doi:10.1016/j.jafrearsci.2002.12.001, 2003.

Brahimi, S., Liégeois, J.-P., Ghienne, J.-F., Munschy, M. and Bourmatte, A.: The Tuareg shield terranes revisited and extended towards the northern Gondwana margin: Magnetic and gravimetric constraints, Earth-Sci. Rev., 185, 572–599, doi:10.1016/j.earscirev.2018.07.002, 2018.

Braun, J., Simon-Labric, T., Murray, K. E. and Reiners, P. W.: Topographic relief driven by variations in surface rock density, Nat. Geosci., 7(7), 534–540, doi:10.1038/ngeo2171, 2014.

de Brito Neves, B. B., Fuck, R. A., Cordani, U. G. and Thomaz F°, A.: Influence of basement structures on the evolution of the major sedimentary basins of Brazil: A case of tectonic heritage, J. Geodyn., 1(3), 495–510, doi:10.1016/0264-3707(84)90021-8, 1984.

Buchanan, P. G. and McClay, K. R.: Sandbox experiments of inverted listric and planar fault systems, Tectonophysics, 188(1), 97–115, doi:10.1016/0040-1951(91)90317-L, 1991.

Burgess, P. M.: Phanerozoic evolution of the sedimentary cover of the North American craton, in Sedimentary Basins of the World, vol. 5, pp. 31–63, Elsevier., 2008.

Burgess, P. M. and Gurnis, M.: Mechanisms for the formation of cratonic stratigraphic sequences, Earth Planet. Sci. Lett., 136(3), 647–663, doi:10.1016/0012-821X(95)00204-P, 1995.

Burgess, P. M., Gurnis, M. and Moresi, L.: Formation of sequences in the cratonic interior of North America by interaction between mantle, eustatic, and stratigraphic processes, Geol. Soc. Am. Bull., 109(12), 1515–1535, 1997.

Burke, K., MacGregor, D. S. and Cameron, N. R.: Africa's petroleum systems: four tectonic 'Aces' in the past 600 million years, Geol. Soc. Lond. Spec. Publ., 207(1), 21–60, 2003.

Burov, E. and Cloetingh, S.: Controls of mantle plumes and lithospheric folding on modes of intraplate continental tectonics: differences and similarities, Geophys. J. Int., 178(3), 1691–1722, doi:10.1111/j.1365-246X.2009.04238.x, 2009.

Butler, R. W. H.: The influence of pre-existing basin structure on thrust system evolution in the Western Alps, Geol. Soc. Lond. Spec. Publ., 44(1), 105–122, doi:10.1144/GSL.SP.1989.044.01.07, 1989.

Caby, R.: Terrane assembly and geodynamic evolution of central–western Hoggar: a synthesis, J. Afr. Earth Sci., 37(3–4), 133–159, doi:10.1016/j.jafrearsci.2003.05.003, 2003.

Cacace, M. and Scheck-Wenderoth, M.: Why intracontinental basins subside longer: 3-D feedback effects of lithospheric cooling and sedimentation on the flexural strength of the lithosphere: Subsidence at Intracontinental Basins, J. Geophys. Res. Solid Earth, 121(5), 3742–3761, doi:10.1002/2015JB012682, 2016.

Cagnard, F., Barbey, P. and Gapais, D.: Transition between “Archaean-type” and “modern-type” tectonics: Insights from the Finnish Lapland Granulite Belt, Precambrian Res., 187(1–2), 127–142, doi:10.1016/j.precamres.2011.02.007, 2011.

Carr, I. D.: Second-Order Sequence Stratigraphy of the Palaeozoic of North Africa, J. Pet. Geol., 25(3), 259–280, doi:10.1111/j.1747-5457.2002.tb00009.x, 2002.

Carruba, S., Perotti, C., Rinaldi, M., Bresciani, I. and Bertozzi, G.: Intraplate deformation of the Al Qarqaf Arch and the southern sector of the Ghadames Basin (SW Libya), J. Afr. Earth Sci., 97, 19–39, doi:10.1016/j.jafrearsci.2014.05.001, 2014.

Catuneanu, O., Abreu, V., Bhattacharya, J. P., Blum, M. D., Dalrymple, R. W., Eriksson, P. G., Fielding, C. R., Fisher, W. L., Galloway, W. E., Gibling, M. R., Giles, K. A., Holbrook, J. M., Jordan, R., Kendall, C. G. S. C., Macurda, B., Martinsen, O. J., Miall, A. D., Neal, J. E., Nummedal, D., Pomar, L., Posamentier, H. W., Pratt, B. R., Sarg, J. F., Shanley, K. W., Steel, R. J., Strasser, A., Tucker, M. E. and Winker, C.: Towards the standardization of sequence stratigraphy, Earth-Sci. Rev., 92(1–2), 1–33, doi:10.1016/j.earscirev.2008.10.003, 2009.

Célérier, J., Sandiford, M., Hansen, D. L. and Quigley, M.: Modes of active intraplate deformation, Flinders Ranges, Australia, Tectonics, 24(6), 1–17, doi:10.1029/2004TC001679, 2005.

Chardon, D., Gapais, D. and Cagnard, F.: Flow of ultra-hot orogens: A view from the Precambrian, clues for the Phanerozoic, Tectonophysics, 477(3–4), 105–118, doi:10.1016/j.tecto.2009.03.008, 2009.

Chaumeau, J., Legrand, P. and Renaud, A.: Contribution a l'etude du Couvinien dans le bassin de Fort-de-Polignac (Sahara), Bull. Société Géologique Fr., S7-III(5), 449–456, doi:10.2113/gssgfbull.S7-III.5.449, 1961.

Chavand, J. C. and Claracq, P.: La disparition du Tassili externe à l'E de Fort-Polignac (Sahara central), CR Soc Géol Fr, 1959, 172–174, 1960.

Choukroune, P., Gapais, D. and Merle, O.: Shear criteria and structural symmetry, J. Struct. Geol., 9(5–6), 525–530, doi:10.1016/0191-8141(87)90137-4, 1987.

Claracq, P., Fabre, C., Freulon, J. M. and Nougarède, F.: Une discordance angulaire dans les ‘‘Grès inférieurs” de l'Adrar Tan Elak (Sahara central), C. r. Somm. Séances Soc. Géologique Fr., 309–310, 1958.

Collomb, G. R.: Étudé géologique du Jebel Fezzan et de sa bordure paléozoique, Compagnie française des pétroles., 1962.

Conrad, J.: Les grandes lignes stratigraphiques et sédimentologiques du Carbonifere de l'Ahnet-Mouydir (Sahara central algérien), Rev. Inst. Fr. Pétrole, 28, 3–18, 1973.

Conrad, J.: Les séries carbonifères du Sahara central algérien: stratigraphie, sédimentation, évolution structurale, Doctoral dissertation, Université Aix-Marseille III, France., 1984.

Coward, M. P. and Ries, A. C.: Tectonic development of North African basins, Geol. Soc. Lond. Spec. Publ., 207(1), 61–83, doi:10.1144/GSL.SP.2003.207.4, 2003.

Cózar, P., Somerville, I. D., Vachard, D., Coronado, I., García-Frank, A., Medina-Varea, P., Said, I., Del Moral, B. and Rodríguez, S.: Upper Mississippian to lower Pennsylvanian biostratigraphic correlation of the Sahara Platform successions on the northern margin of Gondwana (Morocco, Algeria, Libya), Gondwana Res., 36, 459–472, doi:10.1016/j.gr.2015.07.019, 2016.

Craig, J., Rizzi, C., Said, F., Thusu, B., Luning, S., Asbali, A. I., Keeley, M. L., Bell, J. F., Durham, M. J. and Eales, M. H.: Structural styles and prospectivity in the Precambrian and Palaeozoic hydrocarbon systems of North Africa, Geol. East Libya, 4, 51–122, 2008.

Dalrymple, R. W. and Choi, K.: Morphologic and facies trends through the fluvial–marine transition in tide-dominated depositional systems: A schematic framework for environmental and sequence-stratigraphic interpretation, Earth-Sci. Rev., 81(3–4), 135–174, doi:10.1016/j.earscirev.2006.10.002, 2007.

Dalrymple, R. W., Zaitlin, B. A. and Boyd, R.: A conceptual model of estuarine sedimentation, J. Sediment. Petrol., 62(1130–1146), 116, 1992.

Dalrymple, R. W., Mackay, D. A., Ichaso, A. A. and Choi, K. S.: Processes, Morphodynamics, and Facies of Tide-Dominated Estuaries, in Principles of Tidal Sedimentology, pp. 79–107, Springer, Dordrecht., 2012.

Denis, M., Buoncristiani, J.-F., Konaté, M., Ghienne, J.-F. and Guiraud, M.: Hirnantian glacial and deglacial record in SW Djado Basin (NE Niger)., Geodin. Acta, 20(3), 177–195, doi:10.3166/ga.20.177-195, 2007.

Derder, M. E. M., Maouche, S., Liégeois, J. P., Henry, B., Amenna, M., Ouabadi, A., Bellon, H., Bruguier, O., Bayou, B., Bestandji, R., Nouar, O., Bouabdallah, H., Ayache, M. and Beddiaf, M.: Discovery of a Devonian mafic magmatism on the western border of the Murzuq basin (Saharan metacraton): Paleomagnetic dating and geodynamical implications, J. Afr. Earth Sci., 115, 159–176, doi:10.1016/j.jafrearsci.2015.11.019, 2016.

Djouder, H., Lüning, S., Da Silva, A.-C., Abdallah, H. and Boulvain, F.: Silurian deltaic progradation, Tassili n'Ajjer plateau, south-eastern Algeria: Sedimentology, ichnology and sequence stratigraphy, J. Afr. Earth Sci., 142, 170–192, 2018.

Dokka, A. M.: Sedimentological core description WELL: W7, Block - 340, (District - 3) (unpublished), Core description, Sonatrach division exploration direction des operations département assistance aux opérations service géologique, Algérie., 1999.

Dott, R. H. and Bourgeois, J.: Hummocky stratification: Significance of its variable bedding sequences, Geol. Soc. Am. Bull., 93(8), 663, doi:10.1130/0016-7606(1982)93<663:HSSOIV>2.0.CO;2, 1982.

Dubois, P.: Stratigraphie du Cambro-Ordovicien du Tassili n'Ajjer (Sahara central), Bull. Société Géologique Fr., S7-III(2), 206–209, doi:10.2113/gssgfbull.S7-III.2.206, 1961.

Dubois, P. and Mazelet, P.: Stratigraphie du Silurien du Tassili N'Ajjer, Bull. Société Géologique Fr., S7-VI(4), 586–591, doi:10.2113/gssgfbull.S7-VI.4.586, 1964.

Dubois, P., Beuf, S. and Biju-Duval, B.: Lithostratigraphie du Dévonien inférieur gréseux du Tassili n 'Ajjer, in Symposium on the Lower Devonian and its limits: Bur. Recherche Geol. et Minieres Mem, pp. 227–235., 1967.

Dumas, S. and Arnott, R. W. C.: Origin of hummocky and swaley cross-stratification—the controlling influence of unidirectional current strength and aggradation rate, Geology, 34(12), 1073–1076, 2006.

Eaton, D. W. and Darbyshire, F.: Lithospheric architecture and tectonic evolution of the Hudson Bay region, Tectonophysics, 480(1–4), 1–22, doi:10.1016/j.tecto.2009.09.006, 2010.

Echikh, K.: Geology and hydrocarbon occurrences in the Ghadames basin, Algeria, Tunisia, Libya, Geol. Soc. Lond. Spec. Publ., 132(1), 109–129, 1998.

Eschard, R., Desaubliaux, G., Deschamps, R., Montadert, L., Ravenne, C., Bekkouche, D., Abdallah, H., Belhaouas, S., Benkouider, M., Braïk, F., Henniche, M., Maache, N. and Mouaici, R.: Illizi-Berkine Devonian Reservoir Consortium (unpublished), Institut Française du Pétrole - Sontrach, unpublished, Algérie., 1999.

Eschard, R., Abdallah, H., Braik, F. and Desaubliaux, G.: The Lower Paleozoic succession in the Tassili outcrops, Algeria: sedimentology and sequence stratigraphy, First Break, 23(10), 2005.

Eschard, R., Braik, F., Bekkouche, D., Rahuma, M. B., Desaubliaux, G., Deschamps, R. and Proust, J. N.: Palaeohighs: their influence on the North African Palaeozoic petroleum systems, Pet. Geol. Mature Basins New Front. 7th Pet. Geol. Conf., 707–724, 2010.

Fabre, J.: Les séries paléozoïques d'Afrique: une approche, J. Afr. Earth Sci. Middle East, 7(1), 1–40, doi:10.1016/0899-5362(88)90051-6, 1988.

Fabre, J.: Géologie du Sahara occidental et central, Musée royal de l'Afrique centrale., 2005.

Fabre, J., Kaci, A. A., Bouima, T. and Moussine-Pouchkine, A.: Le cycle molassique dans le Rameau trans-saharien de la chaîne panafricaine, J. Afr. Earth Sci., 7, 41–55, doi:10.1016/0899-5362(88)90052-8, 1988.

Fekirine, B. and Abdallah, H.: Palaeozoic lithofacies correlatives and sequence stratigraphy of the Saharan Platform, Algeria, Geol. Soc. Lond. Spec. Publ., 132(1), 97–108, doi:10.1144/GSL.SP.1998.132.01.05, 1998.

Fezaa, N., Liégeois, J.-P., Abdallah, N., Cherfouh, E. H., De Waele, B., Bruguier, O. and Ouabadi, A.: Late Ediacaran geological evolution (575–555Ma) of the Djanet Terrane, Eastern Hoggar, Algeria, evidence for a Murzukian intracontinental episode, Precambrian Res., 180(3–4), 299–327, doi:10.1016/j.precamres.2010.05.011, 2010.

Follot, J.: Sur l'existence de mouvements calédoniens au Mouydir (Sahara Central), Compte Rendus Hebd. Séances L'Académie Sci., 230(25), 2217–2218, 1950.

Frey, R. W., Pemberton, S. G. and Saunders, T. D.: Ichnofacies and bathymetry: a passive relationship, J. Paleontol., 64(1), 155–158, 1990.

Frizon de Lamotte, D., Tavakoli-Shirazi, S., Leturmy, P., Averbuch, O., Mouchot, N., Raulin, C., Leparmentier, F., Blanpied, C. and Ringenbach, J.-C.: Evidence for Late Devonian vertical movements and extensional deformation in northern Africa and Arabia: Integration in the geodynamics of the Devonian world: Devonian evolution Nothern Gondwana, Tectonics, 32(2), 107–122, doi:10.1002/tect.20007, 2013.

Fröhlich, S., Petitpierre, L., Redfern, J., Grech, P., Bodin, S. and Lang, S.: Sedimentological and sequence stratigraphic analysis of Carboniferous deposits in western Libya: Recording the sedimentary response of the northern Gondwana margin to climate and sea-level changes, J. Afr. Earth Sci., 57(4), 279–296, doi:10.1016/j.jafrearsci.2009.09.007, 2010.

Gac, S., Huismans, R. S., Simon, N. S. C., Podladchikov, Y. Y. and Faleide, J. I.: Formation of intracratonic basins by lithospheric shortening and phase changes: a case study from the ultra-deep East Barents Sea basin, Terra Nova, 25(6), 459–464, doi:10.1111/ter.12057, 2013.

Galeazzi, S., Point, O., Haddadi, N., Mather, J. and Druesne, D.: Regional geology and petroleum systems of the Illizi–Berkine area of the Algerian Saharan Platform: An overview, Mar. Pet. Geol., 27(1), 143–178, doi:10.1016/j.marpetgeo.2008.10.002, 2010.

Galloway, W. E.: Genetic Stratigraphic Sequences in Basin Analysis I: Architecture and Genesis of Flooding-Surface Bounded Depositional Units, AAPG Bull., 73(2), 125–142, 1989.

Galushkin, Y. I. and Eloghbi, S.: Thermal history of the Murzuq Basin, Libya, and generation of hydrocarbons in its source rocks, Geochem. Int., 52(6), 486–499, doi:10.1134/S0016702914060032, 2014.

Gariel, O., de Charpal, O. and Bennacef, A.: Sur la sedimentation des gres du Cambro-Ordovicien (Unite II) dans l'Ahnet et le Mouydir (Sahara central): Algerie, Serv. Geol, Bull N Ser, (38), 7–37, 1968.

Ghienne, J.-F., Deynoux, M., Manatschal, G. and Rubino, J.-L.: Palaeovalleys and fault-controlled depocentres in the Late-Ordovician glacial record of the Murzuq Basin (central Libya), Comptes Rendus Geosci., 335(15), 1091–1100, doi:10.1016/j.crte.2003.09.010, 2003.

Ghienne, J.-F., Moreau, J., Degermann, L. and Rubino, J.-L.: Lower Palaeozoic unconformities in an intracratonic platform setting: glacial erosion versus tectonics in the eastern Murzuq Basin (southern Libya), Int. J. Earth Sci., 102(2), 455–482, doi:10.1007/s00531-012-0815-y, 2013.

Gindre, L., Le Heron, D. and Bjørnseth, H. M.: High resolution facies analysis and sequence stratigraphy of the Siluro-Devonian succession of Al Kufrah basin (SE Libya), J. Afr. Earth Sci., 76, 8–26, doi:10.1016/j.jafrearsci.2012.08.002, 2012.

Girard, F., Ghienne, J.-F. and Rubino, J.-L.: Channelized sandstone bodies (‘cordons’) in the Tassili N’Ajjer (Algeria & Libya): snapshots of a Late Ordovician proglacial outwash plain, Geol. Soc. Lond. Spec. Publ., 368(1), 355–379, doi:10.1144/SP368.3, 2012.

Grasemann, B., Martel, S. and Passchier, C.: Reverse and normal drag along a fault, J. Struct. Geol., 27(6), 999–1010, doi:10.1016/j.jsg.2005.04.006, 2005.

Greigertt, J. and Pougnet, R.: Carte Géologique du Niger, 1/2000000, BRGM, Répulbique du Niger, 1965.

Guiraud, R., Bosworth, W., Thierry, J. and Delplanque, A.: Phanerozoic geological evolution of Northern and Central Africa: An overview, J. Afr. Earth Sci., 43(1–3), 83–143, doi:10.1016/j.jafrearsci.2005.07.017, 2005.

Haddoum, H., Guiraud, R. and Moussine-Pouchkine, A.: Hercynian compressional deformations of the Ahnet–Mouydir Basin, Algerian Saharan Platform: far-field stress effects of the Late Palaeozoic orogeny, Terra Nova, 13(3), 220–226, 2001.

Haddoum, H., Mokri, M., Ouzegane, K., Ait-Djaffer, S. and Djemai, S.: Extrusion de l’In Ouzzal vers le Nord (Hoggar occidental, Algérie): une conséquence d’un poinçonnement panafricain, J. Hydrocarb. Mines Environ. Res. Vol., 4(1), 6–16, 2013.

Haq, B. U. and Schutter, S. R.: A Chronology of Paleozoic Sea-Level Changes, Science, 322(5898), 64–68, doi:10.1126/science.1161648, 2008.

Harris, L. B.: Structural and tectonic synthesis for the Perth basin, Western Australia, J. Pet. Geol., 17(2), 129–156, 1994.

Hartley, R. W. and Allen, P. A.: Interior cratonic basins of Africa: relation to continental break-up and role of mantle convection, Basin Res., 6(2–3), 95–113, 1994.

Hassan, A.: Etude palynologique Paléozoïque du sondage Razzal-Allah-Nord (unpublished), Entreprise nationale Sonatrach division hydrocarbures direction Laboratiore central des hydrocarbures, Boumerdès., 1984.

Heine, C., Dietmar Müller, R., Steinberger, B. and Torsvik, T. H.: Subsidence in intracontinental basins due to dynamic topography, Phys. Earth Planet. Inter., 171(1–4), 252–264, doi:10.1016/j.pepi.2008.05.008, 2008.

Henniche, M.: Architecture et modèle de dépôts d'une série sédimentaire paléozoïque en contexte cratonique, Rennes 1, France., 2002.

Holbrook, J. and Schumm, S. A.: Geomorphic and sedimentary response of rivers to tectonic deformation: a brief review and critique of a tool for recognizing subtle epeirogenic deformation in modern and ancient settings, Tectonophysics, 305(1), 287–306, 1999.

Hollard, H., Choubert, G., Bronner, G., Marchand, J. and Sougy, J.: Carte géologique du Maroc, scale 1: 1,000,000, Serv Carte Géol Maroc, 260(2), 1985.

Holt, P. J., Allen, M. B., van Hunen, J. and Bjørnseth, H. M.: Lithospheric cooling and thickening as a basin forming mechanism, Tectonophysics, 495(3–4), 184–194, doi:10.1016/j.tecto.2010.09.014, 2010.

Jacquemont, P., Jutard, G., Plauchut, B., Grégoire, J. and Mouflard, R.: Etude du bassin du Djado, Bur. Rech. Pétroles Rapp., 1215, 1959.

Jäger, H., Lewandowski, E. and Lampart, V.: Palynology of the upper Silurian to middle Devonian in the Reggane Basin, southern Algeria, Ext. Abstr. DGMK-Tagungsbericht 2009-1 DGMKÖGEW Spring Meet. Celle, 47–51, 2009.

Jardiné, S. and Yapaudjian, L.: Lithostratigraphie et palynologie du Dévonien-Gothlandien gréseux du Bassin de Polignac (Sahara), Rev. L'Institut Fr. Pétrole, 23(4), 439–469, 1968.

Joulia, F.: Carte géologique de reconnaissance de la bordure sédimentaire occidentale de l'Aïr au 1/500 000, Éditions BRGM Orléans Fr., 1963.

Kermandji, A. M.: Silurian–Devonian miospores from the western and central Algeria, Rev. Micropaléontologie, 50(1), 109–128, doi:10.1016/j.revmic.2007.01.003, 2007.

Kermandji, A. M. H., Kowalski, M. W. and Pharisat, A.: Palynologie et séquences de l'Emsien de la région d'In Salah, Sahara central Algérien, Bull. Société D'Histoire Nat. Pays Montbél., 301–306, 2003.

Kermandji, A. M. H., Kowalski, W. M. and Touhami, F. K.: Miospore stratigraphy of Lower and early Middle Devonian deposits from Tidikelt, Central Sahara, Algeria, Geobios, 41(2), 227–251, doi:10.1016/j.geobios.2007.05.002, 2008.

Kermandji, A. M. H., Touhami, F. K., Kowalski, W. M., Abbés, S. B., Boularak, M., Chabour, N., Laifa, E. L. and Hannachi, H. B.: Stratigraphie du Dévonien Inférieur du Plateau du Tidikelt d'In Salah (Sahara Central Algérie), Comun. Geológicas, (t. 96), 67–82, 2009.

Khalil, S. M. and McClay, K. R.: Extensional fault-related folding, northwestern Red Sea, Egypt, J. Struct. Geol., 24(4), 743–762, 2002.

Khiar, S.: Résultats palynologiques du sondage Garet El Guefoul (unpublished), Entreprise nationale Sonatrach division hydrocarbures direction Laboratiore central des hydrocarbures, Alger., 1974.

Kracha, N.: Relation entre sédimentologie, fracturation naturelle et diagénèse d'un réservoir à faible perméabilité application aux réservoirs de l'Ordovicien bassin de l'Ahnet, Sahara central, Algèrie, Doctoral dissertation, Université des sciences et technologies de Lille, France., 2011.

Le Heron, D. P.: Interpretation of Late Ordovician glaciogenic reservoirs from 3-D seismic data: an example from the Murzuq Basin, Libya, Geol. Mag., 147(01), 28, doi:10.1017/S0016756809990586, 2010.

Le Heron, D. P., Craig, J., Sutcliffe, O. E. and Whittington, R.: Late Ordovician glaciogenic reservoir heterogeneity: An example from the Murzuq Basin, Libya, Mar. Pet. Geol., 23(6), 655–677, doi:10.1016/j.marpetgeo.2006.05.006, 2006.

Le Heron, D. P., Craig, J. and Etienne, J. L.: Ancient glaciations and hydrocarbon accumulations in North Africa and the Middle East, Earth-Sci. Rev., 93(3–4), 47–76, doi:10.1016/j.earscirev.2009.02.001, 2009.

Leeder, M. R.: Denudation, vertical crustal movements and sedimentary basin infill, Geol. Rundsch., 80(2), 441–458, doi:10.1007/BF01829376, 1991.

Legrand, P.: Le Devonien du Sahara Algerien, Can. Soc. Pet. Geol., 1, 245–284, 1967a.

Legrand, P.: Nouvelles connaissances acquises sur la limite des systèmes Silurien et Dévonien au Sahara algérien, Bull. Bur. Rech. Géologiques Minières, 33, 119–37, 1967b.

Legrand, P.: The lower Silurian graptolites of Oued In Djerane: a study of populations at the Ordovician-Silurian boundary, Geol. Soc. Lond. Spec. Publ., 20(1), 145–153, doi:10.1144/GSL.SP.1986.020.01.15, 1986.

Legrand, P.: Late Ordovician-early Silurian paleogeography of the Algerian Sahara, Bull. Société Géologique Fr., 174(1), 19–32, 2003a.

Legrand, P.: Silurian stratigraphy and paleogeography of the northern African margin of Gondwana, in Silurian Lands and Seas: Paleogeography Outside of Laurentia, edited by E. Landing and M. E. Johson, pp. 59–104, New York., 2003b.

Legrand-Blain, M.: Dynamique des Brachiopodes carbonifères sur la plate-forme carbonatée du Sahara algérien: paléoenvironnements, paléobiogéographie, évolution, Doctoral dissertation, Université de Bordeaux 1, France., 1985.

Lessa, G. and Masselink, G.: Morphodynamic evolution of a macrotidal barrier estuary, Mar. Geol., 129(1–2), 25–46, 1995.

Leuven, J. R. F. W., Kleinhans, M. G., Weisscher, S. A. H. and van der Vegt, M.: Tidal sand bar dimensions and shapes in estuaries, Earth-Sci. Rev., 161, 204–223, doi:10.1016/j.earscirev.2016.08.004, 2016.

Lewis, M. M., Jackson, C. A.-L., Gawthorpe, R. L. and Whipp, P. S.: Early synrift reservoir development on the flanks of extensional forced folds: A seismic-scale outcrop analog from the Hadahid fault system, Suez rift, Egypt, AAPG Bull., 99(06), 985–1012, doi:10.1306/12011414036, 2015.

Liégeois, J. P., Latouche, L., Boughrara, M., Navez, J. and Guiraud, M.: The LATEA metacraton (Central Hoggar, Tuareg shield, Algeria): behaviour of an old passive margin during the Pan-African orogeny, J. Afr. Earth Sci., 37(3–4), 161–190, doi:10.1016/j.jafrearsci.2003.05.004, 2003.

Liégeois, J.-P., Black, R., Navez, J. and Latouche, L.: Early and late Pan-African orogenies in the Air assembly of terranes (Tuareg Shield, Niger), Precambrian Res., 67(1), 59–88, 1994.

Liégeois, J.-P., Benhallou, A., Azzouni-Sekkal, A., Yahiaoui, R. and Bonin, B.: The Hoggar swell and volcanism: Reactivation of the Precambrian Tuareg shield during Alpine convergence and West African Cenozoic volcanism, Geol. Soc. Am. Spec. Pap., 388, 379–400, doi:10.1130/0-8137-2388-4.379, 2005.

Liégeois, J.-P., Abdelsalam, M. G., Ennih, N. and Ouabadi, A.: Metacraton: Nature, genesis and behavior, Gondwana Res., 23(1), 220–237, doi:10.1016/j.gr.2012.02.016, 2013.

Lindsay, J. F. and Leven, J. H.: Evolution of a Neoproterozoic to Palaeozoic intracratonic setting, Officer Basin, South Australia, Basin Res., 8(4), 403–424, doi:10.1046/j.1365-2117.1996.00223.x, 1996.

Logan, P. and Duddy, I.: An investigation of the thermal history of the Ahnet and Reggane Basins, Central Algeria, and the consequences for hydrocarbon generation and accumulation, Geol. Soc. Lond. Spec. Publ., 132(1), 131–155, 1998.

Loi, A., Ghienne, J.-F., Dabard, M. P., Paris, F., Botquelen, A., Christ, N., Elaouad-Debbaj, Z., Gorini, A., Vidal, M., Videt, B. and Destombes, J.: The Late Ordovician glacio-eustatic record from a high-latitude storm-dominated shelf succession: The Bou Ingarf section (Anti-Atlas, Southern Morocco), Palaeogeogr. Palaeoclimatol. Palaeoecol., 296(3–4), 332–358, doi:10.1016/j.palaeo.2010.01.018, 2010.

Lubeseder, S.: Silurian and Devonian sequence stratigraphy of North Africa; Regional correlation and sedimentology (Marocco, Algeria, Libya), Doctoral dissertation, University of Manchester, UK., 2005.

Lubeseder, S., Redfern, J., Petitpierre, L. and Fröhlich, S.: Stratigraphic trapping potential in the Carboniferous of North Africa: developing new play concepts based on integrated outcrop sedimentology and regional sequence stratigraphy (Morocco, Algeria, Libya), in Geological

Society, London, Petroleum Geology Conference series, vol. 7, pp. 725–734, Geological Society of London., 2010.

Lüning, S.: North African Phanerozoic, in Phanerozoic in the Northern african basins, Encyclopedia of Geology, pp. 152–172, Elsevier., 2005.

Lüning, S., Craig, J., Loydell, D. K., Štorch, P. and Fitches, B.: Lower Silurian `hot shales' in North Africa and Arabia: regional distribution and depositional model, Earth-Sci. Rev., 49(1–4), 121–200, doi:10.1016/S0012-8252(99)00060-4, 2000.

Lüning, S., Adamson, K. and Craig, J.: Frasnian organic-rich shales in North Africa: regional distribution and depositional model, Geol. Soc. Lond. Spec. Publ., 207(1), 165–184, doi:10.1144/GSL.SP.2003.207.9, 2003.

Lüning, S., Wendt, J., Belka, Z. and Kaufmann, B.: Temporal–spatial reconstruction of the early Frasnian (Late Devonian) anoxia in NW Africa: new field data from the Ahnet Basin (Algeria), Sediment. Geol., 163(3–4), 237–264, doi:10.1016/S0037-0738(03)00210-0, 2004.

Madritsch, H., Schmid, S. M. and Fabbri, O.: Interactions between thin-and thick-skinned tectonics at the northwestern front of the Jura fold-and-thrust belt (eastern France), Tectonics, 27(5), 1–31, doi:10.1029/2008TC002282, 2008.

Magloire, L.: Étude stratigraphique, par la Palynologie, des dépôts argilo-gréseux du Silurien et du Dévonien inférieur dans la Région du Grand Erg Occidental (Sahara Algérien), Can. Soc. Pet. Geol., 2, 473–491, 1967.

Makhous, M. and Galushkin, Y. I.: Burial history and thermal evolution of the northern and eastern Saharan basins, AAPG Bull., 87(10), 1623–1651, doi:10.1306/04300301122, 2003a.

Makhous, M. and Galushkin, Y. I.: Burial history and thermal evolution of the southern and western Saharan basins: Synthesis and comparison with the eastern and northern Saharan basins, AAPG Bull., 87(11), 1799–1822, 2003b.

Marchal, D., Guiraud, M., Rives, T. and van den Driessche, J.: Space and time propagation processes of normal faults, Geol. Soc. Lond. Spec. Publ., 147(1), 51–70, doi:10.1144/GSL.SP.1998.147.01.04, 1998.

Marchal, D., Guiraud, M. and Rives, T.: Geometric and morphologic evolution of normal fault planes and traces from 2D to 4D data, J. Struct. Geol., 25(1), 135–158, doi:10.1016/S0191-8141(02)00011-1, 2003.

Massa, D.: Paléozoïque de Libye occidentale : stratigraphie et paléogéographie, Doctoral dissertation, Université de Nice, France., 1988.

Mélou, M., Oulebsir, L. and Paris, F.: Brachiopodes et chitinozoaires ordoviciens dans le NE du Sahara algérien: Implications stratigraphiques et paléogéographiques, Geobios, 32(6), 822–839, doi:10.1016/S0016-6995(99)80865-1, 1999.

Milani, E. J. and Zalan, P. V.: An outline of the geology and petroleum systems of the Paleozoic interior basins of South America, Episodes, 22, 199–205, 1999.

Milton, N. J., Bertram, G. T. and Vann, I. R.: Early Palaeogene tectonics and sedimentation in the Central North Sea, Geol. Soc. Lond. Spec. Publ., 55(1), 339–351, 1990.

Moreau, C., Demaiffe, D., Bellion, Y. and Boullier, A.-M.: A tectonic model for the location of Palaeozoic ring complexes in Air (Niger, West Africa), Tectonophysics, 234(1), 129–146, 1994.

Mory, A. J., Zhan, Y., Haines, P. W., Hocking, R. M., Thomas, C. M. and Copp, I. A.: A paleozoic perspective of Western Australia, Geological Survey of Western Australia., 2017.

Najem, A., El-Arnauti, A. and Bosnina, S.: Delineation of Paleozoic Tecto-stratigraphic Complexities in the Northern Part of Murzuq Basin-Southwest Libya, in SPE North Africa Technical Conference and Exhibition, Society of Petroleum Engineers., 2015.

Nikishin, A. M., Ziegler, P. A., Stephenson, R. A., Cloetingh, S., Furne, A. V., Fokin, P. A., Ershov, A. V., Bolotov, S. N., Korotaev, M. V. and Alekseev, A. S.: Late Precambrian to Triassic history of the East European Craton: dynamics of sedimentary basin evolution, Tectonophysics, 268(1–4), 23–63, 1996.

Ogg, J. G., Ogg, G. and Gradstein, F. M.: Introduction, in A Concise Geologic Time Scale: 2016, p. 3, Elsevier., 2016.

de Oliveira, D. C. and Mohriak, W. U.: Jaibaras trough: an important element in the early tectonic evolution of the Parnaíba interior sag basin, Northern Brazil, Mar. Pet. Geol., 20(3), 351–383, doi:https://doi.org/10.1016/S0264-8172(03)00044-8, 2003.

Oudra, M., Beraaouz, H., Ikenne, M., Gasquet, D. and Soulaimani, A.: La Tectonique Panafricaine du Secteur d'Igherm: Implication des dômes extensifs tardi à post-orogéniques (Anti-Atlas occidental, Maroc), Estud. Geológicos, 61(3–6), 177–189, 2005.

Oulebsir, L. and Paris, F.: Chitinozoaires ordoviciens du Sahara algérien: biostratigraphie et affinités paléogéographiques, Rev. Palaeobot. Palynol., 86(1), 49–68, doi:10.1016/0034-6667(94)00098-5, 1995.

Owen, G.: Senni Beds of the Devonian Old Red Sandstone, Dyfed, Wales: anatomy of a semi-arid floodplain, Sediment. Geol., 95(3–4), 221–235, 1995.

Paris, F.: The Ordovician chitinozoan biozones of the Northern Gondwana domain, Rev. Palaeobot. Palynol., 66(3–4), 181–209, doi:10.1016/0034-6667(90)90038-K, 1990.

Paris, F., Bourahrouh, A. and Hérissé, A. L.: The effects of the final stages of the Late Ordovician glaciation on marine palynomorphs (chitinozoans, acritarchs, leiospheres) in well Nl-2 (NE Algerian Sahara), Rev. Palaeobot. Palynol., 113(1–3), 87–104, doi:10.1016/S0034-6667(00)00054-3, 2000.

Peace, A., McCaffrey, K., Imber, J., van Hunen, J., Hobbs, R. and Wilson, R.: The role of pre-existing structures during rifting, continental breakup and transform system development, offshore West Greenland, Basin Res., 30(3), 373–394, 2018.

Pemberton, S. G. and Frey, R. W.: Trace fossil nomenclature and the Planolites-Palaeophycus dilemma, J. Paleontol., 56(4), 843–881, 1982.

Peucat, J. J., Drareni, A., Latouche, L., Deloule, E. and Vidal, P.: U–Pb zircon (TIMS and SIMS) and Sm–Nd whole-rock geochronology of the Gour Oumelalen granulitic basement, Hoggar massif, Tuareg shield, Algeria, J. Afr. Earth Sci., 37(3–4), 229–239, doi:10.1016/j.jafrearsci.2003.03.001, 2003.

Peucat, J.-J., Capdevila, R., Drareni, A., Mahdjoub, Y. and Kahoui, M.: The Eglab massif in the West African Craton (Algeria), an original segment of the Eburnean orogenic belt: petrology, geochemistry and geochronology, Precambrian Res., 136(3–4), 309–352, doi:10.1016/j.precamres.2004.12.002, 2005.

Phillips, T. B., Jackson, C. A.-L., Bell, R. E. and Duffy, O. B.: Oblique reactivation of lithosphere-scale lineaments controls rift physiography – the upper-crustal expression of the Sorgenfrei–Tornquist Zone, offshore southern Norway, Solid Earth, 9(2), 403–429, doi:10.5194/se-9-403-2018, 2018.

Pinet, N., Lavoie, D., Dietrich, J., Hu, K. and Keating, P.: Architecture and subsidence history of the intracratonic Hudson Bay Basin, northern Canada, Earth-Sci. Rev., 125, 1–23, doi:10.1016/j.earscirev.2013.05.010, 2013.

Potter, D.: Relationships of Cambro-Ordovician Stratigraphy to Paleotopography on the Precambrian Basement, Williston Basin, Sask. Geol. Soc., 63–73, 2006.

Reading, H. G. and Collinson, J. D.: Clastic coasts, in Sedimentary environments: processes, facies, and stratigraphy, pp. 154–231, John Wiley & Sons, Oxford ; Cambridge, Mass., 2009.

Rider, M. H.: Facies, Sequences and Depositional Environments from Logs, in The geological interpretation of well logs, pp. 226–238, Whittles Publishing, Caithness, Scotland., 1996.

Rougier, S., Missenard, Y., Gautheron, C., Barbarand, J., Zeyen, H., Pinna, R., Liégeois, J.-P., Bonin, B., Ouabadi, A., Derder, M. E.-M. and Lamotte, D. F. de: Eocene exhumation of the Tuareg Shield (Sahara Desert, Africa), Geology, 41(5), 615–618, doi:10.1130/G33731.1, 2013.

Sabaou, N., Ait-Salem, H. and Zazoun, R. S.: Chemostratigraphy, tectonic setting and provenance of the Cambro-Ordovician clastic deposits of the subsurface Algerian Sahara, J. Afr. Earth Sci., 55(3–4), 158–174, doi:10.1016/j.jafrearsci.2009.04.006, 2009.

Schlische, R. W.: Geometry and origin of fault-related folds in extensional settings, AAPG Bull., 79(11), 1661–1678, 1995.

Sclater, J. G. and Christie, P. A. F.: Continental stretching: An explanation of the Post-Mid-Cretaceous subsidence of the central North Sea Basin, J. Geophys. Res. Solid Earth, 85(B7), 3711–3739, doi:10.1029/JB085iB07p03711, 1980.

Scotese, C. R., Boucot, A. J. and McKerrow, W. S.: Gondwanan palaeogeography and paleoclimatology, J. Afr. Earth Sci., 28(1), 99–114, doi:10.1016/S0899-5362(98)00084-0, 1999.

Serra, O. and Serra, L.: Well logging, facies, sequence and environment, in Well logging and geology, pp. 197–238, Technip Editions, France., 2003.

Sharata, S., Röth, J. and Reicherter, K.: Basin evolution in the North African Platform, Geotecton. Res., 97(1), 80–81, doi:10.1127/1864-5658/2015-31, 2015.

Shaw, J. H., Connors, C. D. and Suppe, J.: Recognizing growth strata, in Seismic interpretation of contractional fault-related folds: an AAPG seismic atlas, vol. 53, pp. 11–14, American Association of Petroleum Geologists, Tulsa, Okla., U.S.A., 2005.

Sloss, L. L.: Sequences in the cratonic interior of North America, Geol. Soc. Am. Bull., 74(2), 93–114, 1963.

Smart, J.: Seismic expressions of depositional processes in the upper Ordovician succession of the Murzuq Basin, SW Libya, in Geological Exploration in Murzuq Basin, edited by M. A. Sola and D. Worsley, pp. 397–415, Elsevier Science B.V., Amsterdam., 2000.

Soares, P. C., Landim, P. M. B. and Fulfaro, V. J.: Tectonic cycles and sedimentary sequences in the Brazilian intracratonic basins, GSA Bull., 89(2), 181–191, doi:10.1130/0016-7606(1978)89<181:TCASSI>2.0.CO;2, 1978.

Stearns, D. W.: Faulting and forced folding in the Rocky Mountains foreland, Laramide Fold. Assoc. Basement Block Faulting West. U. S. Geol. Soc. Am. Mem., 151, 1–37, 1978.

Stow, D. a. V. and Piper, D. J. W.: Deep-water fine-grained sediments: facies models, Geol. Soc. Lond. Spec. Publ., 15(1), 611–646, doi:10.1144/GSL.SP.1984.015.01.38, 1984.

Stow, D. A. V., Huc, A.-Y. and Bertrand, P.: Depositional processes of black shales in deep water, Mar. Pet. Geol., 18(4), 491–498, doi:10.1016/S0264-8172(01)00012-5, 2001.

Suter, J. R.: Facies models revisited: clastic shelves, Spec. Publ.-SEPM, 84, 339, 2006.

Tournier, F.: Mécanismes et contrôle des phénomènes diagénétiques en milieu acide dans les grès de l'Ordovicien glaciaire du bassin de Sbaa, Algérie, Doctoral dissertation, Université de Paris 11, France., 2010.

Trompette, R.: Gondwana evolution; its assembly at around 600 Ma, Comptes Rendus Académie Sci.-Ser. IIA-Earth Planet. Sci., 330(5), 305–315, 2000.

Turner, G. M., Rasson, J. L. and Reeves, C. V.: Observation and Measurement Techniques, in Treatise on Geophysics, vol. 5, edited by G. Schubert, pp. 33–75, Blackwell Pub, Malden, MA., 2007.

Ustaszewski, K., Schumacher, M., Schmid, S. and Nieuwland, D.: Fault reactivation in brittle–viscous wrench systems–dynamically scaled analogue models and application to the Rhine–Bresse transfer zone, Quat. Sci. Rev., 24(3–4), 363–380, doi:10.1016/j.quascirev.2004.03.015, 2005.

Van Hinte, J. E.: Geohistory analysis–application of micropaleontology in exploration geology, AAPG Bull., 62(2), 201–222, 1978.

Vauchez, A., Tommasi, A. and Barruol, G.: Rheological heterogeneity, mechanical anisotropy and deformation of the continental lithosphere, Tectonophysics, 296(1–2), 61–86, doi:10.1016/S0040-1951(98)00137-1, 1998.

Vecoli, M.: Palaeoenvironmental interpretation of microphytoplankton diversity trends in the Cambrian–Ordovician of the northern Sahara Platform, Palaeogeogr. Palaeoclimatol. Palaeoecol., 160(3–4), 329–346, doi:10.1016/S0031-0182(00)00080-8, 2000.

Vecoli, M. and Playford, G.: Stratigraphically significant acritarchs in uppermost Cambrian to basal Ordovician strata of Northwestern Algeria, Grana, 36(1), 17–28, doi:10.1080/00173139709362585, 1997.

Vecoli, M., Albani, R., Ghomari, A., Massa, D. and Tongiorgi, M.: Précisions sur la limite Cambrien-Ordovicien au Sahara Algérien (Secteur de Hassi-Rmel), Comptes Rendus Académie Sci. Sér. 2 Sci. Terre Planètes, 320(6), 515–522, 1995.

Vecoli, M., Tongiorgi, M., Abdesselam-Roughi, F. F., Benzarti, R. and Massa, D.: Palynostratigraphy of upper Cambrian-upper Ordovician intracratonic clastic sequences, North Africa, Boll.-Soc. Paleontol. Ital., 38(2/3), 331–342, 1999.

Vecoli, M., Videt, B. and Paris, F.: First biostratigraphic (palynological) dating of Middle and Late Cambrian strata in the subsurface of northwestern Algeria, North Africa: Implications for regional stratigraphy, Rev. Palaeobot. Palynol., 149(1–2), 57–62, doi:10.1016/j.revpalbo.2007.10.004, 2008.

Videt, B., Paris, F., Rubino, J.-L., Boumendjel, K., Dabard, M.-P., Loi, A., Ghienne, J.-F., Marante, A. and Gorini, A.: Biostratigraphical calibration of third order Ordovician sequences on the northern Gondwana platform, Palaeogeogr. Palaeoclimatol. Palaeoecol., 296(3–4), 359–375, doi:10.1016/j.palaeo.2010.03.050, 2010.

Wagoner, J. C. V., Mitchum, R. M., Campion, K. M. and Rahmanian, V. D.: Siliciclastic Sequence Stratigraphy in Well Logs, Cores, and Outcrops: Concepts for High-Resolution Correlation of Time and Facies, AAPG Methods Explor. Ser. No 7, 174, III–55, 1990.

Watts, A. B.: Isostasy and Flexure of the Lithosphere, Cambridge University Press, Oxford University., 2001.

Wendt, J.: Disintegration of the continental margin of northwestern Gondwana: Late Devonian of the eastern Anti-Atlas (Morocco), Geology, 13(11), 815–818, 1985.

Wendt, J.: Facies Pattern and Paleogeography of the Middle and Late Devonian in the Eastern Anti-Atlas (Morocco), Can. Soc. Pet. Geol., 1(14), 467–480, 1988.

Wendt, J.: Shell directions as a tool in palaeocurrent analysis, Sediment. Geol., 95(3), 161–186, doi:10.1016/0037-0738(94)00104-3, 1995.

Wendt, J. and Kaufmann, B.: Mud buildups on a Middle Devonian carbonate ramp (Algerian Sahara), Geol. Soc. Lond. Spec. Publ., 149(1), 397–415, doi:10.1144/GSL.SP.1999.149.01.18, 1998.

Wendt, J., Belka, Z. and Moussine-Pouchkine, A.: New architectures of deep-water carbonate buildups: Evolution of mud mounds into mud ridges (Middle Devonian, Algerian Sahara), Geology, 21(8), 723–726, 1993.

Wendt, J., Belka, Z., Kaufmann, B., Kostrewa, R. and Hayer, J.: The world's most spectacular carbonate mud mounds (Middle Devonian, Algerian Sahara), J. Sediment. Res., 67(3), 424–436, doi:10.1306/D426858B-2B26-11D7-8648000102C1865D, 1997.

Wendt, J., Kaufmann, B., Belka, Z., Klug, C. and Lubeseder, S.: Sedimentary evolution of a Palaeozoic basin and ridge system: the Middle and Upper Devonian of the Ahnet and Mouydir (Algerian Sahara), Geol. Mag., 143(3), 269–299, doi:10.1017/S0016756806001737, 2006.

Wendt, J., Kaufmann, B., Belka, Z. and Korn, D.: Carboniferous stratigraphy and depositional environments in the Ahnet Mouydir area (Algerian Sahara), Facies, 55(3), 443–472, doi:10.1007/s10347-008-0176-y, 2009a.

Wendt, J., Kaufmann, B. and Belka, Z.: Devonian stratigraphy and depositional environments in the southern Illizi Basin (Algerian Sahara), J. Afr. Earth Sci., 54(3–4), 85–96, doi:10.1016/j.jafrearsci.2009.03.006, 2009b.

Withjack, M. O. and Callaway, S.: Active normal faulting beneath a salt layer: an experimental study of deformation patterns in the cover sequence, AAPG Bull., 84(5), 627–651, 2000.

Withjack, M. O., Olson, J. and Peterson, E.: Experimental models of extensional forced folds, AAPG Bull., 74(7), 1038–1054, 1990.

Withjack, M. O., Schlische, R. W. and Olsen, P. E.: Rift-basin structure and its influence on sedimentary systems, Soc. Sediment. Geol. Spec. Publ., (73), 57–81, 2002.

Xie, X. and Heller, P.: Plate tectonics and basin subsidence history, Geol. Soc. Am. Bull., 121(1–2), 55–64, doi:10.1130/B26398.1, 2009.

Yahi, N.: Petroleum generation and migration in the Berkine (Ghadames) Basin, Eastern Algeria: an organic geochemical and basin modelling study, Doctoral dissertation, Forschungszentrum, Zentralbibliothek, Jülich., 1999.

Zalan, P. V., Wolff, S., Astolfi, M. A. M., Vieira, I. S., Concelcao, J. C. J., Appi, V. T., Neto, E. V. S., Cerqueira, J. R. and Marques, A.: The Parana Basin, Brazil: Chapter 33: Part II. Selected Analog Interior Cratonic Basins: Analog Basins, , 134, 681–708, 1990.

Zazoun, R. S.: Hercynian deformation in the western Ahnet Basin and Bled El-Mass area, Algerian Sahara: a continuous strain, J. Afr. Earth Sci., 32(4), 869–887, 2001.

Zazoun, R. S.: The Fadnoun area, Tassili-n-Azdjer, Algeria: Fracture network geometry analysis, J. Afr. Earth Sci., 50(5), 273–285, doi:10.1016/j.jafrearsci.2007.10.001, 2008.

Zazoun, R. S. and Mahdjoub, Y.: Strain analysis of Late Ordovician tectonic events in the In-Tahouite and Tamadjert Formations (Tassili-n-Ajjers area, Algeria), J. Afr. Earth Sci., 60(3), 63–78, doi:10.1016/j.jafrearsci.2011.02.003, 2011.

## List of figures

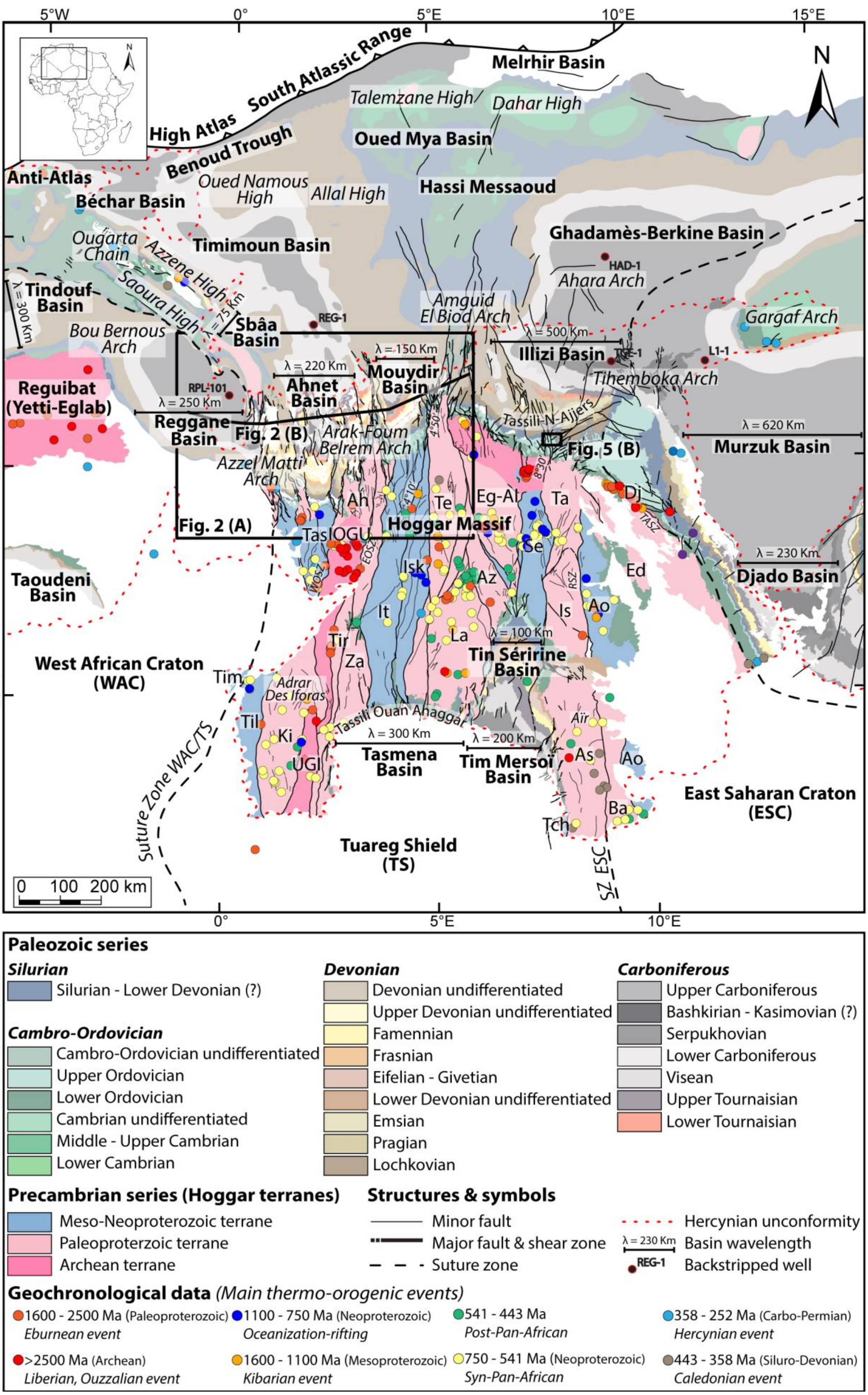

5°W
0°
5°E
10°E
15°E
30°N
25°N
20°N
N
South Atlassic Range
High Atlas
Melrhir Basin
Talemzane High
Dahar High
Oued Mya Basin
Benoud Trough
Anti-Atlas
Oued Namous High
Allal High
Hassi Messaoud
Béchar Basin
Ghadamès-Berkine Basin
Ougarta Chain
Timimoun Basin
HAD-1
Azzene High
Ahara Arch
Tindouf Basin
λ = 300 Km
Saoura High
λ = 75 Km
REG-1
Amguid El Biod Arch
Gargaf Arch
Bou Bernous Arch
Sbâa Basin
λ = 500 Km
λ = 150 Km
Illizi Basin
TGE-1
L1-1
λ = 220 Km
Mouydir Basin
Reguibat (Yetti-Eglab)
RPL-101
Ahnet Basin
Tihemboka Arch
λ = 250 Km
Reggane Basin
Tassili-N-Ajjers
λ = 620 Km
Fig. 2 (B)
Arak-Foum Belrem Arch
Fig. 5 (B)
Murzuk Basin
Azzel Matti Arch
Eg-At
Ta
Dj
Ah
Te
Fig. 2 (A)
Hoggar Massif
Tas
OGU
Se
λ = 230 Km
Taoudeni Basin
Isk
Az
Ed
Djado Basin
It
Is
Ao
La
λ = 100 Km
West African Craton (WAC)
Tir
Tin Séririne Basin
Za
Tim
Adrar Des Iforas
Tassili Ouan Ahaggar
Til
Aïr
Ki
λ = 300 Km
λ = 200 Km
As
Ao
UGI
Tasmena Basin
Tim Mersoï Basin
East Saharan Craton (ESC)
Ba
Suture Zone WAC/TS
Tch
Tuareg Shield (TS)
SZ ESC
0 100 200 km
Paleozoic series
Silurian
Silurian - Lower Devonian (?)
Cambro-Ordovician
Cambro-Ordovician undifferentiated
Upper Ordovician
Lower Ordovician
Cambrian undifferentiated
Middle - Upper Cambrian
Lower Cambrian
Devonian
Devonian undifferentiated
Upper Devonian undifferentiated
Famennian
Frasnian
Eifelian - Givetian
Lower Devonian undifferentiated
Emsian
Pragian
Lochkovian
Carboniferous
Upper Carboniferous
Bashkirian - Kasimovian (?)
Serpukhovian
Lower Carboniferous
Visean
Upper Tournaisian
Lower Tournaisian
Precambrian series (Hoggar terranes)
Meso-Neoproterozoic terrane
Paleoproterzoic terrane
Archean terrane
Structures & symbols
Minor fault
Major fault & shear zone
Suture zone
Hercynian unconformity
Basin wavelength
Backstripped well
Geochronological data (Main thermo-orogenic events)
1600 - 2500 Ma (Paleoproterozoic) Eburnean event
1100 - 750 Ma (Neoproterozoic) Oceanization-rifting
541 - 443 Ma Post-Pan-African
358 - 252 Ma (Carbo-Permian) Hercynian event
>2500 Ma (Archean) Liberian, Ouzzalian event
1600 - 1100 Ma (Mesoproterozoic) Kibarian event
750 - 541 Ma (Neoproterozoic) Syn-Pan-African
443 - 358 Ma (Siluro-Devonian) Caledonian event

Figure 1: Geological map of the Paleozoic North Saharan Platform (North Gondwana) georeferenced, compiled and modified from (1) Paleozoic subcrop distribution below the Hercynian unconformity geology of the Saharan Platform (Boote et al., 1998; Galeazzi et al., 2010); (2) Geological map (1/500,000) of the Djado basin (Jacquemont et al., 1959); (3) Geological map (1/200,000) of Algeria (Bennacef et al., 1974; Bensalah et al., 1971), (4) Geological map (1/50,000) of Aïr (Joulia, 1963), (5) Geological map (1/2,000,000) of Niger (Greigertt and Pougnet, 1965), (6) Geological map (1/5,000,000 ) of the Lower Paleozoic of the Central Sahara (Beuf et al., 1971), (7) Geological map (1/1,000,000) of Morocco (Hollard et al., 1985), (8) Geological map of the Djebel Fezzan (Massa, 1988); Basement characterization of the different terranes from geochronological data compilation (see supplementary data) and geological maps (Berger et al., 2014; Bertrand and Caby, 1978; Black et al., 1994; Caby, 2003; Fezaa et al., 2010; Liégeois et al., 1994, 2003, 2005, 2013); Terrane names: Tassendjanet (Tas), Tassendjanet nappe (Tas n.), Ahnet (Ah), In Ouzzal Granulitic Unit (IOGU), Iforas Granulitic Unit (UGI), Kidal (Ki), Timétrine (Tim), Tilemsi (Til), Tirek (Tir), In Zaouatene (Za), In Teidini (It), Iskel (Isk), Tefedest (Te), Laouni (La), Azrou-n-Fad (Az), Egéré-Aleskod (Eg-Al), Serouenout (Se), Tazat (Ta), Issalane (Is), Assodé (As), Barghot (Ba), Tchilit (Tch), Aouzegueur (Ao), Edembo (Ed), Djanet (Dj); Shear zone and lineament names: Suture Zone East Saharan Craton (SZ ESC), West Ouzzal Shear Zone (WOSZ), East Ouzzal Shear Zone (EOSZ), Raghane Shear Zone (RSZ), Tin Amali Shear Zone (TASZ), 4°10’ Shear Zone, 4°50’ Shear Zone, 8°30’ Shear Zone.

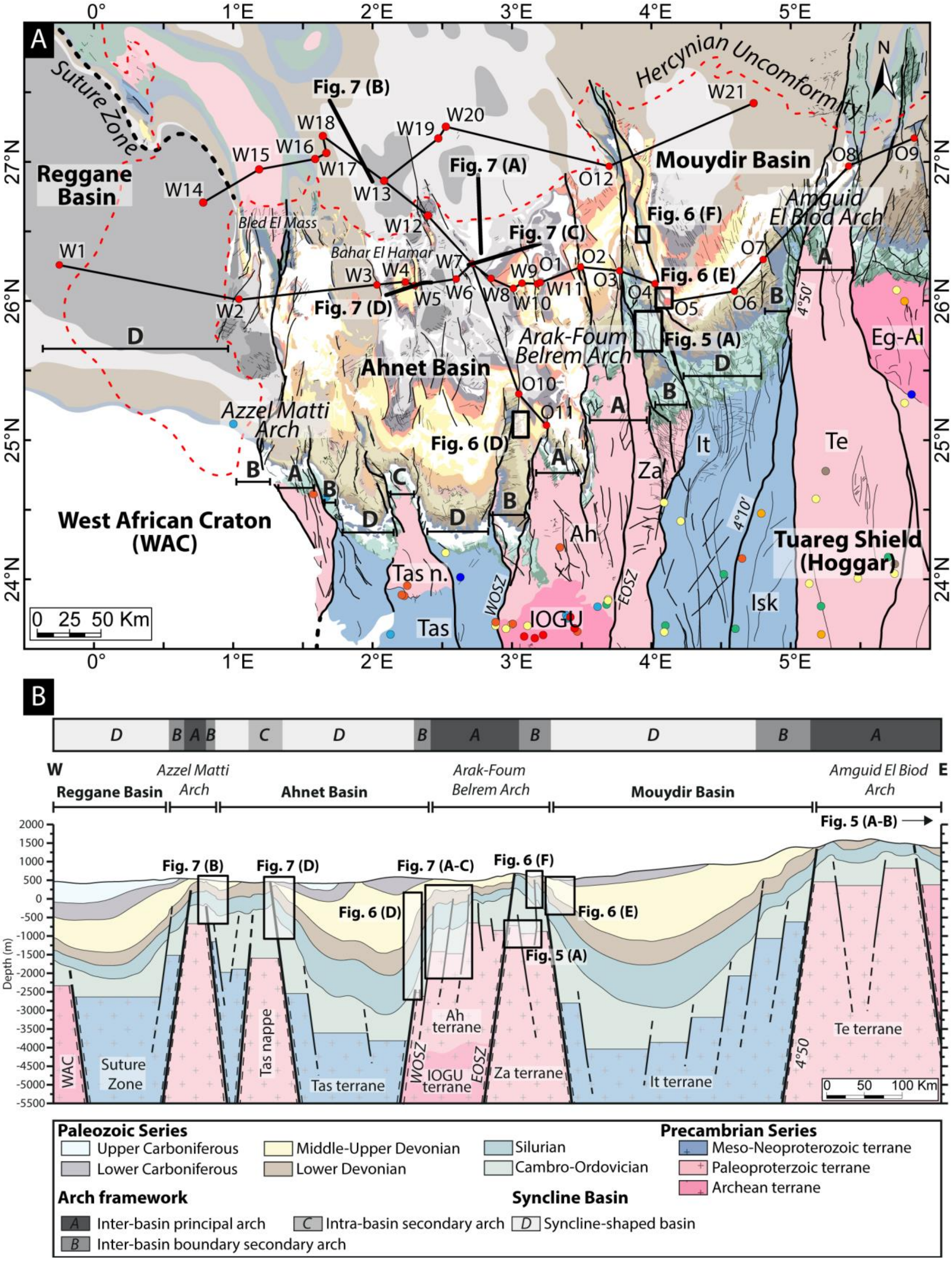


Figure 2: (A) Geological map of the Paleozoic of the Reggane, Ahnet, and Mouydir basins. Legend and references see Fig. 1. (B) E–W cross-section of the Reggane, Ahnet, and Mouydir

basins associated with the different terranes and highlighting the classification of the different structural units. Localization of the interpreted sections (seismic profiles and satellite images). W=Well and O=Outcrop. See figure 1 for location of the geological map A and cross section B.

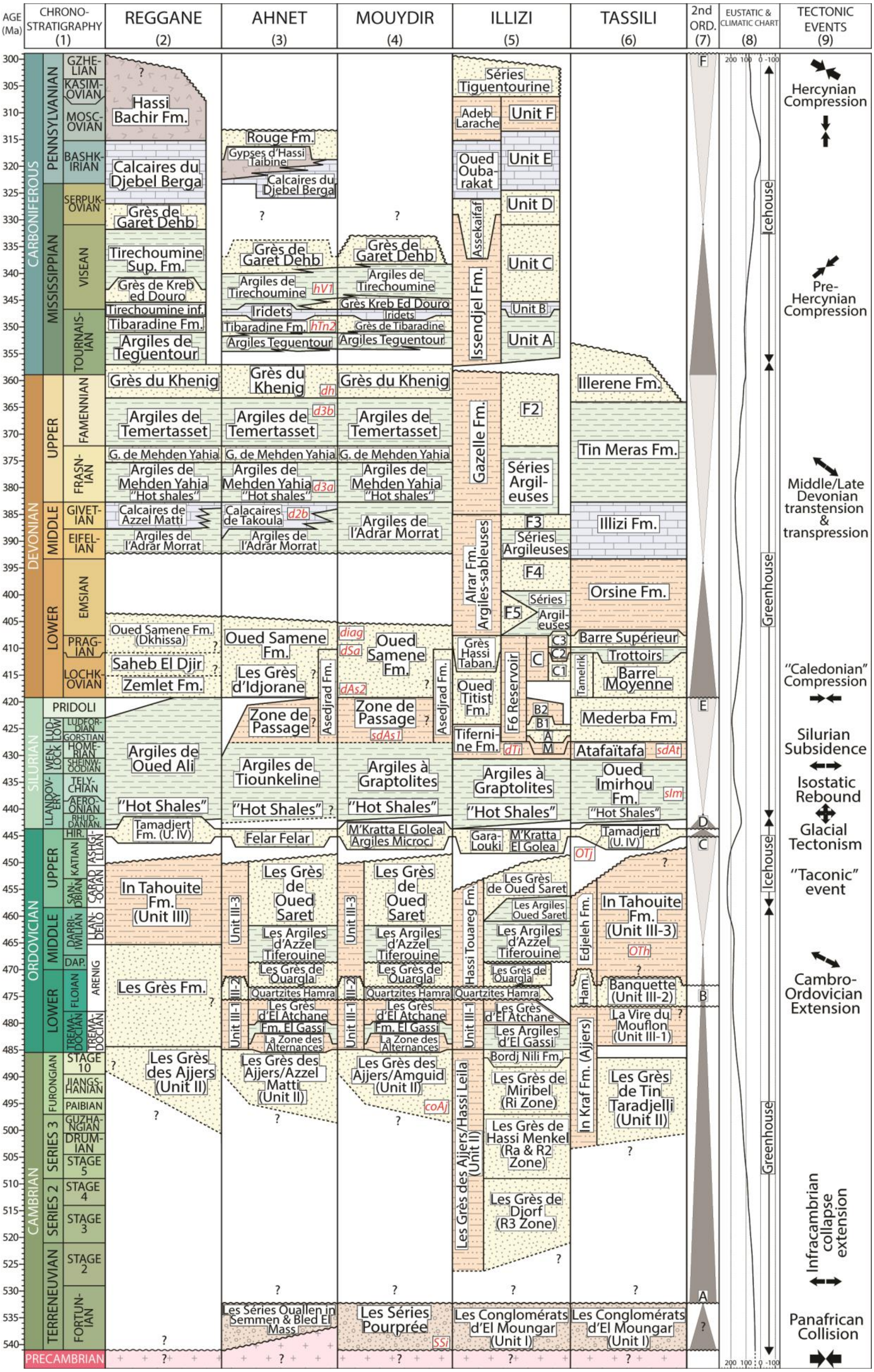
AGE (Ma)
CHRONO-STRATIGRAPHY (1)
REGGANE (2)
AHNET (3)
MOUYDIR (4)
ILLIZI (5)
TASSILI (6)
2nd ORD. (7)
EUSTATIC & CLIMATIC CHART (8)
TECTONIC EVENTS (9)
CARBONIFEROUS
PENNSYLVANIAN
MISSISSIPPIAN
GZHELIAN
KASIMOVIAN
MOSCOVIAN
BASHKIRIAN
SERPUKOVIAN
VISEAN
TOURNAISIAN
DEVONIAN
UPPER
MIDDLE
LOWER
FAMENNIAN
FRASNIAN
GIVETIAN
EIFELIAN
EMSIAN
PRAGIAN
LOCHKOVIAN
SILURIAN
PRIDOLI
LUDLOW
LUDFORDIAN
GORSTIAN
WENLOCK
HOMERIAN
SHEINWOODIAN
LLANDOVERY
TELYCHIAN
AERONIAN
RHUDDANIAN
ORDOVICIAN
HIR.
KATIAN
SANDBIAN
DARRIWILIAN
DAP.
FLOIAN
TREMADOCIAN
ASHGILLIAN
CARADOCIAN
LLANDEILO
ARENIG
TREMADOCIAN
CAMBRIAN
FURONGIAN
SERIES 3
SERIES 2
TERRENEUVIAN
STAGE 10
JIANGSHANIAN
PAIBIAN
GUZHANGIAN
DRUMIAN
STAGE 5
STAGE 4
STAGE 3
STAGE 2
FORTUNIAN
PRECAMBRIAN
Hassi Bachir Fm.
Calcaires du Djebel Berga
Grès de Garet Dehb
Tirechoumine Sup. Fm.
Grès de Kreb ed Douro
Tirechoumine inf.
Tibaradine Fm.
Argiles de Teguentour
Grès du Khenig
Argiles de Temertasset
G. de Mehden Yahia
Argiles de Mehden Yahia
"Hot shales"
Calcaires de Azzel Matti
Argiles de l'Adrar Morrat
Oued Samene Fm. (Dkhissa)
Saheb El Djir
Zemlet Fm.
Argiles de Oued Ali
"Hot Shales"
Tamadjert Fm. (U. IV)
In Tahouite Fm. (Unit III)
Les Grès Fm.
Les Grès des Ajjers (Unit II)
Rouge Fm.
Gypses d'Hassi Taibine
Calcaires du Djebel Berga
Grès de Garet Dehb
Argiles de Tirechoumine
hV1
Iridets
Tibaradine Fm.
hTn2
Argiles Teguentour
Grès du Khenig
dh
d3b
d3a
Calcaires de Takoula
d2b
Oued Samene Fm.
Les Grès d'Idjorane
Asedjrad Fm.
Zone de Passage
Argiles de Tiounkeline
Felar Felar
Unit III-3
Les Grès de Oued Saret
Les Argiles d'Azzel Tiferouine
Les Grès de Ouargla
Quartzites Hamra
Unit III-2
Unit III-1
Les Grès d'El Atchane
Fm. El Gassi
La Zone des Alternances
Les Grès des Ajjers/Azzel Matti (Unit II)
Les Séries Ouallen in Semmen & Bled El Mass
Grès Kreb Ed Douro
Grès de Tibaradine
diag
dSa
dAs2
sdAs1
Argiles à Graptolites
M'Kratta El Golea
Argiles Microc.
Les Grès des Ajjers/Amguid (Unit II)
coAj
Les Séries Pourprée
SSi
Séries Tiguentourine
Adeb Larache
Unit F
Oued Oubarakat
Unit E
Unit D
Assekaifaf
Unit C
Unit B
Unit A
Issendjel Fm.
Gazelle Fm.
F2
Séries Argileuses
F3
F4
F5
Alrar Fm.
Argiles-sableuses
Grès Hassi Taban
C3
C2
C1
C
Oued Titist Fm.
F6 Reservoir
B2
B1
A
M
Tiferniне Fm.
dTi
Gara-Louki
M'Kratta El Golea
Hassi Touareg Fm.
Les Grès de Oued Saret
Les Argiles Oued Saret
Les Argiles d'Azzel Tiferouine
Les Grès de Ouargla
Les Grès d'El Atchane
Les Argiles d'El Gassi
Bordj Nili Fm.
Les Grès de Miribel (Ri Zone)
Les Grès de Hassi Menkel (Ra & R2 Zone)
Les Grès de Djorf (R3 Zone)
Les Grès des Ajjers/Hassi Leila (Unit II)
Les Conglomérats d'El Moungar (Unit I)
Illerene Fm.
Tin Meras Fm.
Illizi Fm.
Orsine Fm.
Barre Supérieur
Tamelrik
Trottoirs
Barre Moyenne
Mederba Fm.
Atafaïtafa
sdAt
Oued Imirhou Fm.
slm
OTj
Edjeleh Fm.
In Tahouite Fm. (Unit III-3)
OTh
Ham.
Banquette (Unit III-2)
La Vire du Mouflon (Unit III-1)
In Kraf Fm. (Ajjers)
Les Grès de Tin Taradjelli (Unit II)
F
E
D
C
B
A
200 100 0 -100
Icehouse
Greenhouse
Hercynian Compression
Pre-Hercynian Compression
Middle/Late Devonian transtension & transpression
"Caledonian" Compression
Silurian Subsidence
Isostatic Rebound
Glacial Tectonism
"Taconic" event
Cambro-Ordovician Extension
Infracambrian collapse extension
Panafrican Collision

1371

Figure 3: Paleozoic litho-stratigraphic, sequence stratigraphy and tectonic framework of the North Peri-Hoggar basins (North African Saharan Platform) compiled from (1) Chronostratigraphic chart (Ogg et al., 2016), (2) The Cambrian–Silurian (Askri et al., 1995) and the Devonian–Carboniferous stratigraphy of the Reggane basin (Cózar et al., 2016; Lubeseder, 2005; Lubeseder et al., 2010; Magloire, 1967; Wendt et al., 2006), (3) The Cambrian–Silurian (Paris, 1990; Wendt et al., 2006) and the Devonian–Carboniferous stratigraphy of the Ahnet basin (Beuf et al., 1971; Conrad, 1973, 1984; Legrand-Blain, 1985; Wendt et al., 2006, 2009a), (4) The Cambrian–Silurian (Askri et al., 1995; Paris, 1990; Videt et al., 2010) and the Devonian–Carboniferous stratigraphy of the Mouydir basin (Askri et al., 1995; Beuf et al., 1971; Conrad, 1973, 1984; Wendt et al., 2006, 2009a), (5) The Cambrian–Silurian (Eschard et al., 2005; Fekirine and Abdallah, 1998; Jardiné and Yapaudjian, 1968; Videt et al., 2010) and the Devonian–Carboniferous stratigraphy of the Illizi basin (Eschard et al., 2005; Fekirine and Abdallah, 1998; Jardiné and Yapaudjian, 1968), (6) The Cambrian–Silurian (Dubois, 1961; Dubois and Mazelet, 1964; Eschard et al., 2005; Henniche, 2002; Videt et al., 2010) and the Devonian–Carboniferous stratigraphy of the Tassili-N-Ajjers (Dubois et al., 1967; Eschard et al., 2005; Henniche, 2002; Wendt et al., 2009a), (7) Sequence stratigraphy of the Saharan Platform (Carr, 2002; Eschard et al., 2005; Fekirine and Abdallah, 1998), (8) Eustatic and climatic chart (Haq and Schutter, 2008; Scotese et al., 1999), (9) Tectonic events (Boudjema, 1987; Coward and Ries, 2003; Craig et al., 2008; Guiraud et al., 2005; Lüning, 2005); (A) Infra-Tassilian (Pan-African) unconformity, (B) Intra-Arenig unconformity, (C) Taconic and glacial unconformity, (D) Isostatic rebound unconformity, (E) Caledonian unconformity, (F) Hercynian unconformity.

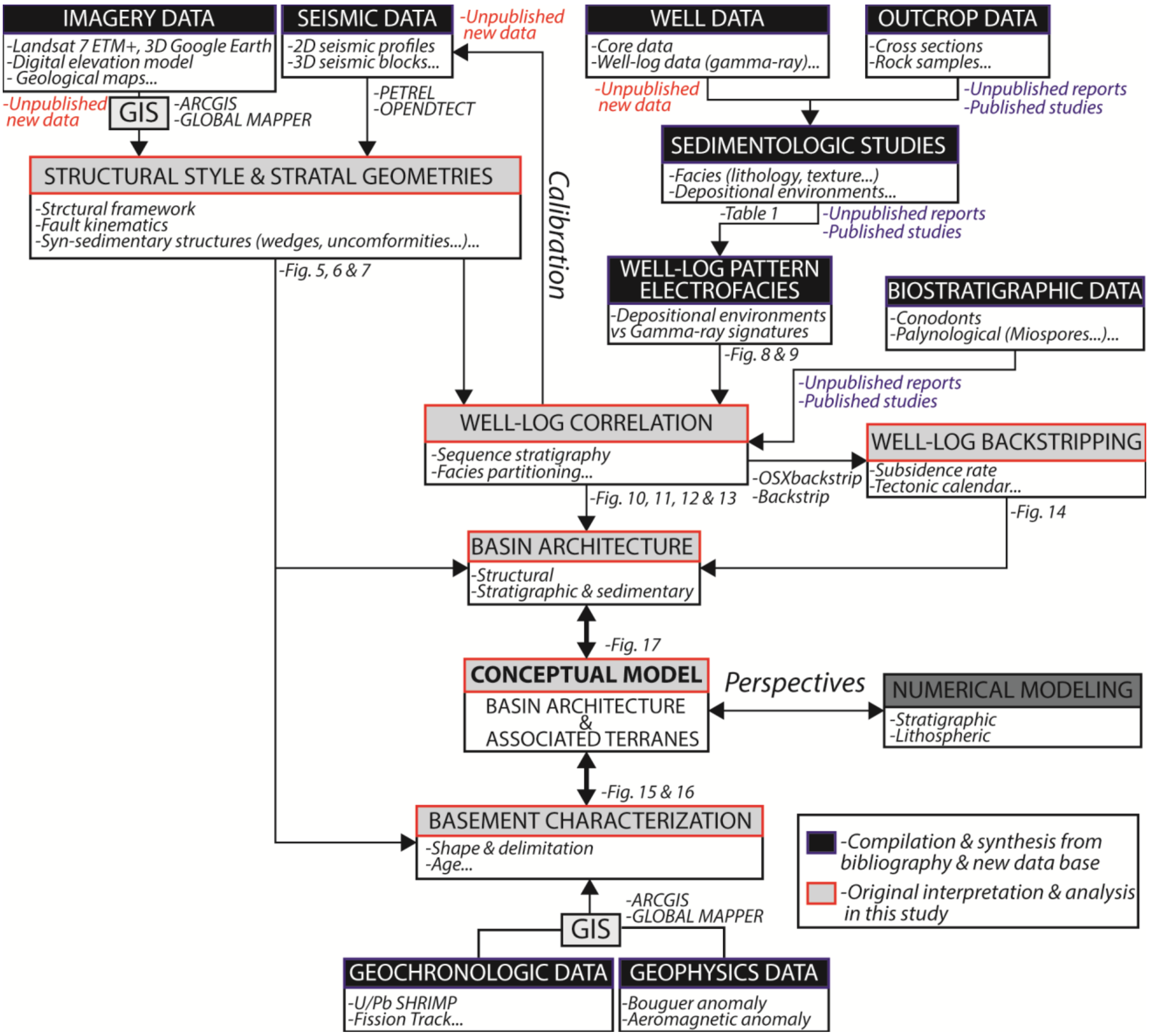


Figure 4: Schematic synthesis of the integrated method of basin analysis in this study.

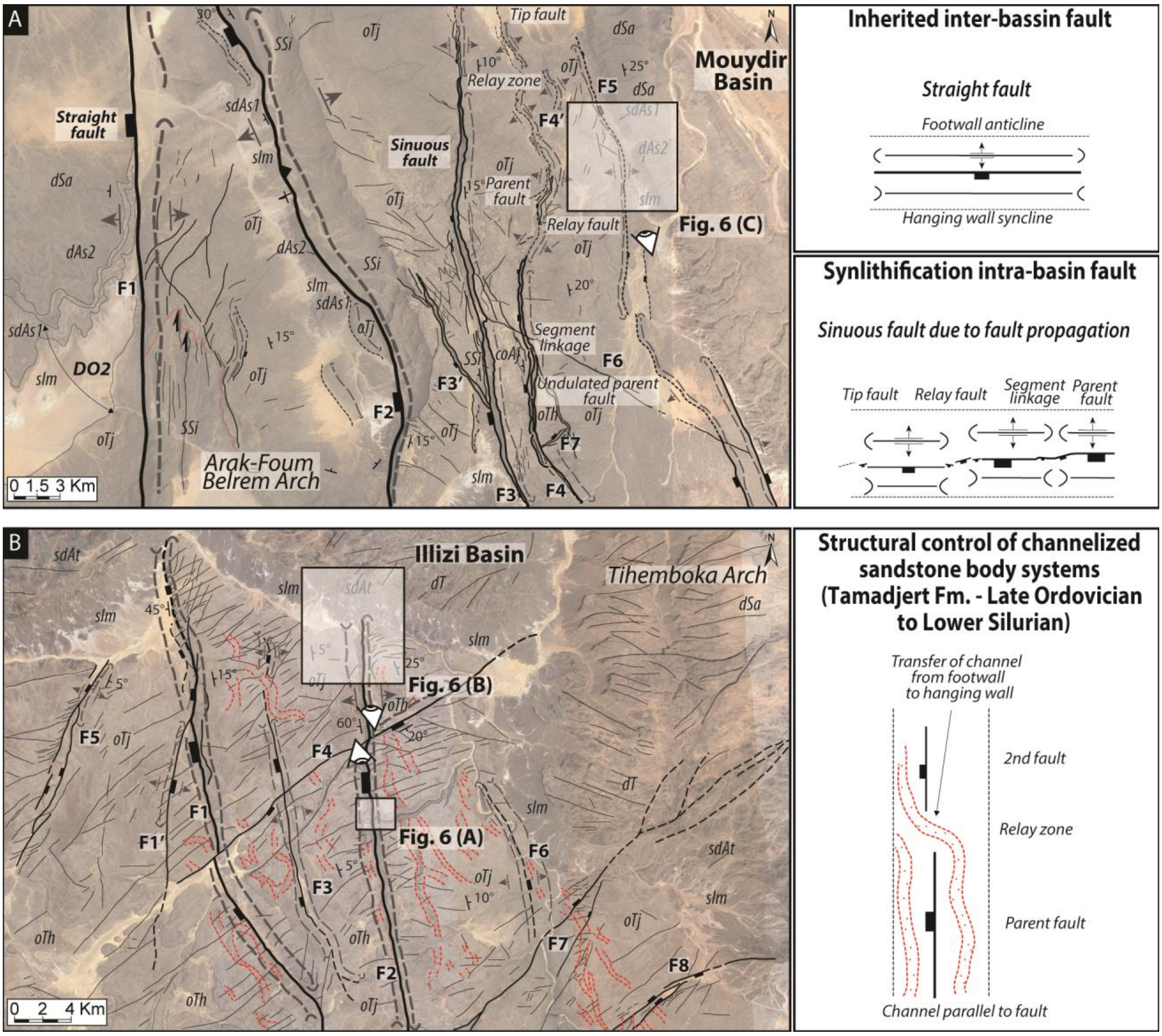


Figure 5: (A) Typology of different types of faults (inherited straight faults vs sinuous short synlithification propagation faults) in the Cambrian–Ordovician series of the Djebel Settaf (Arak-Foum Belrem arch; inter-basin boundary secondary arch between the Ahnet and Mouydir basins). (B) Structural control of channelized sandstone bodies in Late Ordovician series of South Adrar Assaouatene, Tassili-N-Ajjers (Tihemboka inter-basin boundary secondary arch between the Illizi and Murzuq basins). Dotted red line: Tamadjert Fm. channelized sandstone bodies. *OTh*: In Tahouite Fm. (Early to Late Ordovician, Floian to Katian), *OTj*: Tamadjert Fm. (Late Ordovician, Hirnantian), *sIm*: Imirhou Fm. (Early Silurian), *sdAs1*: Asedjrad Fm. 1 (Late Silurian to Early Devonian), *dAs2*: Asedjrad Fm. 2

(Early Devonian, Lochkovian), *dSa*: Oued Samene Fm. (Lower Devonian, Pragian). See Fig. 2 for map and cross-section location.

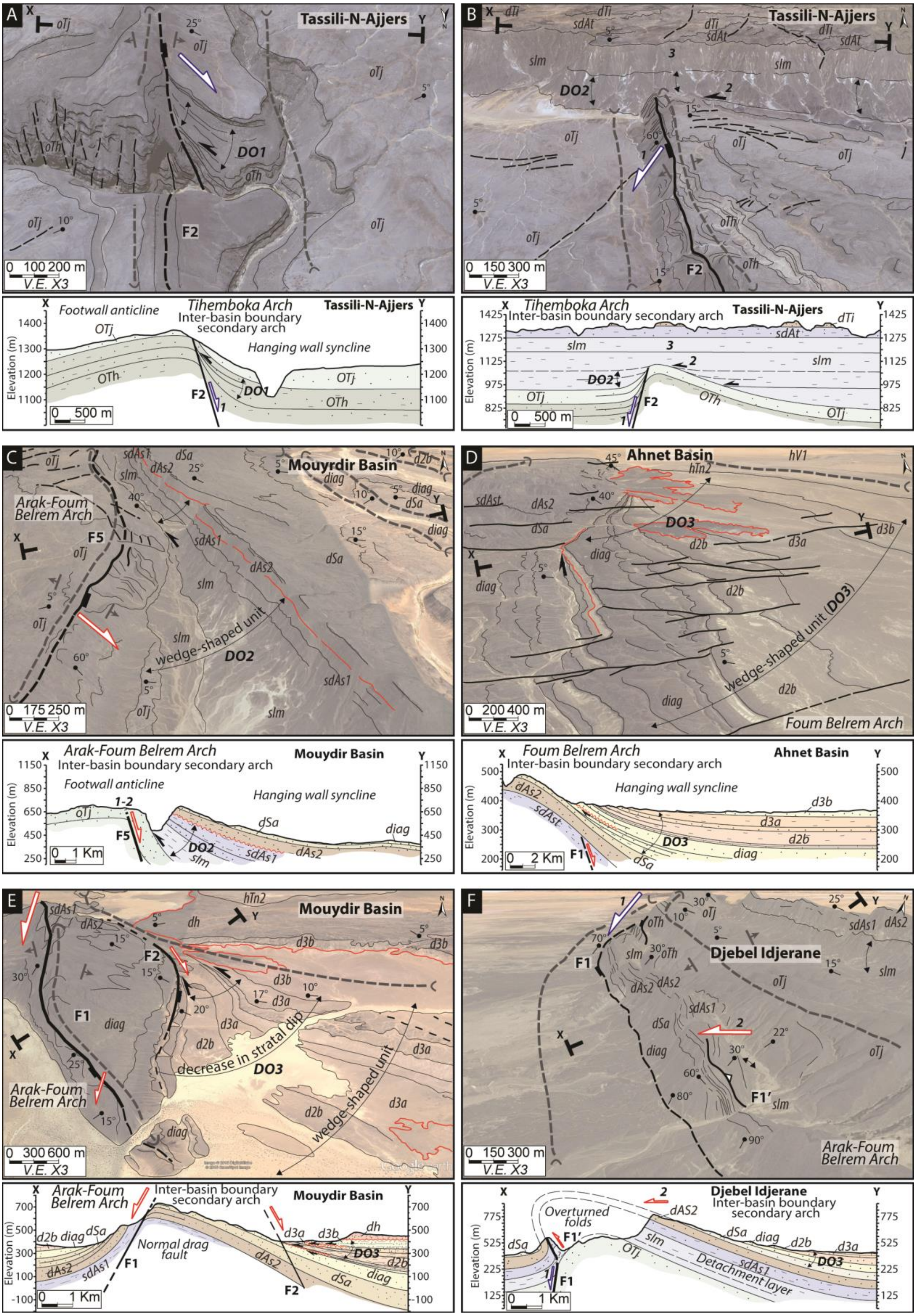
A
Tassili-N-Ajjers
oTj
oTh
DO1
F2
0 100 200 m
V.E. X3
Footwall anticline
Tihemboka Arch
Inter-basin boundary secondary arch
Hanging wall syncline
Elevation (m)
0 500 m
B
Tassili-N-Ajjers
dTi
sdAt
slm
DO2
oTj
oTh
F2
0 150 300 m
V.E. X3
Tihemboka Arch
Inter-basin boundary secondary arch
C
Mouyrdir Basin
Arak-Foum Belrem Arch
F5
sdAs1
dAs2
dSa
diag
slm
wedge-shaped unit
DO2
0 175 250 m
V.E. X3
Arak-Foum Belrem Arch
Inter-basin boundary secondary arch
Moudyir Basin
Footwall anticline
Hanging wall syncline
0 1 Km
D
Ahnet Basin
hV1
hTn2
sdAst
dAs2
dSa
DO3
d2b
d3a
d3b
diag
wedge-shaped unit (DO3)
Foum Belrem Arch
0 200 400 m
V.E. X3
Foum Belrem Arch
Inter-basin boundary secondary arch
Ahnet Basin
Hanging wall syncline
0 2 Km
F1
E
Mouydir Basin
dh
F1
F2
decrease in stratal dip
DO3
wedge-shaped unit
Arak-Foum Belrem Arch
0 300 600 m
V.E. X3
Arak-Foum Belrem Arch
Inter-basin boundary secondary arch
Mouydir Basin
Normal drag fault
0 1 Km
F
Djebel Idjerane
F1
F1'
Arak-Foum Belrem Arch
0 150 300 m
V.E. X3
Djebel Idjerane
Inter-basin boundary secondary arch
Overturned folds
Detachment layer
0 1 Km

Figure 6: (A) Normal fault (F2) associated with a footwall anticline and a hanging wall syncline with divergent onlaps (i.e. wedge-shaped unit DO1) in the Early to Late Ordovician In Tahouite series (Tassili-N-Ajjers, Tihemboka inter-basin boundary secondary arch between the Illizi and Murzuq basins). (B) Ancient normal fault F2 escarpment reactivated and sealed during Silurian deposition (poly-historic paleo-reliefs) linked to thickness variation, divergent onlaps (DO2) in the hanging wall synclines, and onlaps on the fold hinge anticline (Tassili-N-Ajjers, Tihemboka inter-basin boundary secondary arch between the Illizi and Murzuq basins). 1: Early to Late Ordovician extension, 2: Late Ordovician to Early Silurian extension, 3: Middle to Late Silurian sealing (horizontal drape). (C) Normal fault (F5) associated with forced fold with divergent strata (syncline-shaped hanging wall syncline and associated wedge-shaped unit DO2) and truncation in Silurian–Devonian series of Dejbel Settaf (Arak-Foum Belrem arch; inter-basin boundary secondary arch between the Mouydir and Ahnet basins). 1: Cambrian–Ordovician extension, 2: Silurian–Devonian extensional reactivation (Caledonian extension). (D) Blind basement normal fault (F1) associated with forced fold with in the hanging wall syncline divergent onlaps of Lower to Upper Devonian series (wedge-shaped unit DO3) and intra-Emsian truncation (Arak-Foum Belrem arch; inter-basin boundary secondary arch between the Mouydir and Ahnet basins). (E) N170° normal blind faults F1 and F2 forming a horst-graben system associated with forced fold with Lower to Upper Devonian series divergent onlaps (wedge-shaped unit DO3) and intra-Emsian truncation in the hanging-wall syncline (in the Mouydir basin near Arak-Foum Belrem arch, eastward inter-basin boundary secondary arch). (F) Inherited normal fault F1 transported from footwall to hanging wall associated with inverse fault F1' and accommodated by a detachment layer in Silurian shales series (thickness variation of Imirhou Fm. between footwall and hanging wall) and spilled dip strata markers of overturned folding (Djebel Idjerane, Arak-Foum Belrem arch, eastwards inter-basin boundary secondary arch). 1:

Cambrian–Ordovician extension, 2: Middle to Late Devonian compression. *OTh*: In Tahouite Fm. (Early to Late Ordovician, Floian to Katian), *OTj*: Tamadjert Fm (Late Ordovician, Hirnantian), *sIm*: Imirhou Fm. (Early to Mid-Silurian), *sdAt*: Atafaïtafa Fm. (Middle Silurian), *dTi*: Tifernine Fm. (Middle Silurian), *sdAs1*: Asedjrad Fm. 1 (Late Silurian to Early Devonian), *dAs2*: Asedjrad Fm. 2 (Early Devonian, Lochkovian), *dSa*: Oued Samene Fm. (Early Devonian, Pragian), *diag*: Oued Samene shaly-sandstones Fm. (Early Devonian, Emsian?), *d2b*: Givetian, *d3a*: Mehden Yahia Fm. (Late Devonian, Frasnian), *d3b*: Mehden Yahia Fm. (Late Devonian, Famennian), *dh*: Khenig sandstones (late Famennian to early Tournaisian), *hTn2*: late Tournaisian, *hV1*: early Visean. Red line: Unconformity. See Figs. 1, 2 and 5 for map and cross-section location.

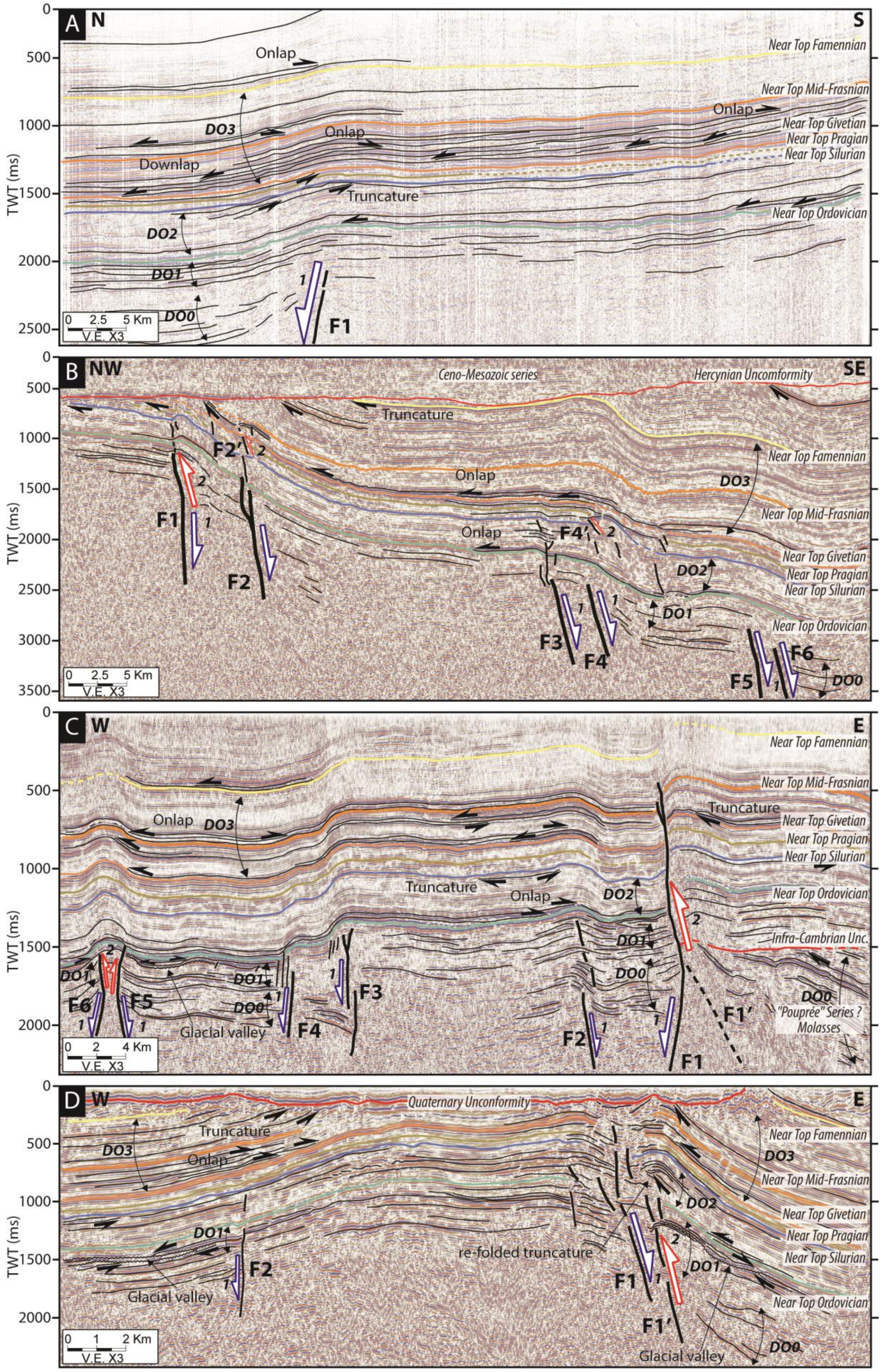
A
N
S
TWT (ms)
Near Top Famennian
Near Top Mid-Frasnian
Near Top Givetian
Near Top Pragian
Near Top Silurian
Near Top Ordovician
Onlap
Downlap
Truncature
DO3
DO2
DO1
DO0
F1
0 2.5 5 Km
V.E. X3
B
NW
SE
Ceno-Mesozoic series
Hercynian Uncomformity
Truncature
Onlap
F1
F2
F2'
F3
F4
F4'
F5
F6
C
W
E
Infra-Cambrian Unc.
"Pouprée" Series ?
Molasses
Glacial valley
F1'
0 2 4 Km
D
Quaternary Unconformity
re-folded truncature
0 1 2 Km

Figure 7: (A) N–S interpreted seismic profile in the Ahnet basin near Erg Tegunentour (near Arak-Foum Belrem arch, westward inter-basin boundary secondary arch) showing steeply-dipping northward basement normal blind faults associated with forced folding. (B) NW–SE interpreted seismic profile of near Azzel Matti arch (inter-basin principal arch) showing steeply-dipping south-eastwards basement normal blind faults associated with forced folds. The westernmost structures are featured by reverse fault related propagation fold. (C) W–E interpreted profile of the Ahnet basin (Arak-Foum Belrem arch, westward inter-basin boundary secondary arch) showing horst and graben structures influencing Paleozoic tectonics associated with forced folds. (D) W–E interpreted seismic profile of Bahar el Hammar in the Ahnet basin (Ahnet intra-basin secondary arch) showing steeply-dipping normal faults F1 and F2 forming a horst positively inverted associated with folding. Multiple activation and inversion of normal faults are correlated to divergent onlaps (wedge-shaped units): DO0 Infra-Cambrian extension, DO1 Cambrian–Ordovician extension, DO2 Silurian extension with local Silurian–Devonian positive inversion, and DO3 Frasnian–Famennian extension-local compression. See figure 2 for map and cross-section location.

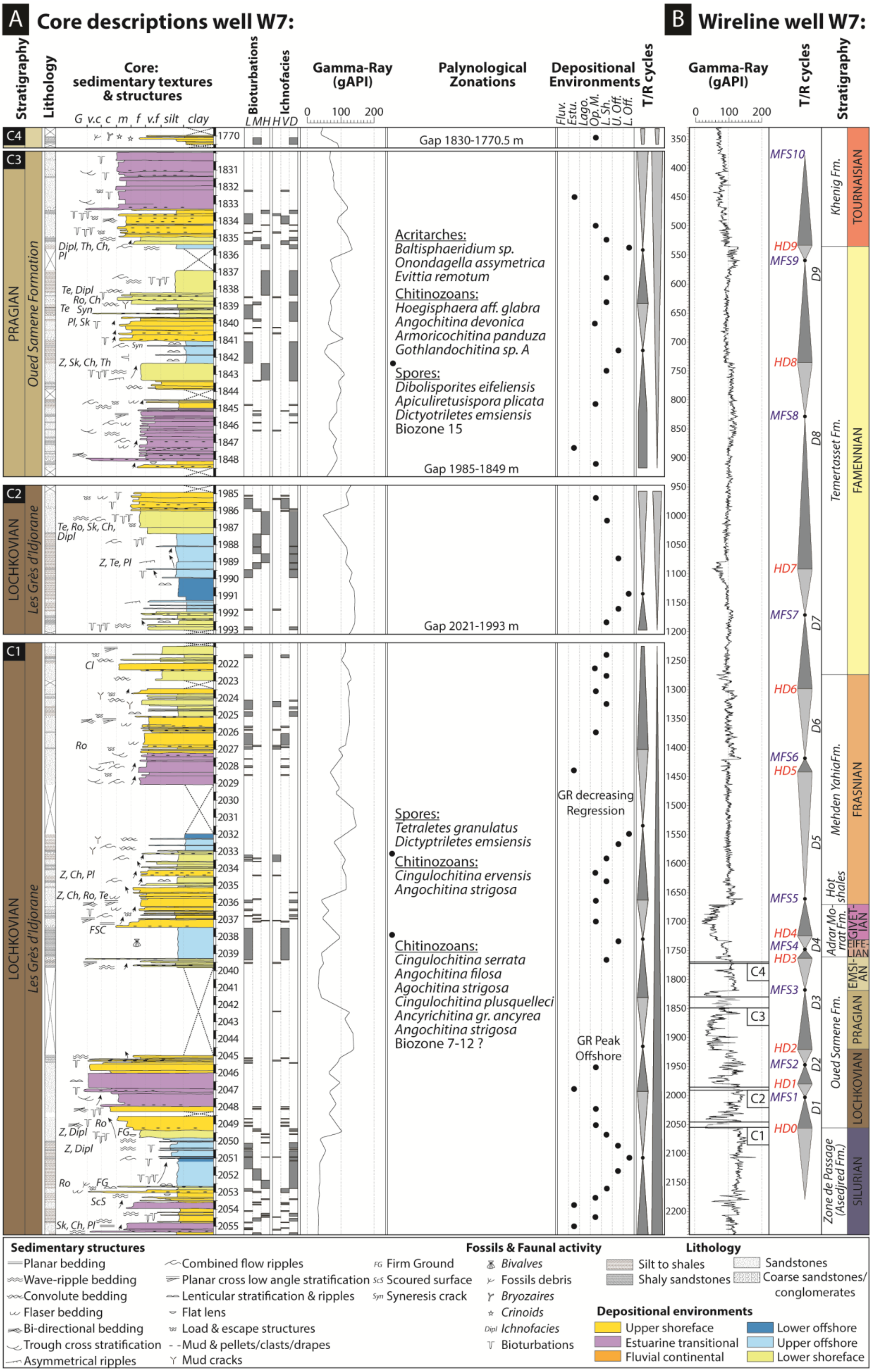
A Core descriptions well W7:
B Wireline well W7:
Stratigraphy
Lithology
Core: sedimentary textures & structures
Bioturbations
Ichnofacies
Gamma-Ray (gAPI)
Palynological Zonations
Depositional Environments
T/R cycles
Gap 1830-1770.5 m
PRAGIAN
Oued Samene Formation
Acritarches:
Baltisphaeridium sp.
Onondagella assymetrica
Evittia remotum
Chitinozoans:
Hoegisphaera aff. glabra
Angochitina devonica
Armoricochitina panduza
Gothlandochitina sp. A
Spores:
Dibolisporites eifeliensis
Apiculiretusispora plicata
Dictyotriletes emsiensis
Biozone 15
Gap 1985-1849 m
LOCHKOVIAN
Les Grès d'Idjorane
Gap 2021-1993 m
GR decreasing Regression
Spores:
Tetraletes granulatus
Dictyptriletes emsiensis
Chitinozoans:
Cingulochitina ervensis
Angochitina strigosa
Chitinozoans:
Cingulochitina serrata
Angochitina filosa
Agochitina strigosa
Cingulochitina plusquelleci
Ancyrichitina gr. ancyrea
Angochitina strigosa
Biozone 7-12 ?
GR Peak Offshore
Khenig Fm.
TOURNAISIAN
Temertasset Fm.
FAMENNIAN
Mehden YahiaFm.
FRASNIAN
Hot shales
Adrar Mo-rrat Fm.
GIVET-IAN
EIFE-LIAN
EMSI-AN
Oued Samene Fm.
PRAGIAN
LOCHKOVIAN
Zone de Passage (Asedjred Fm.)
SILURIAN
MFS10 HD9 MFS9 HD8 MFS8 HD7 MFS7 HD6 MFS6 HD5 MFS5 HD4 MFS4 HD3 MFS3 HD2 MFS2 HD1 MFS1 HD0
Sedimentary structures
Planar bedding
Wave-ripple bedding
Convolute bedding
Flaser bedding
Bi-directional bedding
Trough cross stratification
Asymmetrical ripples
Combined flow ripples
Planar cross low angle stratification
Lenticular stratification & ripples
Flat lens
Load & escape structures
Mud & pellets/clasts/drapes
Mud cracks
Firm Ground
Scoured surface
Syneresis crack
Fossils & Faunal activity
Bivalves
Fossils debris
Bryozaires
Crinoids
Ichnofacies
Bioturbations
Lithology
Silt to shales
Shaly sandstones
Sandstones
Coarse sandstones/ conglomerates
Depositional environments
Upper shoreface
Estuarine transitional
Fluvial continental
Lower offshore
Upper offshore
Lower shoreface

Figure 8: (A) Core description, palynological calibration and gamma-ray signatures of well W7 modified from internal core description report (Dokka, 1999) and internal palynological report (Azzoune, 1999). (B) Devonian sequential stratigraphy of well-log W7. For location of well W7 see figure 2A.

| Criteria & characteristics | | | | | Formations | Depositional environments | |
|---|---|---|---|---|---|---|---|
| Facies associations | Textures/Lithology | Sedimentary structures | Biotic/non biotic grains | Ichnofacies | | | |
| AF1 | Conglomerates, mid to coarse sandstones, siltstones, shales | Trough cross-bedding, mud clasts, lag deposits, fluidal and overturn structures, imbricated grains, lenticular laminations, oblique stratification | Rare oolitic intercalations, imbricated pebbles, sandstones, ironstones, phosphorites, corroded quartz grains, calcareous matrix, brachiopod coquinas, phosphatized pebbles, hematite, azurite, quartz | Rare bioturbation | Oued Samene Fm., Barre Supérieur, Barre Moyenne | Fluvial | Continental (Fluvial) |
| AF2 | Silt to argillaceous fine sandstone | Current ripples, climbing ripples, crevasse splay, root traces, paleosols, plant debris | Nodules, ferruginous horizon | | Oued Samene Fm., Barre Supérieur, Barre Moyenne | Flood plain | Continental (Fluvial) |
| AF3a | Fine to coarse sandstones, argillaceous siltstones, shales (heterolithic) | Trough cross-bedding, some planar bedding, flaser bedding, mud clasts, mud drapes, root trace, desiccation cracks, water escape, wavy bedding, shale pebble, sigmoidal cross-bedding | Brachiopods, trilobites, tentaculites graptolites | Bioturbations, *Skolithos* (Sk), *Planolites*, (Pl) | Oued Samene Fm., Grès du Khenig, Barre Supérieur, Barre Moyenne | Delta/Estuarine channels | Coastal Plain (Transitional Marine/Continental) |
| AF3b | Very coarse-grained poorly sorted sandstone | Trough cross-bedding, sigmoidal cross-bedding, abundant mud clasts and mud drapes | | Increasing upward bioturbation *Skolithos* (Sk) | Oued Samene Fm., Grès du Khenig, Barre Supérieur, Barre Moyenne | Fluvial/Tidal distributary channels | Coastal Plain (Transitional Marine/Continental) |
| AF3c | Fine-grained to very coarse-grained heterolithic sandstone | Sigmoidal cross-bedding with multidirectional tidal bundles, wavy, lenticular, flaser bedding, occasional current and oscillation ripples, occasional mud cracks | | Intense bioturbation, *Skolithos* (Sk), *Planolites*, (Pl), *Thalassinoides* (Th) | Talus à Tigillites | Tidal sand flat | Coastal Plain (Transitional Marine/Continental) |
| AF3d | Mudstones, varicolored shales, thin sandstone layers | Occasional wave ripples, mud cracks, horizontal lamination, rare multi-directional ripples | Absence of ammonoids, goniatites, calymenids, pelecypod molds, brachiopods coquinas | Intense bioturbation, *Skolithos* (Sk), *Planolites*, (Pl), *Thalassinoides* (Th) | Oued Samene Fm., Grès du Khenig, Atafaitafa Fm. | Lagoon/Mudflat | Coastal Plain (Transitional Marine/Continental) |
| AF4a | Silty mudstone associated with coarse to very coarse argillaceous sandstone, poorly sorted, heterolithic silty mudstone | Sigmoidal cross-bedding, abundant mud clasts, wavy, lenticular cross-bedding and flaser bedding, abundant current and oscillation ripples, mud drapes | Shell debris (crinoids, brachiopods) | Strongly bioturbated *Skolithos* (Sk), *Planolites*, (Pl) | Oued Samene Fm., Talus à Tigillites | Subtidal | Shoreface |
| AF4b | Fine to mid grained sandstones interbedded with argillaceous siltstone and mudstone, bioclastic carbonates sandstones, brownish sandstones and clays, silts | Oscillation ripples, swaley cross-bedding, bidirectional bedding, flaser bedding, rare hummocky cross-bedding, mud cracks (syneresis), convolute bedding, wavy bedding, combined flow ripples, planar cross low angle stratification, cross-bedding, ripple marks, centimetric bedding, shale pebbles | Ooids, crinoids, bryozoans, coral clasts, fossil debris, stromatoporoids, tabulates, colonial rugose corals, myriad pelagic styliolinids, neritic tentaculitids, brachiopods, iron ooliths, abundant micas | *Skolithos* (Sk), *Cruziana*, *Planolites*, (Pl) *Chondrites* (Ch), *Teichichnus* (Te), *Spirophytons* (Sp) | Atafaitafa Fm., Zone de passage, Grès de Mehden Yahia, Calcaires d'Azzel Matti | Open marine-upper shoreface | Shoreface |
| AF4c | Silty shales to fine sandstones (heterolithic) | Hummocky cross-bedding, planar bedding, combined flow ripples, convolute bedding, dish structures, mud drapes, remnant ripples, flat lenses, slumping | Intense bioturbation, *Cruziana* | *Thalassinoides* (Th), *Planolites* (Pl), *Skolithos* (Sk), *Diplocraterion* (Dipl), *Teichichnus* (Te), *Chondrites* (Ch), *Rogerella* (Ro), *Climactichnites* (Cl) | Atafaitafa Fm., Zone de passage, Grès de Mehden Yahia, Calcaires d'Azzel Matti | Lower shoreface | Shoreface |
| AF5a | Grey silty-shales, bundles of skeletal wackestones, silty greenish shale interlayers fine grained sandstones, calcareous mudstones, black shales, polychrome clays (black, brown, grey, green, red, pink), grey and reddish shales | Lenticular sandstones, rare hummocky cross-bedding, mud mounds, mud buildups, low-angle cross-bedding, tempestite bedding, slumping, deep groove marks | Intensive burrowing, bivalve debris, horizontal burrows, skeletal remains (goniatites, orthoconic, nautiloids, styliolinids, trilobites, crinoids, solitary rugose, corals, limestones nodules, ironstone nodules and layers | *Zoophycos* (Z), *Teichichnus* (Te), *Planolites* (Pl) | Argiles à Graptolites, Orsine Fm., Argiles de Mehden Yahia, Argiles de Temertasset | Upper offshore | Offshore |
| AF5b | Black silty-shales (mudstones), bituminous mudstones-wackestones, packstones | Rare structures | parallel-aligned styliolinids, gonitaties, orthoconic nautiloids, pelagic pelecypod *Buchiola*, anoxic conditions, limestone nodules, goniatites, *Buchiola*, *tentaculitids*, ostracods and rare fish remains, *Tornoceras*, *Aulatornoceras*, *Lobotornoceras*, *Manticoceras*, *Costamanticoceras* and *Virginoceras*, graptolites | *Zoophycos* (Z) | Argiles à Graptolites, Orsine Fm., Argiles de Mehden Yahia, Argiles de Temertasset | Lower offshore | Offshore |

Table 1: Synthesis of facies associations (AF1 to AF5), depositional environments, and electrofacies in the Devonian series compiled from internal (Eschard et al., 1999) and published studies (Beuf et al., 1971; Biju-Duval et al., 1968; Wendt et al., 2006).

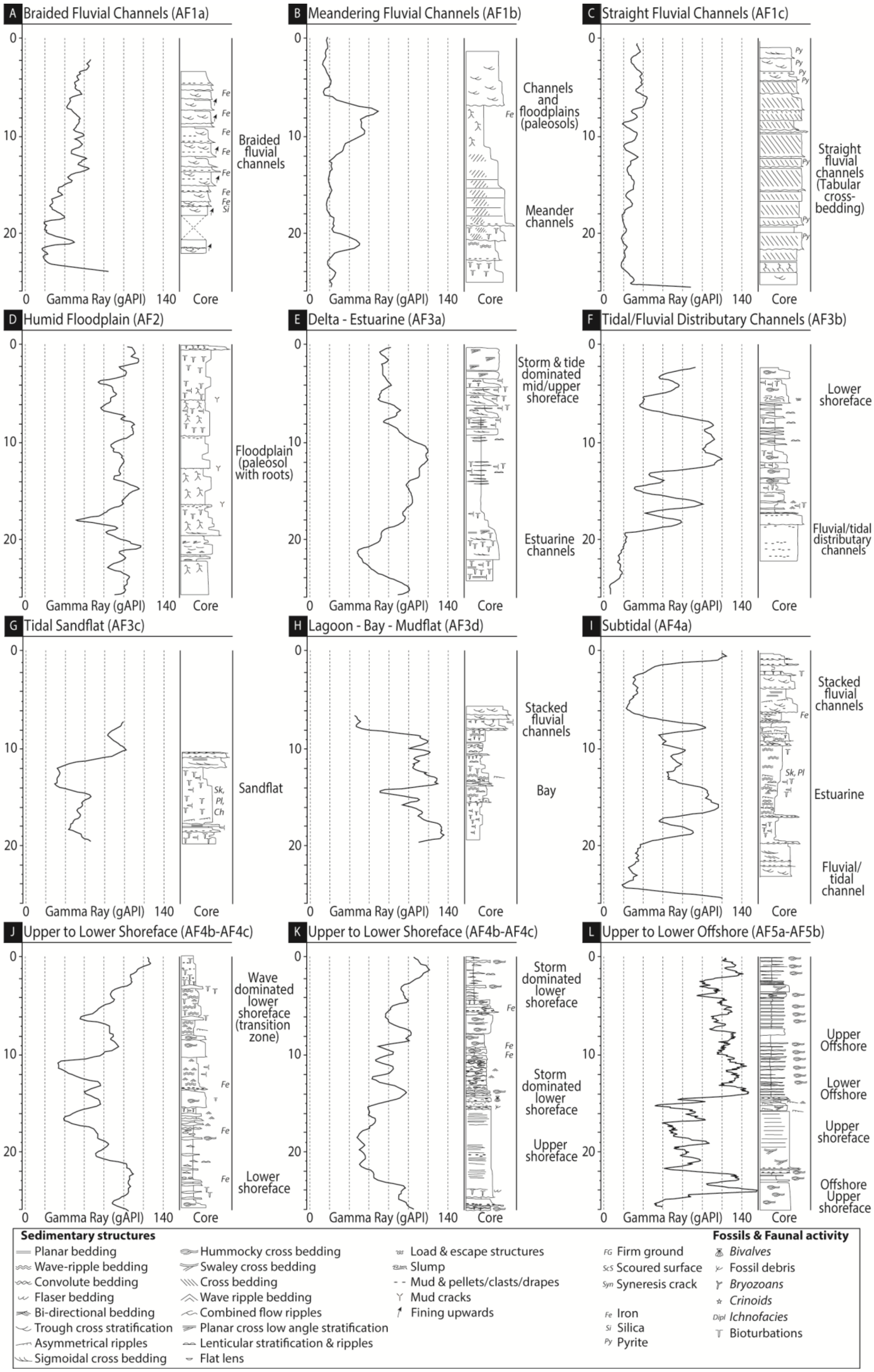
A Braided Fluvial Channels (AF1a)
Braided fluvial channels
B Meandering Fluvial Channels (AF1b)
Channels and floodplains (paleosols)
Meander channels
C Straight Fluvial Channels (AF1c)
Straight fluvial channels (Tabular cross-bedding)
D Humid Floodplain (AF2)
Floodplain (paleosol with roots)
E Delta - Estuarine (AF3a)
Storm & tide dominated mid/upper shoreface
Estuarine channels
F Tidal/Fluvial Distributary Channels (AF3b)
Lower shoreface
Fluvial/tidal distributary channels
G Tidal Sandflat (AF3c)
Sandflat
H Lagoon - Bay - Mudflat (AF3d)
Stacked fluvial channels
Bay
I Subtidal (AF4a)
Stacked fluvial channels
Estuarine
Fluvial/ tidal channel
J Upper to Lower Shoreface (AF4b-AF4c)
Wave dominated lower shoreface (transition zone)
Lower shoreface
K Upper to Lower Shoreface (AF4b-AF4c)
Storm dominated lower shoreface
Storm dominated lower shoreface
Upper shoreface
L Upper to Lower Offshore (AF5a-AF5b)
Upper Offshore
Lower Offshore
Upper shoreface
Offshore
Upper shoreface
0 Gamma Ray (gAPI) 140 Core
Sedimentary structures
Planar bedding
Wave-ripple bedding
Convolute bedding
Flaser bedding
Bi-directional bedding
Trough cross stratification
Asymmetrical ripples
Sigmoidal cross bedding
Hummocky cross bedding
Swaley cross bedding
Cross bedding
Wave ripple bedding
Combined flow ripples
Planar cross low angle stratification
Lenticular stratification & ripples
Flat lens
Load & escape structures
Slump
Mud & pellets/clasts/drapes
Mud cracks
Fining upwards
FG Firm ground
ScS Scoured surface
Syn Syneresis crack
Fe Iron
Si Silica
Py Pyrite
Fossils & Faunal activity
Bivalves
Fossil debris
Bryozoans
Crinoids
Dipl Ichnofacies
Bioturbations

Figure 9: The main depositional environments (A to L) and their associated electrofacies (i.e. gamma-ray patterns) modified and compiled from (Eschard et al., 1999).

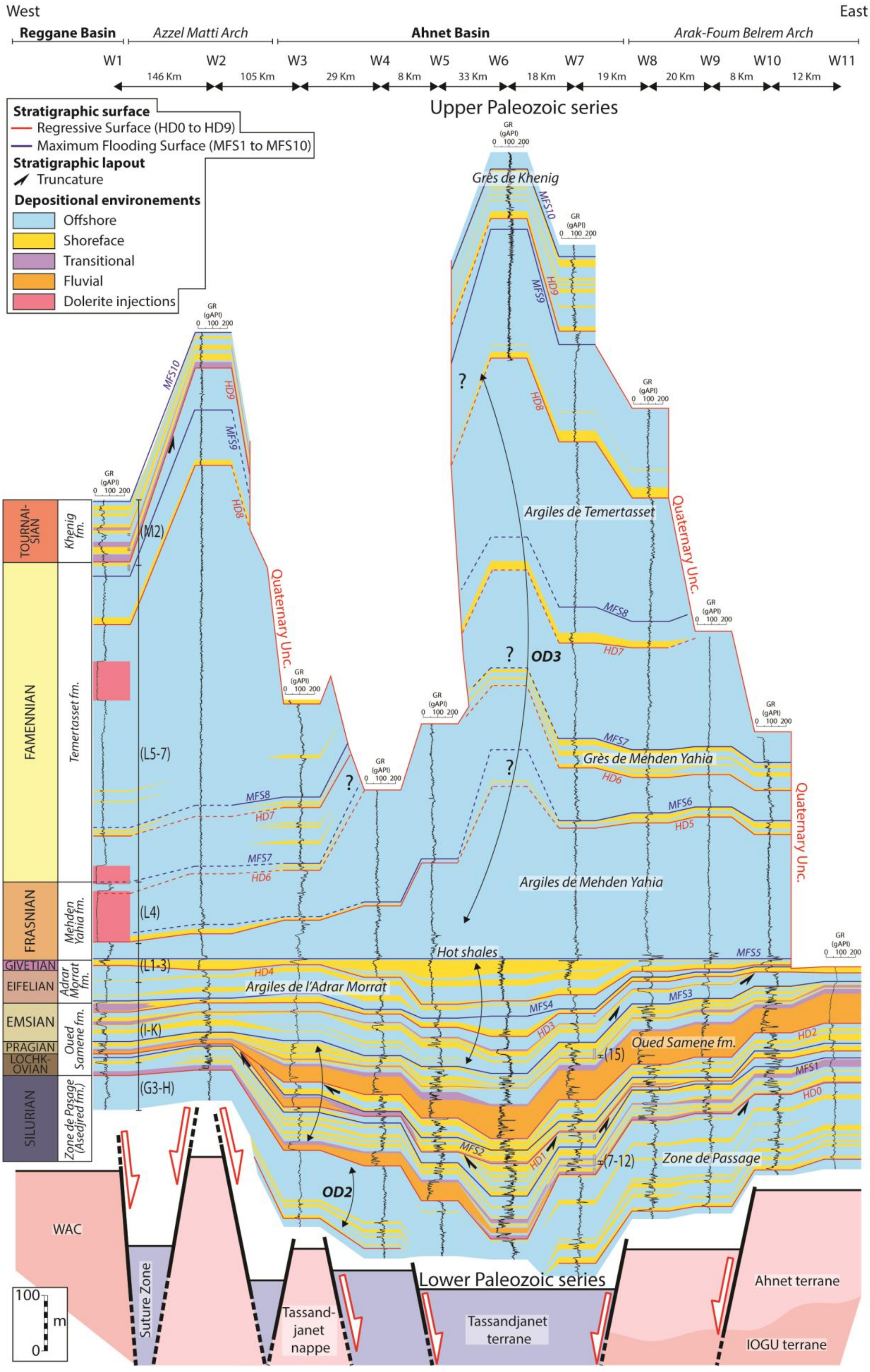

West
East
Reggane Basin
Azzel Matti Arch
Ahnet Basin
Arak-Foum Belrem Arch
W1 W2 W3 W4 W5 W6 W7 W8 W9 W10 W11
146 Km
105 Km
29 Km
8 Km
33 Km
18 Km
19 Km
20 Km
8 Km
12 Km
Upper Paleozoic series
Stratigraphic surface
Regressive Surface (HD0 to HD9)
Maximum Flooding Surface (MFS1 to MFS10)
Stratigraphic lapout
Truncature
Depositional environements
Offshore
Shoreface
Transitional
Fluvial
Dolerite injections
Grès de Khenig
Argiles de Temertasset
Quaternary Unc.
OD3
Grès de Mehden Yahia
Argiles de Mehden Yahia
Hot shales
Argiles de l'Adrar Morrat
Oued Samene fm.
Zone de Passage
OD2
TOURNAI-SIAN
FAMENNIAN
FRASNIAN
GIVETIAN
EIFELIAN
EMSIAN
PRAGIAN
LOCHK-OVIAN
SILURIAN
Khenig fm.
Temertasset fm.
Mehden Yahia fm.
Adrar Morrat fm.
Oued Samene fm.
Zone de Pasage (Asedjred fm.)
(M2)
(L5-7)
(L4)
(L1-3)
(I-K)
(G3-H)
WAC
Suture Zone
Tassand-janet nappe
Lower Paleozoic series
Tassandjanet terrane
Ahnet terrane
IOGU terrane
100 m 0


1478

Figure 10: SE–W cross-section between the Reggane basin, Azzel Matti arch, Ahnet basin, Arak-Foum Belrem arch, Mouydir basin, and Amguid El Biod arch (well locations in fig. 3). Well W1 biozone calibration from Hassan, (1984) internal report is based on Magloire, (1967) classification: biozone G3-H (Wenlock–Ludlow, Upper Silurian), biozone I-K (Lochkovian–Emsian, Lower Devonian), biozone L1-3 (Eifelian–Givetian, Middle Devonian), biozone L4 (Frasnian, Upper Devonian), biozone L5-7 (Famennian, Upper Devonian), biozone M2 (Tournaisian–Lower Carboniferous). Well W7 biozone calibration from Azzoune, (1999) internal report is based on Boumendjel, (1987) classification: biozone 7-12 (Lochkovian, Lower Devonian), biozone 15 (Emsian, Lower Devonian). Interpretation of the basement is based on Figs. 1, 2 and 15. Well location is in Fig. 2.

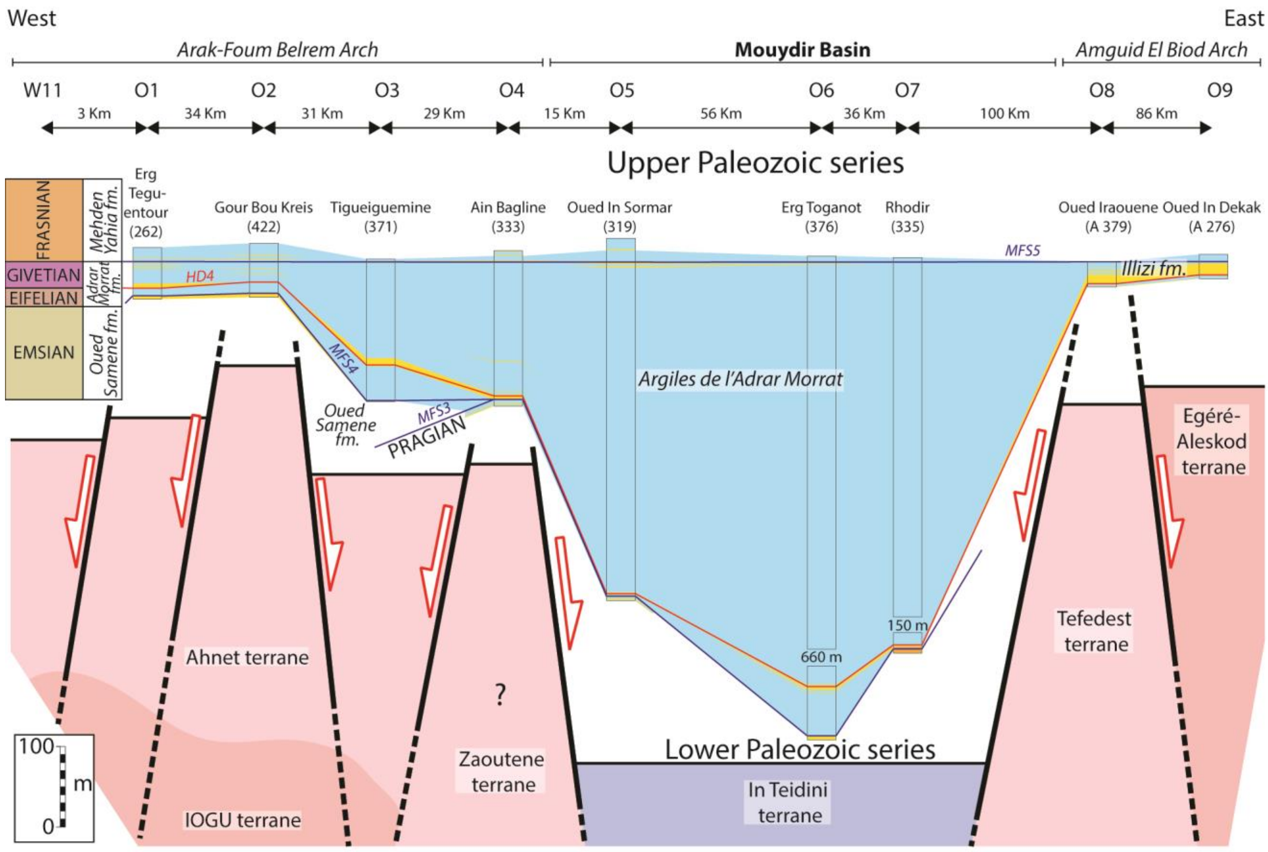


Figure 11: SE–W cross-section between the Arak-Foum Belrem arch, the Mouydir basin and the Amguid El Biod arch. Outcrop cross-section correlations and biostratigraphic calibrations

are based on the compilation of published papers (Wendt et al., 2006, 2009b). Interpretation of the basement is based on Figs. 1, 2 and 15. Outcrop location is in Fig. 2.

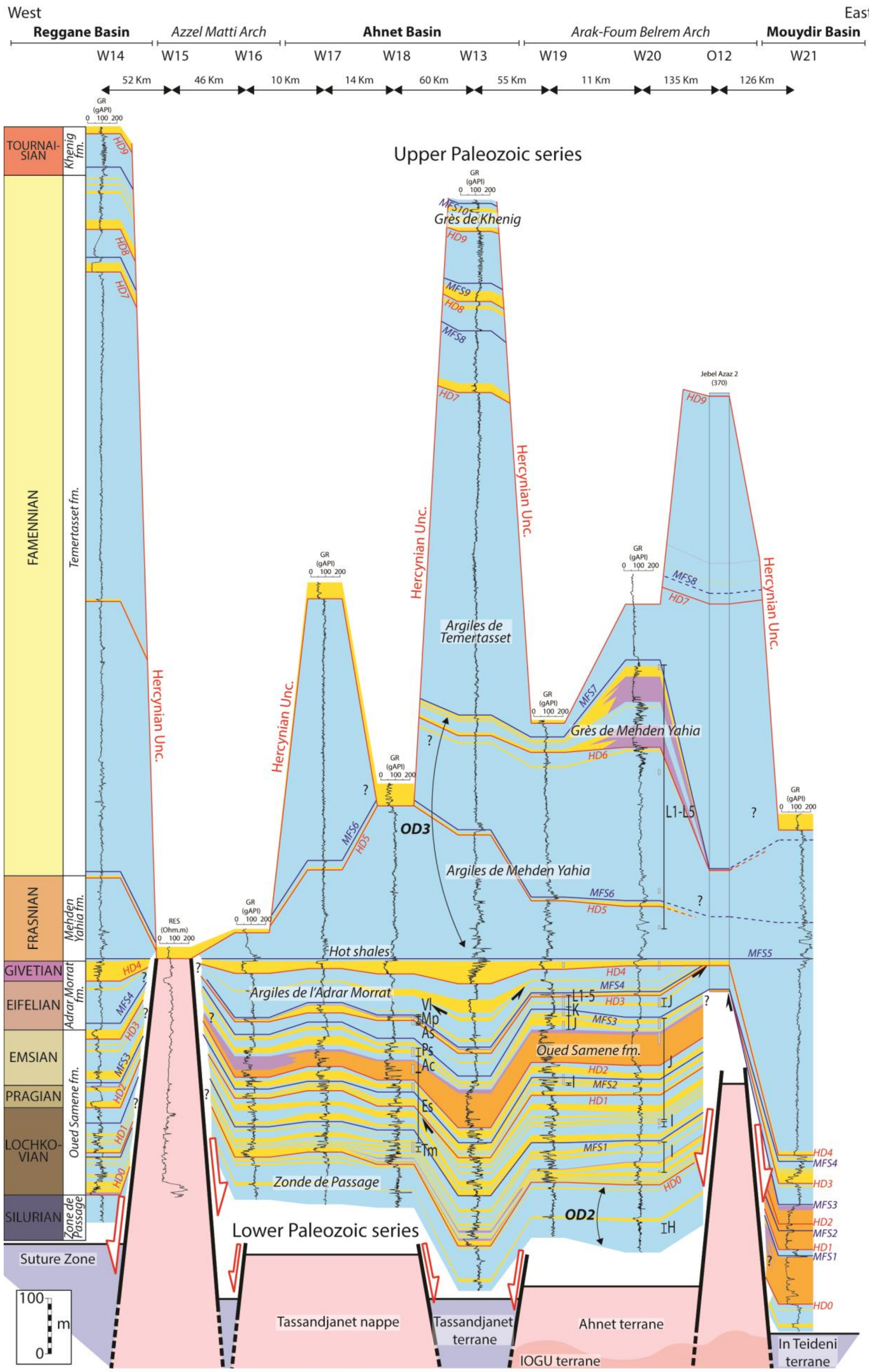
West
East
Reggane Basin
Azzel Matti Arch
Ahnet Basin
Arak-Foum Belrem Arch
Mouydir Basin
W14
W15
W16
W17
W18
W13
W19
W20
O12
W21
52 Km
46 Km
10 Km
14 Km
60 Km
55 Km
11 Km
135 Km
126 Km
TOURNAISIAN
FAMENNIAN
FRASNIAN
GIVETIAN
EIFELIAN
EMSIAN
PRAGIAN
LOCHKOVIAN
SILURIAN
Khenig fm.
Temertasset fm.
Mehden Yahia fm.
Adrar Morrat fm.
Oued Samene fm.
Zone de Passage
Upper Paleozoic series
Lower Paleozoic series
Grès de Khenig
Argiles de Temertasset
Grès de Mehden Yahia
Argiles de Mehden Yahia
Hot shales
Argiles de l'Adrar Morrat
Oued Samene fm.
Zonde de Passage
Hercynian Unc.
OD3
OD2
L1-L5
Jebel Azaz 2 (370)
GR (gAPI)
RES (Ohm.m)
Suture Zone
Tassandjanet nappe
Tassandjanet terrane
Ahnet terrane
IOGU terrane
In Teideni terrane
100 m 0

Figure 12: NE–W cross-section between the Reggane basin, Azzel Matti arch, Ahnet basin, Arak-Foum Belrem arch, Mouydir basin, and Amguid El Biod arch. Well W18 biozone calibration is based on Kermandji et al., (2009): biozone (Tm) *tidikeltense microbaculatus* (Lochkovian, Lower Devonian), biozone (Es) *emsiensis spinaeformis* (Lochkovian-Pragian, Lower Devonian), biozone (Ac) *arenorugosa caperatus* (Pragian, Lower Devonian), biozone (Ps) *poligonalis subgranifer* (Pragian–Emsian, Lower Devonian), biozone (As) *annulatus svalbardiae* (Emsian, Lower Devonian), biozone (Mp) *microancyreus protea* (Emsian–Eifelian, Lower to Middle Devonian), biozone (Vl) *velatus langii* (Eifelian, Middle Devonian). Well W19 and W20 biozones calibration from internal reports (Abdesselam-Rouighi, 1991; Khiar, 1974) is based on Magloire, (1967) classification: biozone H (Pridoli, Upper Silurian), biozone I (Lochkovian, Lower Devonian), biozone J (Pragian, Lower Devonian), biozone K (Emsian, Lower Devonian), biozone L1-5 (Middle Devonian to Upper Devonian). Interpretation of the basement is based on Figs. 1, 2 and 15. Outcrop and well location is in Fig. 2.

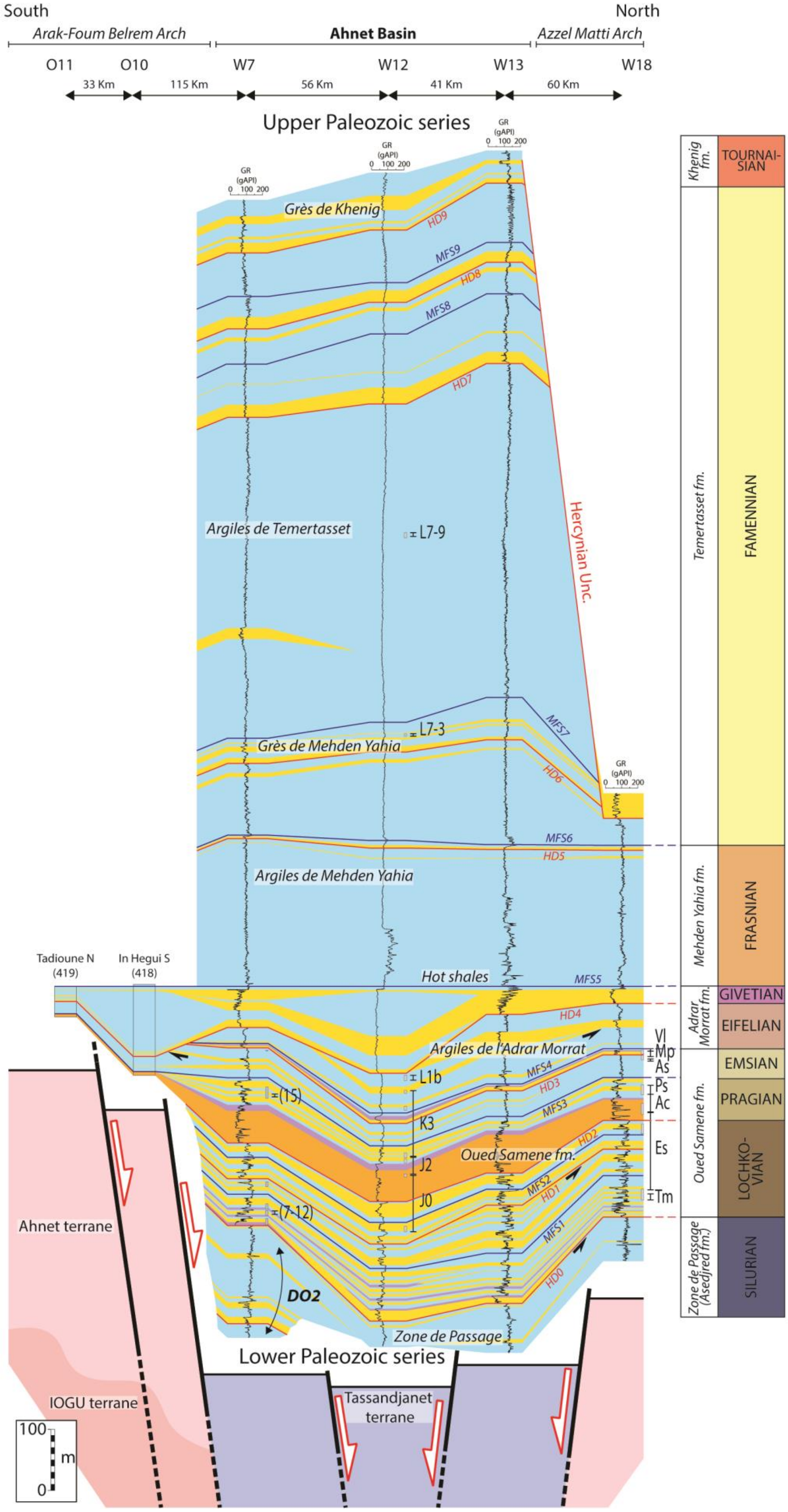
South
North
Arak-Foum Belrem Arch
Ahnet Basin
Azzel Matti Arch
O11
O10
W7
W12
W13
W18
33 Km
115 Km
56 Km
41 Km
60 Km
Upper Paleozoic series
Grès de Khenig
HD9
MFS9
HD8
MFS8
HD7
Argiles de Temertasset
L7-9
Hercynian Unc.
MFS7
L7-3
Grès de Mehden Yahia
HD6
MFS6
HD5
Argiles de Mehden Yahia
Tadioune N (419)
In Hegui S (418)
Hot shales
MFS5
HD4
Argiles de l'Adrar Morrat
MFS4
HD3
MFS3
HD2
Oued Samene fm.
MFS2
HD1
MFS1
HD0
L1b
(15)
K3
J2
J0
(7-12)
DO2
Zone de Passage
Lower Paleozoic series
Vl
Mp
As
Ps
Ac
Es
Tm
Ahnet terrane
IOGU terrane
Tassandjanet terrane
100
m
0
Khenig fm.
Temertasset fm.
Mehden Yahia fm.
Adrar Morrat fm.
Oued Samene fm.
Zone de Passage (Asedjred fm.)
TOURNAISIAN
FAMENNIAN
FRASNIAN
GIVETIAN
EIFELIAN
EMSIAN
PRAGIAN
LOCHKOVIAN
SILURIAN
GR (gAPI) 0 100 200

1511

Figure 13: N–S cross-section in the Ahnet basin between Azzel Matti arch and Arak-Foum Belrem arch; Well W7 biozone calibration from Azzoune, (1999) internal report based on Boumendjel, (1987) classification: biozones 7–12 (Lochkovian, Lower Devonian), biozone 15 (Emsian, Lower Devonian). Well W18 biozone calibration is based on Kermandji et al., (2009): biozone (Tm) *tidikeltense microbaculatus* (Lochkovian, Lower Devonian), biozone (Es) *emsiensis spinaeformis* (Lochkovian-Pragian, Lower Devonian), biozone (Ac) *arenorugosa caperatus* (Pragian, Lower Devonian), biozone (Ps) *poligonalis subgranifer* (Pragian-Emsian, Lower Devonian), biozone (As) *annulatus svalbardiae* (Emsian, Lower Devonian), biozone (Mp) *microancyreus protea* (Emsian-Eifelian, Lower to Middle Devonian), biozone (Vl) *velatus langii* (Eifelian, Middle Devonian). Well W12 biozone calibration from Abdesselam-Rouighi, (1977) internal report is based on (Boumendjel, (1987) classification: biozone J (Pragian, Lower Devonian), biozone K (Emsian, Lower Devonian), biozone L1 (Eifelian, Middle Devonian), biozone L7-3, L7-9 (Frasnian-Famennian, Upper Devonian). Interpretation of the basement is based on Figs. 1, 2 and 15. Outcrop and well location is in Fig. 2.

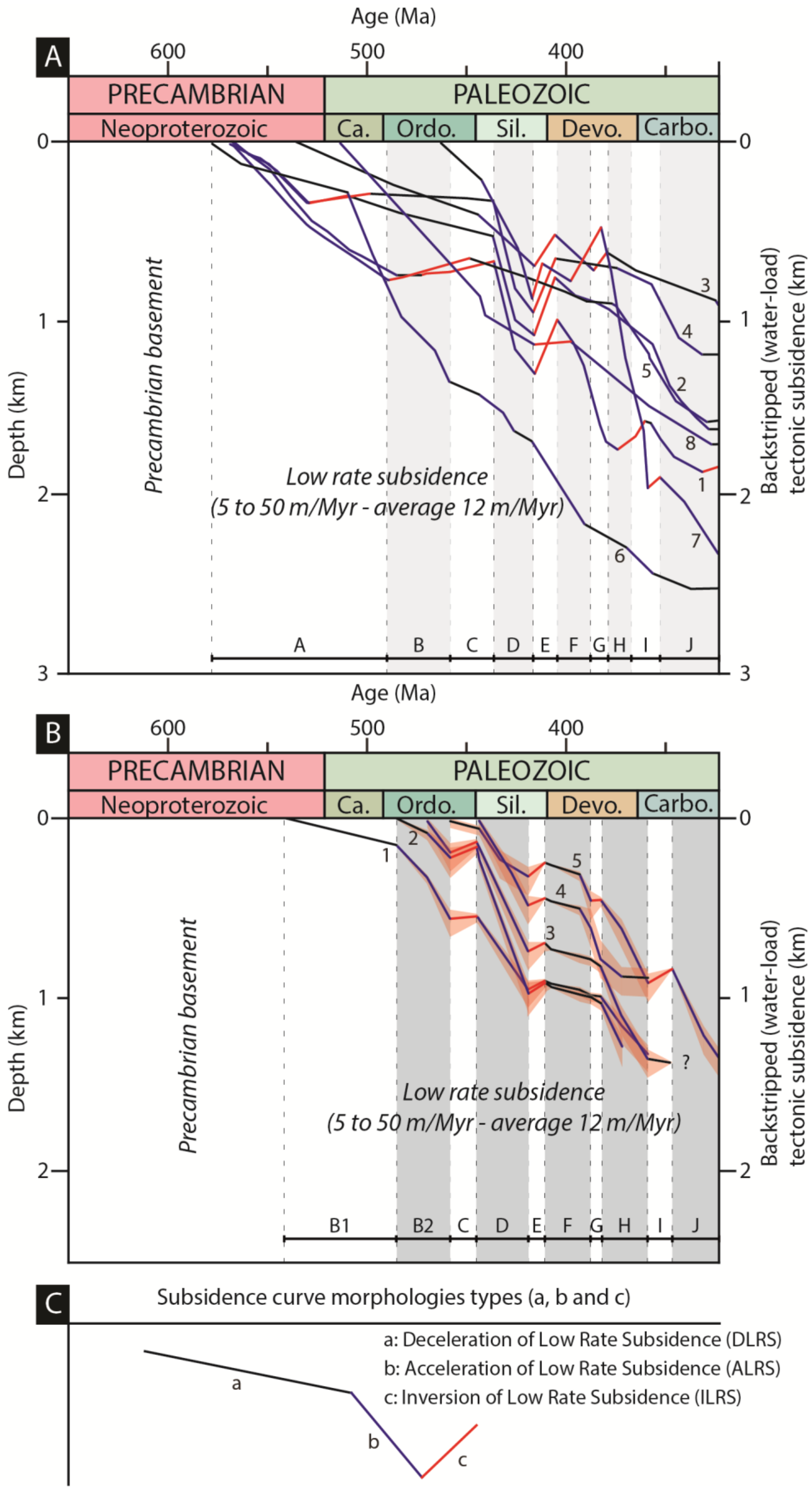
A
Age (Ma)
600
500
400
PRECAMBRIAN
PALEOZOIC
Neoproterozoic
Ca.
Ordo.
Sil.
Devo.
Carbo.
Depth (km)
Backstripped (water-load) tectonic subsidence (km)
Precambrian basement
Low rate subsidence
(5 to 50 m/Myr - average 12 m/Myr)
A B C D E F G H I J
B
Age (Ma)
600
500
400
PRECAMBRIAN
PALEOZOIC
Neoproterozoic
Ca.
Ordo.
Sil.
Devo.
Carbo.
Depth (km)
Backstripped (water-load) tectonic subsidence (km)
Precambrian basement
Low rate subsidence
(5 to 50 m/Myr - average 12 m/Myr)
B1 B2 C D E F G H I J
C
Subsidence curve morphologies types (a, b and c)
a: Deceleration of Low Rate Subsidence (DLRS)
b: Acceleration of Low Rate Subsidence (ALRS)
c: Inversion of Low Rate Subsidence (ILRS)
a
b
c

Figure 14: (A) Tectonic backstripped curves of the Paleozoic North Saharan Platform (peri-Hoggar basins) compiled from literature. 1: HAD-1 well in Ghadamès basin (Makhous and Galushkin, 2003b); 2: Well RPL-101 in Reggane basin (Makhous and Galushkin, 2003b); 3: L1-1 well in Murzuq basin (Galushkin and Eloghbi, 2014); 4: TGE-1 in Illizi basin (Makhous and Galushkin, 2003a); 5: REG-1 in Timimoun basin (Makhous and Galushkin, 2003b); 6: Ghadamès-Berkine basin (Allen and Armitage, 2011; Yahi, 1999); 7: well in Sbâa basin (Tournier, 2010); 8: well B1NC43 in Al Kufrah basin (Holt et al., 2010). (B) Tectonic backstripped curves of wells in the study area (1: well W17 in Ahnet basin; 2: well W5 in Ahnet basin; 3: well W7 in Ahnet basin; 4: well W21 in Mouydir basin; 5: well W1 in Reggane basin; (C) Typologies of subsidence curves morphologies. A: Late Pan-African compression and collapse (type a, b, and c subsidence), B: Undifferentiated Cambrian–Ordovician (type a, b, and c subsidence), B1: Cambrian–Ordovician tectonic quiescence (type a subsidence), B2: Cambrian–Ordovician extension (type b subsidence), C: Late Ordovician glacial and isostatic rebound (type c subsidence), D: Silurian extension (type b subsidence), E: Late Silurian Caledonian compression (type c subsidence), F: Early Devonian tectonic quiescence (type a subsidence), G-H: Middle to late Devonian extension with local compression (i.e. inversion structures, type b and c subsidence), I: Early Carboniferous extension with local tectonic pre-Hercynian compression (type c and b subsidence), J: Middle Carboniferous tectonic extension (type b subsidence).

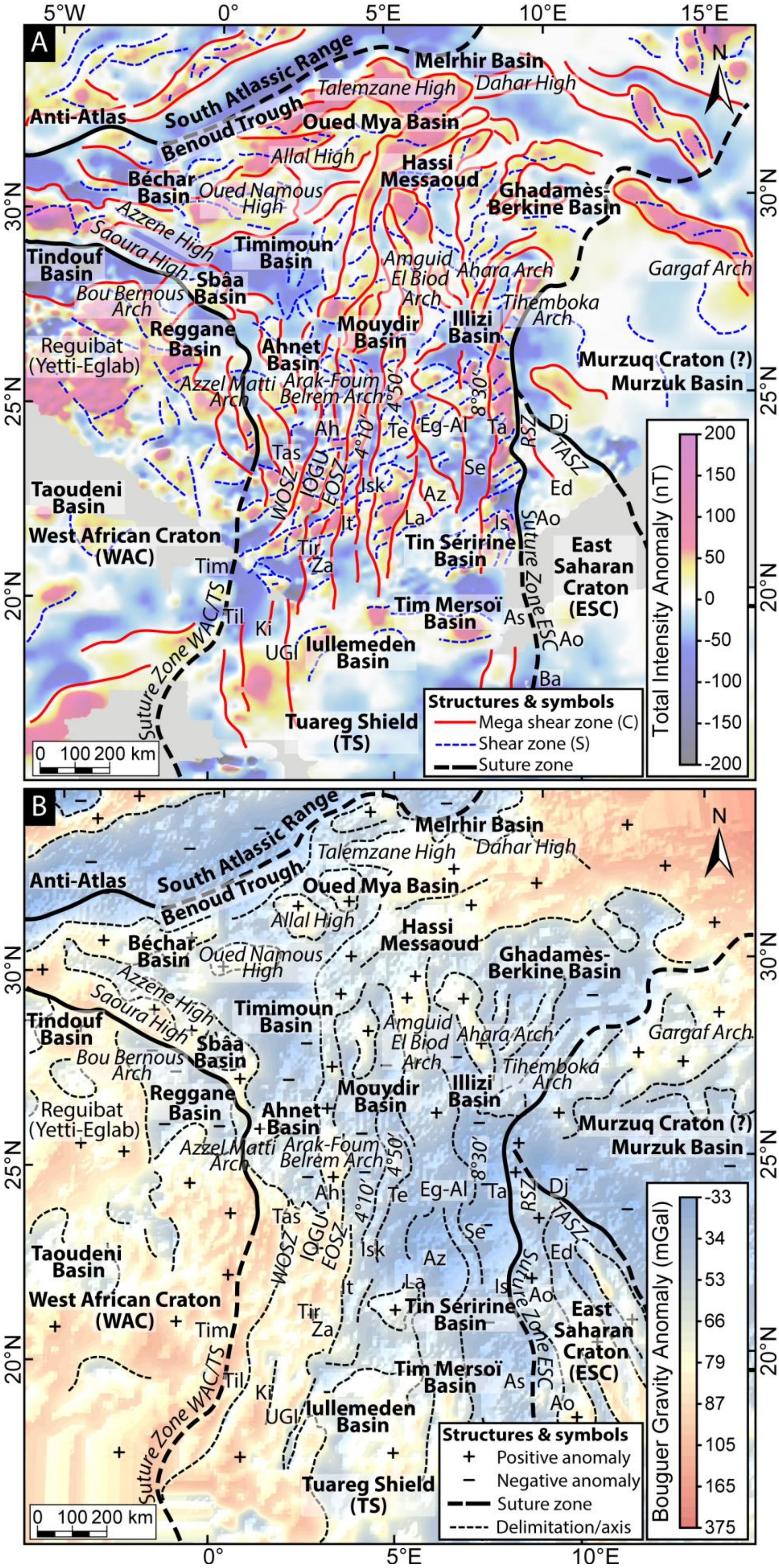
A
B
5°W
0°
5°E
10°E
15°E
30°N
25°N
20°N
South Atlassic Range
Melrhir Basin
Talemzane High
Dahar High
Anti-Atlas
Benoud Trough
Oued Mya Basin
Allal High
Hassi Messaoud
Béchar Basin
Oued Namous High
Ghadamès-Berkine Basin
Azzene High
Saoura High
Tindouf Basin
Timimoun Basin
Amguid El Biod Arch
Ahara Arch
Gargaf Arch
Sbâa Basin
Bou Bernous Arch
Tihemboka Arch
Reguibat (Yetti-Eglab)
Reggane Basin
Ahnet Basin
Mouydir Basin
Illizi Basin
Murzuq Craton (?)
Murzuk Basin
Azzel Matti Arch
Arak-Foum Belrem Arch
4°50'
8°30'
4°10'
Ah
Te
Eg-Al
Ta
Dj
RSZ
TASZ
Tas
WOSZ
IOGU
EOSZ
Isk
Se
Az
Ed
Taoudeni Basin
It
La
Is
Ao
West African Craton (WAC)
Tin Séririne Basin
East Saharan Craton (ESC)
Tir
Za
Tim
Suture Zone ESC
Suture Zone WAC/TS
Tim Mersoï Basin
Til
Ki
As
UGI
Iullemeden Basin
Ba
Tuareg Shield (TS)
0 100 200 km
N
Structures & symbols
Mega shear zone (C)
Shear zone (S)
Suture zone
Total Intensity Anomaly (nT)
200
150
100
50
0
-50
-100
-150
-200
Positive anomaly
Negative anomaly
Delimitation/axis
Bouguer Gravity Anomaly (mGal)
-33
34
53
66
79
87
105
165
375

Figure 15: (A) Interpreted aeromagnetic anomaly map (https://www.geomag.us/) of the Paleozoic North Saharan Platform (peri-Hoggar basins) showing the different terranes delimited by NS, NW–SE and NE–SW lineaments and mega-sigmoid structures (SC shear fabrics); (B) Bouguer anomaly map (from International Gravimetric Bureau: http://bgi.omp.obs-mip.fr/) of North Saharan Platform (peri-Hoggar basins) presenting evidence of positive anomalies under arches and negative anomalies under basins.

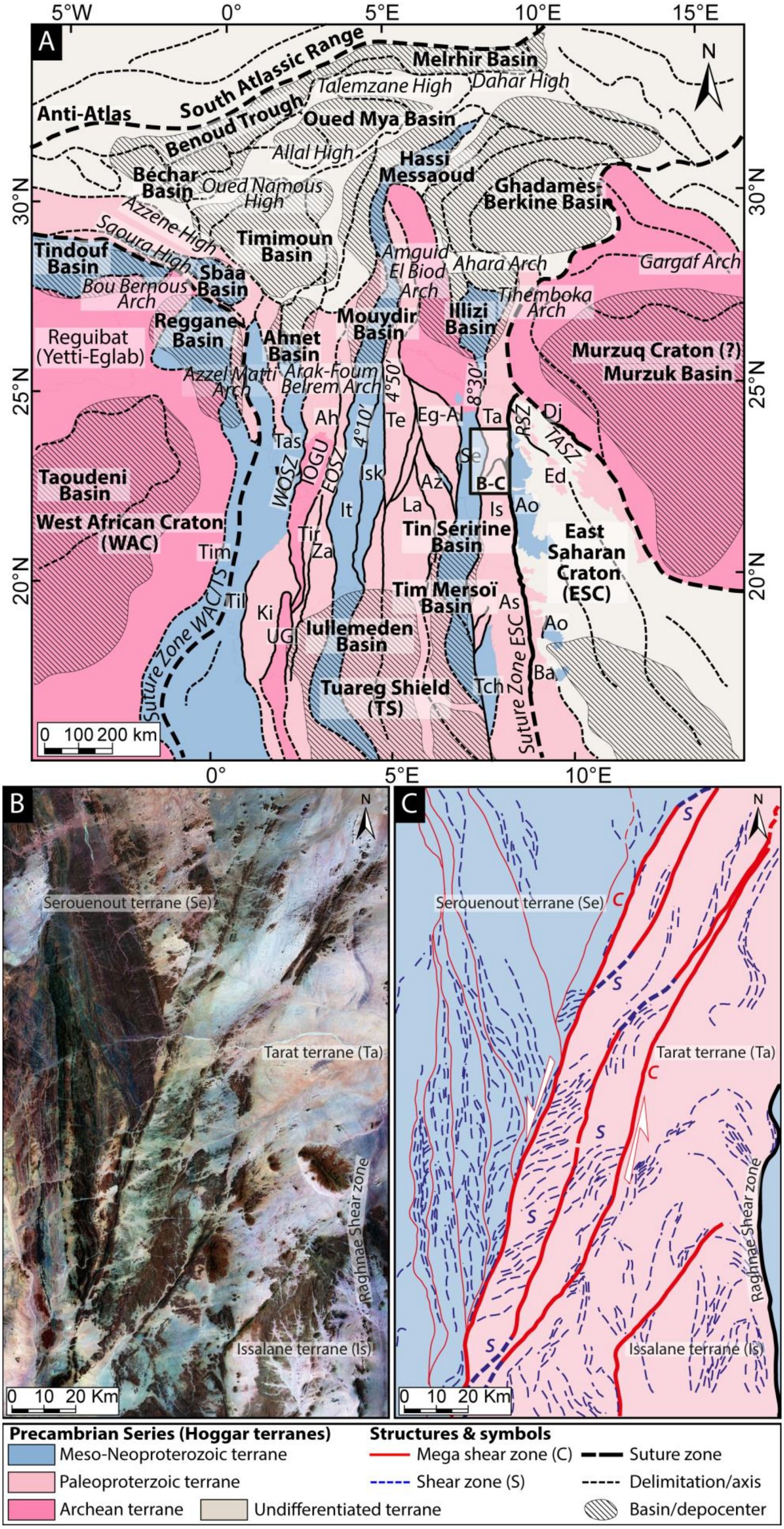
A
B
C
5°W
0°
5°E
10°E
15°E
30°N
25°N
20°N
South Atlassic Range
Melrhir Basin
Talemzane High
Dahar High
Anti-Atlas
Benoud Trough
Oued Mya Basin
Allal High
Hassi Messaoud
Béchar Basin
Oued Namous High
Ghadames-Berkine Basin
Azzene High
Saoura High
Timimoun Basin
Tindouf Basin
Sbaa Basin
Bou Bernous Arch
Amguid El Biod Arch
Ahara Arch
Gargaf Arch
Tihemboka Arch
Reguibat (Yetti-Eglab)
Reggane Basin
Ahnet Basin
Mouydir Basin
Illizi Basin
Murzuq Craton (?)
Murzuk Basin
Azzel Matti Arch
Arak-Foum Belrem Arch
Taoudeni Basin
West African Craton (WAC)
Tin Seririne Basin
East Saharan Craton (ESC)
Tim Mersoï Basin
Iullemeden Basin
Tuareg Shield (TS)
Suture Zone WACTS
Suture Zone ESC
WOSZ
IOGU
EOSZ
4°10'
4°50'
8°30'
RSZ
TASZ
B-C
0 100 200 km
Serouenout terrane (Se)
Tarat terrane (Ta)
Raghnae Shear zone
Issalane terrane (Is)
0 10 20 Km
Precambrian Series (Hoggar terranes)
Meso-Neoproterozoic terrane
Paleoproterzoic terrane
Archean terrane
Undifferentiated terrane
Structures & symbols
Mega shear zone (C)
Shear zone (S)
Suture zone
Delimitation/axis
Basin/depocenter

1555

Figure 16: (A) Interpreted map of basement terranes according to their age (compilation of data sets in Fig. 1 and supplementary data 1); (B) Satellite images (7ETM+ from USGS: https://earthexplorer.usgs.gov/) of Paleoproterozoic Issalane-Tarat terrane, Central Hoggar (see C for location); (C) Interpreted satellite images of Paleoproterozoic Issalane-Tarat terrane showing sinistral sigmoid mega-structures associated with transcurrent lithospheric shear fabrics SC.

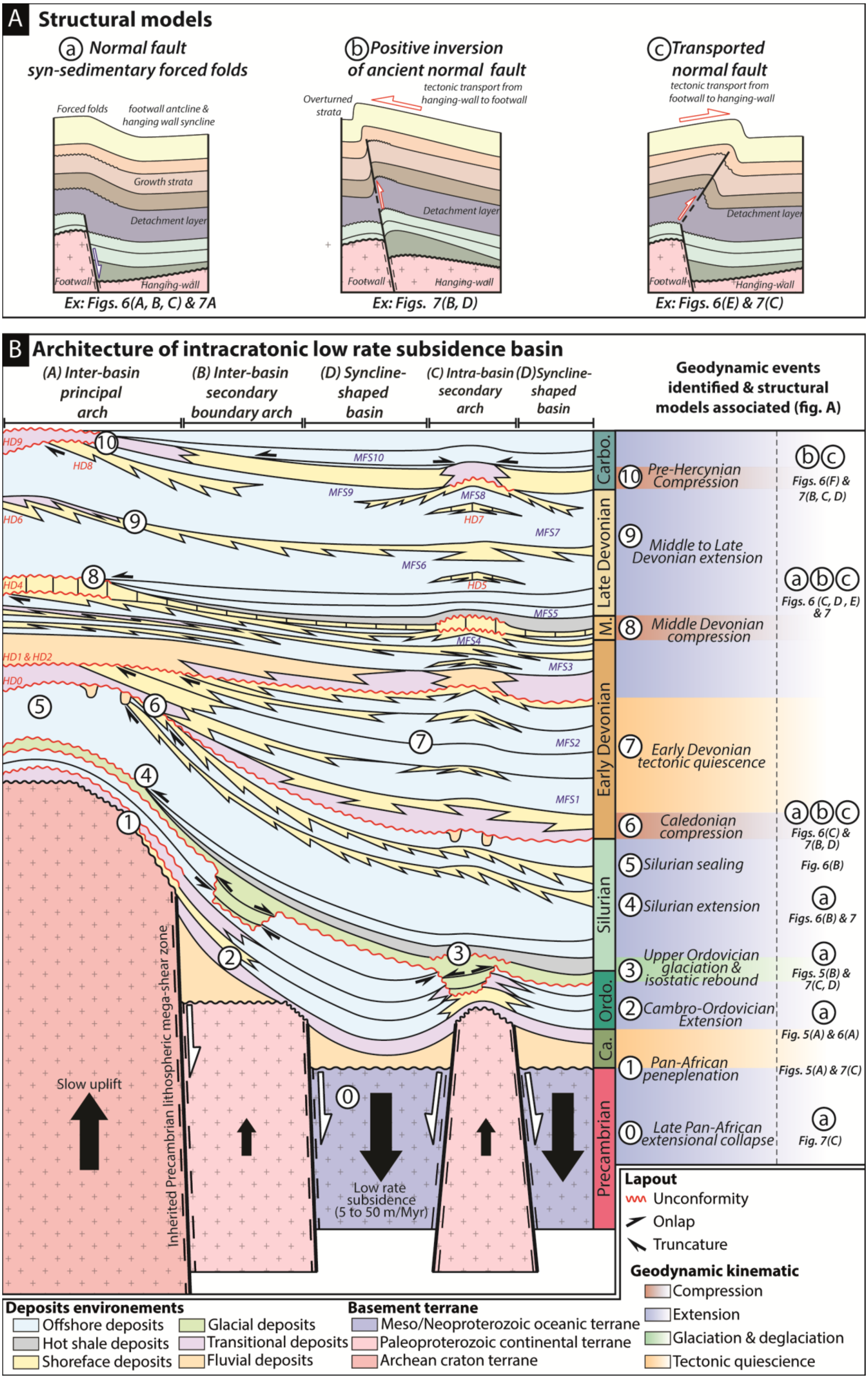
A Structural models
a Normal fault syn-sedimentary forced folds
Forced folds
footwall antcline & hanging wall syncline
Growth strata
Detachment layer
Footwall
Hanging-wall
Ex: Figs. 6(A, B, C) & 7A
b Positive inversion of ancient normal fault
tectonic transport from hanging-wall to footwall
Overturned strata
Detachment layer
Footwall
Hanging-wall
Ex: Figs. 7(B, D)
c Transported normal fault
tectonic transport from footwall to hanging-wall
Detachment layer
Footwall
Hanging-wall
Ex: Figs. 6(E) & 7(C)
B Architecture of intracratonic low rate subsidence basin
(A) Inter-basin principal arch
(B) Inter-basin secondary boundary arch
(D) Syncline-shaped basin
(C) Intra-basin secondary arch
(D) Syncline-shaped basin
Geodynamic events identified & structural models associated (fig. A)
HD9
HD8
MFS10
MFS9
MFS8
HD7
HD6
MFS7
MFS6
HD4
HD5
MFS5
MFS4
HD1 & HD2
MFS3
HD0
MFS2
MFS1
Inherited Precambrian lithospheric mega-shear zone
Slow uplift
Low rate subsidence (5 to 50 m/Myr)
Carbo.
Late Devonian
M.
Early Devonian
Silurian
Ordo.
Ca.
Precambrian
10 Pre-Hercynian Compression
9 Middle to Late Devonian extension
8 Middle Devonian compression
7 Early Devonian tectonic quiescence
6 Caledonian compression
5 Silurian sealing
4 Silurian extension
3 Upper Ordovician glaciation & isostatic rebound
2 Cambro-Ordovician Extension
1 Pan-African peneplenation
0 Late Pan-African extensional collapse
b c Figs. 6(F) & 7(B, C, D)
a b c Figs. 6 (C, D, E) & 7
a b c Figs. 6(C) & 7(B, D)
Fig. 6(B)
a Figs. 6(B) & 7
a Figs. 5(B) & 7(C, D)
a Fig. 5(A) & 6(A)
Figs. 5(A) & 7(C)
a Fig. 7(C)
Lapout
Unconformity
Onlap
Truncature
Geodynamic kinematic
Compression
Extension
Glaciation & deglaciation
Tectonic quiescence
Deposits environements
Offshore deposits
Hot shale deposits
Shoreface deposits
Glacial deposits
Transitional deposits
Fluvial deposits
Basement terrane
Meso/Neoproterozoic oceanic terrane
Paleoproterozoic continental terrane
Archean craton terrane

Figure 17: (A) Different structural model styles identified from the analysis of seismic profiles and from interpretation of the satellite images; (B) Conceptual model of the architecture of intracratonic low rate subsidence basin and synthesis of the tectonic kinematics during the Paleozoic. Note that the differential subsidence between arches and basins is controlled by terrane heterogeneity (i.e. thermo-chronologic age, rheology, etc.).

Supplementary data 1: Georeferenced geochronological dating data compilation of the study area.